Virginia Commonwealth University
VCU Scholars Compass

Theses and Dissertations | Graduate School

2014

MOLECULAR DYNAMICS SIMULATIONS OF PURE POLYTETRAFLUOROETHYLENE NEAR GLASSY TRANSITION TEMPERATURE FOR DIFFERENT MOLECULAR WEIGHTS

Rawan Al-Nsour

Follow this and additional works at: https://scholarscompass.vcu.edu/etd

 Part of the Mechanical Engineering Commons

© The Author

Downloaded from
https://scholarscompass.vcu.edu/etd/3845

This Dissertation is brought to you for free and open access by the Graduate School at VCU Scholars Compass. It has been accepted for inclusion in Theses and Dissertations by an authorized administrator of VCU Scholars Compass. For more information, please contact libcompass@vcu.edu.

MOLECULAR DYNAMICS SIMULATIONS OF PURE POLY-TETRAFLUOROETHYLENE NEAR GLASSY TRANSITION TEMPERATURE FOR DIFFERENT MOLECULAR WEIGHTS

A thesis submitted in partial fulfillment of the requirements for the degree of Doctor of Philosophy Degree at Virginia Commonwealth University

by

RAWAN AL-NSOUR

M.Sc., Industrial Engineering, University of Jordan, Jordan, 2006
B.Sc., Mechanical Engineering, Jordan University of Science and Technology, Jordan, 2002

Director: Hani El-Kaderi, PhD
Associate Professor in Department of Chemistry

Virginia Commonwealth University
Richmond, Virginia
December, 2014

Acknowledgment

I would like first to express my gratitude to my family; my father, my mother, my lovely husband (Basil), my adorable son (Yazan), my siblings, my father and mother in law and all my big family for their continuous and great support. Basil and Yazan, it was long and challenging journey that will not end with success without your patience, love and encouragement.

I want also to express my sincere gratefulness to my doctoral committee, Dr. Hani El-kaderi (Chair), Dr. Brian Hinderliter (Co-Chair), Dr. John Hackett (Co-Chair), Dr. Karla Mossi, and Dr. James McLeskey, for their patience and gaudiness. Each, in their own way, contributed to the quality of my dissertation research and the completion of my doctoral work.

My sincere thanks also to Dr. Barbara Boyan, Dr. Gary Tepper, Dr. Neel Scarsdale, and Dr. Justin Elenewski.

Table of Contents

List of Figures

List of Tables

List of Abbreviations

AA	All Atom
AFMM	Automated Frequency Matching Method
AMBER	Assisted Model Building with Energy Refinement
AM1	Austin Model 1
CED	Cohesive Energy Density
CHARMM	Chemistry at HARvard Macromolecular Mechanics
CHELPG	CHarges from Electrostatic Potentials using a Grid based method
DFT	Density Functional Theory
DP	Degree of Polymerization
GROMOS	GROningen MOlecular Simulation
GTT	Glassy Transition Temperature
HF	Hartree-Fock
MD	Molecular Dynamics
MM	Molecular Mechanics
MOPAC	Molecular Orbital PACkage
NAMD®	NAnoscale Molecular Dynamics program
NPT	Isothermal-isobaric ensemble, the number of particles, the pressure and the temperature are constant.
NVT	Canonical ensemble, the number of particles, the volume and the temperature are constant
NVE	Micro-canonical ensemble, the number of particles, the volume and the energies are constant
NWCHEM®	Northwest Computational Chemistry
OPLS	Optimized Potentials for Liquid Simulations
PBC's	Periodic Boundary Conditions
PDB	Protein Data Bank
PE	Polyethylene
PME	Particle Mesh Ewald
PMMA	Polymethylmethacrylate
PM3	Parametric Method 3
PP	Polypropylene
PSF	Protein Structure File
PTFE	Polytetrafluoroethylene
QM	Quantum Mechanics
RESP	Restrained Electrostatic Potential
RMSD	Root Mean Square Deviation
SA	Simulated Annealing
UA	United Atom
VDW	Van der Waals
VMD	Visual Molecular Dynamics
μVT	Grand-canonical ensemble, the chemical potential, the volume and the temperature are constant

Abstract

Fluoropolymers are employed in countless end-user applications across several industries. One such fluoropolymer is polytetrafluoroethylene. This research is concerned with studying and understanding the thermal behavior of polytetrafluoroethylene. Such understanding is critical to predict its behavior in diverse service environments as the polymer ages and for allowing bottom up design of improved polymers for specific applications.

While a plethora of experiments have investigated the thermal properties of polytetrafluoroethylene, examining these properties using molecular dynamics simulations remains in its infancy. In particular, the current body of molecular dynamics research on polytetrafluoroethylene has primarily focused on studying polytetrafluoroethylene phases, its physical nature, and its helical conformational structure. The present study is the first molecular dynamics simulations research to study polytetrafluoroethylene behavior near the glassy transition temperature. Specifically, the current research utilizes molecular dynamics simulations to achieve the following objectives: (a) model and predict polytetrafluoroethylene glassy transition temperature at different molecular weights, (b) examine the impact of glassy transition temperature on the volume-temperature and thermal properties, (c) study the influence of molecular weight on polytetrafluoroethylene melt and glassy state, and (d) determine the governing forces at the molecular level that control polytetrafluoroethylene glassy transition temperature. Achieving the aforementioned objectives requires performing four major tasks. Motivated by the scarcity of polytetrafluoroethylene force fields research, the first task aims to generate and test polytetrafluoroethylene force fields. The parameters were produced based on the Optimized Potentials for Liquid Simulations All Atom model. The intramolecular parameters were generated using the automated frequency matching method while the torsional terms were

fitted using the nonlinear least squares algorithm. The intermolecular partial atomic charges were obtained using Northwest Computational Chemistry software and fitted using the restrained electrostatic potential at (MP2/6-31G*) level of theory. The final set of parameter was tested by calculating polytetrafluoroethylene density using molecular dynamics simulations.

The second task involves building polytetrafluoroethylene amorphous structure using molecular dynamics at periodic boundary conditions for polytetrafluoroethylene cell at different molecular weights. We use the amorphous structure in the molecular dynamics simulations in consistence with research evidence which reveals that polymer properties such as the specific volume will differ as the polymer passes the glassy transition when it is in the amorphous phase structure whereas no variation occurs when the polymer passes the glassy transition while it is in the crystalline structure. The third task includes testing polytetrafluoroethylene melt phase properties: density, specific heat, boiling point, and enthalpy of vaporization. In the fourth and final task, we performed molecular dynamics simulations using NAnoscale Molecular Dynamics program. This task involves the polymer relaxation process to predict polytetrafluoroethylene mechanical behavior around the glassy transition temperature. Properties that are affected by this transition such as density, heat capacity, volumetric thermal expansion, the specific volume, and the bulk modulus were examined and the simulated results were in good agreement with experimental findings.

1 Introduction

1.1 Motivations

Polymers continue to be a critical component in numerous materials across a wide range of manufacturing and industrial sectors. Polymers are divided into two types, natural and synthetic. Natural polymers are found in nature such as proteins, cellulose, enzymes and starch. Synthetic polymers are man-made materials that are processed under specific conditions (e.g. polymerization) such as polytetrafluoroethylene (PTFE), polyethylene and epoxy. Synthetic polymers could be categorized according to their thermal response into two well-known types, thermosets, and thermoplastics.

Thermosets are defined as a network forming materials that are exposed to chemical reactions which cause these polymers to cross-link and become rigid (Goodman, 1998, Prime, 2010). The treatment of these polymers could be thermally induced by using chemical reactions or radiation. Examples of well-known thermosets include epoxy, polyurethane and melamine.

Thermoplastics are materials which have a rubbery and elastic behavior under heating process (Margolis, 1985). Examples of such polymers include polypropylene (PP), polymethylmethacrylate (PMMA) and polytetrafluoroethylene (PTFE). Therefore, changes in temperature would affect the mechanical behavior and properties of these polymers. One such property is the glassy transition temperature where plastics transform their behavior from the glassy state to the rubbery state.

Special interest to this research is PTFE. PTFE has been researched extensively, especially in the medical and engineering fields. Medical research and applications involving PTFE include, but are not limited to, organ preservation (Brasile and Clarke, 1997), eye surgical instruments, drug delivery and blood substitutes containers and tools (Gross et al., 1993, Riess, 1992, Long

Jr, 1998). In engineering applications, PTFE continues to play a significant role due to its thermal stability, hydrophobicity, low dielectric coefficient, low friction coefficient, and high surface resistivity (Ebnesajjad, 2011). In addition to its effective performance, PTFE is easily recycled which makes it safe and friendly to the environment (Hopewell et al., 2009).

A review of the literature on PTFE reveals two research approaches: experimental-based research and modeling-based research. Until recently, the experimental research has been the primary approach to study PTFE. The legacy of the experimental research enriches the literature with a wealth of details about PTFE important features and significant properties thereby allowing for a comprehensive understanding of PTFE structure and mechanical behavior. Recently, MD simulations emerged as a new theoretical approach for studying materials including polymers such as PTFE. Today, MD as a research approach is widely-recognized in both practice and academia due to its ability not only to understand the experimental findings and also to study the materials' properties at the molecular level, an aspect that is lacking in experimental research. Specifically, this research is concerned with studying the glassy transition temperature of PTFE and its implication on other properties. The thermo-physical effects of the glassy transitional temperature cause conformational rearrangement and molecular vibrations state of population change with temperature, which in turn cause significant changes in the polymers mechanical properties such as the elasticity, compressibility, specific volume and specific enthalpy.

While there has been a considerable effort to study the glassy transition temperature of PTFE experimentally (Lau et al., 1984, Durrell et al., 1965, Sauer and Kline, 1955, Rae and Dattelbaum, 2004, Rae and Brown, 2005), there is yet to be seen a comparable effort to study the glassy transition temperature of PTFE using MD simulations. This is contrary to other polymers

such as polyethylene where a host of MD studies have been conducted to investigate its glassy transition temperature (Han et al., 1994, Rigby and Roe, 1987, Capaldi et al., 2004, Hossain et al., 2010). To fill in the aforementioned gap in the current body of research, this work will employ MD approach to study the glassy transition temperature of PTFE.

1.2 Outline

The remainder of this thesis is organized as follows. Chapter Two presents a comprehensive background and inclusive literature review of PTFE phases, modeling and simulations. Chapter Three demonstrates the research approach, molecular dynamics simulations. Chapter Four presents the Methodology of the parameterization and MD simulations tasks in addition to the research tools. Chapter Five presents the discussions and results. Chapter six presents this research full analysis for PTFE different molecular weight melt phase characterization and the behavior near the glassy transition temperature. The conclusions, contribution, and future research are presented in Chapter Seven.

2 Background

2.1 Introductory Remarks

Polytetrafluoroethylene (PTFE) was discovered accidentally in 1938 by research chemist Dr. Roy J. Plunkett from DuPont Company's Jackson laboratories in the state of New Jersey (Plunkett, 1986). At the time, Dr. Plunkett was working on characterizing different refrigerants gases including methane, ethane and fluorocarbons to find an alternative to Freon® coolant gas. He found that one of the tetrafluoroethylene frozen samples was no longer gas. Instead, it had polymerized and turned to the solid state phase with white color and waxy nature. This material has become to be known as polytetrafluoroethylene scientifically and Teflon® commercially.

Since its introduction commercially, PTFE has played an important role in numerous industries including the weaponry industry. For example, the US military used PTFE in critical high temperature application for the first time in weaponry shell fuses and in producing a nuclear material for the Manhattan Project during World War II (Havens Jr, 1968). Today, PTFE can be found in applications such as gaskets, valve seals, pumps, laboratory ware, electrical insulation, chemically resistant coating and nonstick surfaces.

The purpose of this chapter is to briefly review the current body of literature on PTFE modeling and simulation. Specifically, PTFE physical nature is presented followed by a literature review for the PTFE research fields and PTFE macroscopic properties.

2.2 Physical Nature

PTFE is an artificial linear polymer made of the amalgamation of tetrafluoroethylene monomer units during the polymerization process. These monomers are connected to each other by a strong covalent bond (C—C) according to the molecular formula shown in Figure 1 $(C_2F_4)_n$.

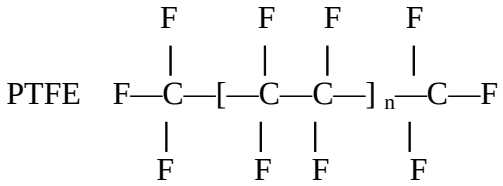

Figure 1: PTFE molecular formula

There are many risks associated with the polymerization process of tetrafluoroethylene, mainly due to its explosive nature (Peterson, 1945). For example, the highly exothermic polymerization (about -42 kcal/mole) of tetrafluoroethylene caused deadly accidents twenty years ago (Eleuterio, 1991). PTFE has a unique set of properties (Arkles and Schireson, 1976, Ebnesajjad, 2011, Sperati and Starkweather, 1961) due to its high content of fluorine atoms. Comparing the fluorine atom to hydrogen atom fluorine is larger, heavier, more reactive, has a stronger bond with carbon, and it has more electronegativity. Listed below are properties correspond to PTFE mixture of chain lengths:

- High molecular weight
- Thermal stability with high resistance to flame and high melting point (327 C°)
- Excellent chemical properties such as its resistance to corrosive chemicals and outstanding weatherability

- Physical properties such as its insolubility in organic solvents
- Superior optical properties and photo-stability (Feiring et al., 1994)
- Electrical properties: the high performance electrical properties make PTFE a very competitive insulator with high dielectric strength and low dielectric loss factor (of about 0.0002 F/m). In addition, PTFE has high electric resistivity (about 10^{19} ohm-cm). The non-polarity features of the PTFE result in a low dielectric constant (about 1.891) ; it is a dimensionless ratio of the permittivity of a material to the permittivity of free space where the permittivity unit is in farads per meter (Hanford and Joyce, 1946). Radiation is used to improve PTFE electrical conductivity (Fowler and Farmer, 1954).
- Mechanical properties: PTFE is the most slippery material and known for its unique mechanical properties. For example, PTFE has low friction coefficient about 0.01 to 0.04; it is a dimensionless value represents the ratio between the frictional force and the normal reaction force where the force unit in the international system units is Newton (Shooter and Thomas, 1949, Flom and Porile, 1955).

2.3 Literature Review

A review of PTFE literature reveals three broad research approaches: (a) the experimental approach, (b) the computational approach (force fields), and (c) the molecular dynamics simulations (MD) approach. The next sections presents a brief review of each research approach as it pertains to PTFE.

2.3.1 **Experimental Approach**

The experimental research is mainly concerned with identifying and examining the different properties of the PTFE based on the analysis of the crystal structure and the phase transitions. Studies within this stream of research utilize various tools such as x-ray diffraction (Ryland, 1958) and NMR spectroscopy (Gunther, 1994). Early studies on PTFE were concerned with studying the structure and the phase transitions of PTFE under specific conditions such as temperature and pressure. These studies represented the building block for PTFE modeling. Based on these studies, the structure of the PTFE was found to have four phases as shown in Figure 2 with three of them being low pressure phases and one being a high pressure phase (Weir, 1953, Hirakawa and Takemura, 1969). The three low pressure phases are found at pressure 1 atm. These are: (a) Phase I which exists at temperature above 30 °C, (b) Phase II which exists at temperature below 20 °C, and (c) Phase IV which exists at temperature between 19 °C and 30 °C. The high pressure phase (Phase III) is found above 4840 atm (5000 kg/cm^2).

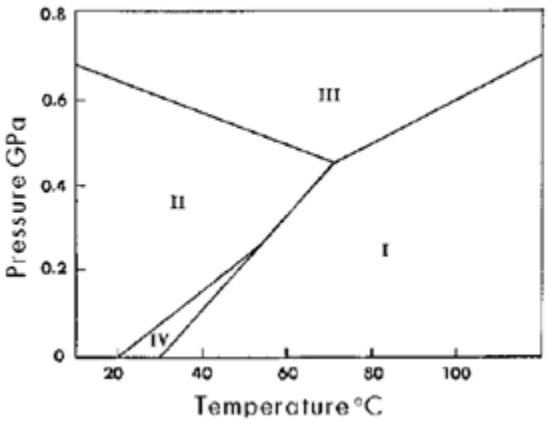

Figure 2: PTFE phases adopted from Clark (1999)

The detailed crystal structure of PTFE phases has been studied extensively. Below is a brief description of these phases, listed by temperature from low to high:

Phase II exists at low temperatures (less than 20 °C). In this phase, the PTFE adopts a helical conformation of (13/6) (Clark, 1999) as shown in Figure 3 and has a strong level of crystallinity (Weeks et al., 1981, Bunn and Howells, 1954). The strong level of crystallinity is supported by the capability of PTFE chains to be oriented and the accurate transition degree (Hanford and Joyce, 1946).

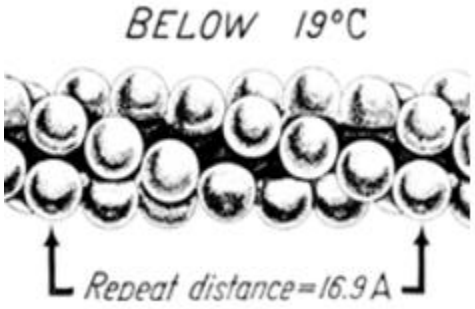

Figure 3: PTFE Phase II helical conformation adopted from Sperati and Starkweather (1961)

Phase IV exists between limited temperature ranges (19 °C to 30 °C). In this phase, the PTFE adopts (15/7) helical conformation as shown in Figure 4. With increasing the temperature, the molecules become more disordered and the conformation becomes less crystalline. Clark and Muus (1962) studied the disorder pattern in PTFE crystal structure at low temperatures (i.e., between 19 °C and 30 °C) and found that the angular displacement at 19 °C is much less than the angular displacement at 30 °C.

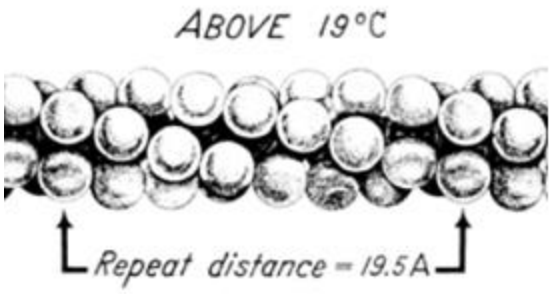

Figure 4: PTFE Phase IV helical conformation adopted from Sperati and Starkweather (1961)

Phase I exists above 30 °C and is situated in a wide range of high temperatures. After passing the melting point (at 327 °C), PTFE converts to its amorphous structure; therefore it is called semi-crystalline polymer. Clark (2006) studied the crystal structure and the possibility of another transition phase within **phase I**. In addition, the structure of PTFE was studied at the thermal degradation which occurs at a very high temperatures (i.e. more than 450 °C) (Bunn et al., 1958, Hanford and Joyce, 1946).

Phase III represents the crystal structure of PTFE at high pressure in which PTFE looks like planar zigzag in contrast to the helical conformation at atmospheric pressure (Nakafuku and Takemura, 1975). Matsushige et al. (1977) studied the crystal structure and chain conformation for the transition phase from phase III to phase I. The researchers found that there is a new region at the high temperature phase near phase I, where the conformation appears like a planar-zigzag due to the right and left handed nature of PTFE molecular chains.

2.3.2 **Computational Chemistry Approach**

Computational chemistry is a multidisciplinary area concerned with solving real world problems based on quantum chemistry basics with the use of computer software packages

(Lipkowitz and Boyd, 1995). The quantum chemistry basics concentrate specifically on equations and approximations which are derived from quantum mechanics by solving the Schrödinger equation (Sadlej and Cooper, 1985) for atomic level systems. Performing calculations using methods that do not consist of any empirical parameters or experimental data is known as *Ab Initio* Quantum Chemistry (Roos and Lawley, 1987). Many properties can be calculated with ab initio quantum chemistry for simple as well as complex molecular systems. However, large systems of atoms require simplifying Schrödinger equation through approximations before the equation can be solved numerically and vast time storage in computer. There are three components to solving the Schrödinger equation for molecular systems. The first component is Born-Oppenheimer Approximation (Combes et al., 1977) which examines the molecule surface potential energy and the wave-function.

The Born-Oppenheimer approximation is an approach to clarify the complex Schrödinger equation. The nucleus and electrons in a molecule are exerted forces on each other with the same amount of electric charge. Although applying the same momentum, the nucleus which has bigger mass to the electron, will have insignificant velocity. Born-Oppenheimer uses this fact and makes the assumption that the nucleus motion can be disregarded in solving the electronic Schrödinger equation; it is assumed to be static (i.e., nucleus) and electrons move around it. The motion of the nuclei and the electrons can be separated and solved with independent wave-functions (Simon and McQuarrie, 1997).

Electron wave function for electron interactions could be solved using different approximation methods such as Hartree-Fock (HF) (Fischer, 1977). Another alternative to consider the electrons energy is to calculate the electron density utilizing Density Functional Theory (DFT) (Gross and

Dreizler, 1995). The molecular orbital usually is described by atom centered functions or basis functions. The basis functions are also called the basis set.

Quantum chemistry studies have extracted the parameters that predict the properties and the conformation of the PTFE based on the minimum potential energy and force fields calculations. These studies used different computational chemistry models such as semi-empirical and ab initio. A detailed review of PTFE computational chemistry research until the mid-90's can be found in Holt et al. (1999). Below is a topical summary of PTFE modeling research from Holt et al. (1999):

- Bates and Stockmayer (1966), (Accelrys, Bates, 1967, Bates and Stockmayer, 1968b, Bates and Stockmayer, 1968a) describe PTFE helical structure based on investigating the conformational energy and the non-bonded parameters. Bates (1967) calculates the conformational potential energies for perfluoroalkanes using semi-empirical calculations. The conformational energy is represented by a function of the rotational angle about the CF_2-CF_2. The energy equation was made of three terms: the non-bonded interactions, the dipole-dipole interaction energy and the three-fold torsion potential for molecules with tetrahedral valence angle. In Bates and Stockmayer (1968a) paper, they investigate the dipole moment (Leonard Jr et al., 1965) for five perfluoroalkanes in benzene solution. The dipole moment measurements were modified using the semi-empirical calculations and implemented in explaining some PTFE properties. Bates and Stockmayer (1968b) use potential energy calculations to predict the chain conformational properties (the fraction of gauche and trans states, characteristic ratio, temperature coefficient of chain dimensions, and change in conformational entropy on melting) for

polytetrafluoroethylene at temperature higher than 600K. The calculated properties were consistent with experimental data.

- Studies that examined PTFE structural properties at solid state using computational and analytical models: De Santis et al. (1963) investigates the helical chains stability for variety of linear polymers such as PTFE and polyethylene (PE). The researchers found that the non-bonding interactions play a significant role in polymer chain stability. Iwasaki (1963) studied the helical structure of PTFE and the most stable structure of it, where the potential energy was the minimum, he found that the steric interactions has stronger effect on PTFE structure than the electrostatic interactions. D'Ilario and Giglio (1974) investigate the influence of Van der Waals (VDW) forces on PTFE helical structure, the researchers found that PTFE is a free rotating polymer around its helical axes. Corradini and Guerra (1977) studied the stability of PTFE confirmation above 30 °C, the results shows that the chain pseudo hexagonal adjustment matches to the disorderly successions of the PTFE helical conformation. Banerjea and Taylor (1982) (1984), this paper examines the non-bonding interactions parameters for three types of interactions: the VDW, the electrostatic and the torsional interactions. The parameter sets were obtained based on previous studies: set A (Hopfinger and Hopfinger, 1973), set B (McCullough and McMahon, 1964) and set C (Farmer and Eby, 1981). The PTFE helical structure is predicted in this work. The three sets were reproduced using the potential 6-12 form. Heinonen and Taylor (1989) studied the dynamic in PTFE chain reversal defects and found that the specific morphology of PTFE seems to allow the right and left handed reversal chain defects to traverse a lamellar width in the order of 10 ns. Napolitano et al. (1990) investigated PTFE structure at low temperature (i.e., phase II), the researchers

found that there is a chain disorder even at the crystalline phase. Villani et al. (1991) studied the thermal behavior and transitions of PTFE at room temperature and found that these transition affected by the morphology such as triclinic-hexagonal and pseudo-hexagonal structure transition crystals. Smith et al. (1994) characterized PTFE structures using ab intio calculations on PTFE small oligomers, they presented six-state model for PTFE conformations which is consistent with experimental findings.

- PTFE studies which were conducted using computational models, analytical and Monte Carlo models: McMahon and McCullough (1965) refer some polymers properties to the defects that exist in the polymer chain, they use analytical method to simulate the polymer defect structure and found the fold of fewer than seven dihedral indicates high bonding structure energy, ineffective non-bonding energy and stable or fixed structure. Farmer and Eby (1981), this paper highlights the importance of energy calculations and analysis in predicting some PTFE properties and describing its structure. The calculated energy is a function of transitional and rotational displacement. More specifically, the paper investigates the PTFE crystal structure in specific conformations (i.e. 13/6 and 54/5) under low temperature with the objective of finding the lowest energy level. The parameters were obtained from two sources: crystal structure data and/or previous studies. The results were consistent with diffraction experimental data and showed disorder conformation at phase II. Farmer and Eby (1985), This paper examines and contrasts the conformational energies of PTFE phases under high temperature with the PTFE phases under low temperatures as studied in (Farmer and Eby, 1981). In addition, the paper examines the lowest energy level structure and investigated the defects which resulted in high energy levels under high temperature condition. The results were not

consistent with experimental data except for one conformation (i.e. 15/7 conformation). Weeks et al. (1981) studied phase II of PTFE after its transformation from phase IV using electron diffraction and x-ray diffraction methods. Eby et al. (1990), they studied PTFE conformational properties at high pressure conditions and found that phase III (i.e., high pressure phase) form monoclinic structure which provides high entropy.

The main limitation in the force fields parameters which were computed in the aforementioned early studies is the deficiency of accurate parameters. This problem forces the researchers to fix the geometry in order to reproduce the experimental results. Over the past decade, a handful of studies were conducted to derive the fluorocarbons force fields with complete optimization and energies at all degrees of freedom (Hougham, 1999) using semi-empirical and ab initio calculations. These studies are listed below:

- Hariharan and Harris (1994) found the force field parameters for PTFE and hydrocarbon small oligomers. The united atoms models (UA), consider a group of atoms such as CH_3 or CF_3 as one united atom (i.e., one bead), and were used to perform copolymer equilibrium liquid-vapor simulation. The intra-molecular interactions included the dihedral and angle potentials while the bonds were constrained to specific values. The study yielded inaccurate Van Der Waals (VDW) parameters. In this study the force field parameters failed to calculate some of the properties such as the low surface tension.
- Holt et al. (1996) used the semi-empirical Austin Model 1 (AM1) (Stewart, 1990) to generate the PTFE force fields in its solid state for perfluorohexadecane. The results were scheduled in two sets: set (I) which was used with VDW^{6-12} and set (II) which was used with VDW^{6-9}. The parameters were refined again by scaling the *ab initio* data with the semi-empirical energies to yield two adjusted sets: set (III) (used with VDW^{6-12}) and set

(IV) (used with VDW^{6-9}). The force field potential energy formula is the same formula that was used in Biosym Discover (Guide, 1993). The partial charges were derived from Molecular Orbital PACkage (MOPAC) AM1 charges. However, the authors dropped the torsional term (i.e. the torsional barrier equal to zero) from the model to get results that agree with the experimental finding.

- In a subsequent study, Holt and Farmer (1999a) used the MOPAC Parametric Method 3 (PM3) Hamiltonian semi-empirical model to derive the force field parameters with the purpose of having more accurate and reasonable simulations than those in Holt et al. (1996). The dihedral potential is added to describe the backbone torsional conformation. Based on this change, an additional set was added (i.e. Set VI calculated for only VDW^{6-9}). The partial charges were derived using semi-empirical MO calculations (F= -0.09, C= +0.18). All sets are shown in Table 1.

Noteworthy is that the 1996 and 1999 studies by Holt and Farmer were based on finding the force fields parameter using the united atom model and not the all atom model. The all atom (AA) models study considers all the atoms in the simulation while the UA models as I mentioned earlier, consider a group of atoms such as CH_3 or CF_3 as one united atom (i.e., one bead). As the UA model method does not consume as much time and resources, it yields less accurate results. In contrast, the AA models method consumes more resources and time but offers more accurate results (Breneman and Wiberg, 2004). The Assisted Model Building with Energy Refinement (AMBER) (Cardelli, 1986) and Chemistry at HARvard Macromolecular Mechanics (CHARMM) (Brooks et al., 1983) are force fields belong to the AA models. An example of the UA models is the Dreiding potential force fields (Mayo et al., 1990).

Table 1: PTFE united atom force fields adopted from Hougham (1999)

Derived Force Field Parameters

(a) van der Waals Parameters

Interaction	Set I[a]		Set II[b]		Set III[a]		Set IV[b]		Set VI[b]	
	ε (kcal/mol)	r_{min} (Å)	ε (kcal/mol)	r_{min} (Å)	ε (kcal/mol)	r_{min} (Å)	ε (kcal/mol)	r_{min} (Å)	ε (kcal/mol)	r_{min} (Å)
F–F	0.0115	3.207	0.0245	3.248	0.2500	3.074	0.3328	3.200	0.0211	3.538
C–C	0.0050	3.400	0.0050	3.450	0.0500	2.805	0.0500	3.000	0.0844	3.884
F–C[c]	0.0076	3.304	0.0111	3.349	0.1118	2.940	0.1290	3.100	0.0422	3.711

(b) Valence Force Field Parameters for Quadratic Bond Stretching and Angle Bending Terms[d]

	Set I		Set II		Set III		Set IV		Set VI	
Interaction	FC	EQV	FC	EQC	FC	EQC	FC	EQV	FC	EQV
C–C stretch	402.43	1.610 Å	402.43	1.610 Å	402.43	1.595 Å	402.43	1.595 Å	722.46	1.540 Å
F–C stretch	871.69	1.360 Å	892.50	1.360 Å	861.85	1.360 Å	892.65	1.360 Å	892.60	1.340 Å
C–C–C bend	193.36	109.4°	174.65	109.4°	120.15	107.5°	120.15	107.5°	110.30	108.5°
F–C–C bend	159.54	110.0°	157.57	110.0°	152.98	110.0°	152.98	110.0°	152.98	111.2°
F–C–F bend	256.72	104.3°	256.72	104.3°	212.07	104.4°	256.72	104.4°	256.80	104.8°

(c) Coefficients for Six-Term Dihedral Potential (kcal/mol) Used with Set VI

$V_1 = -0.4005$ $V_2 = -0.9980$ $V_3 = -2.3612$ $V_4 = -1.6149$ $V_5 = -1.1447$ $V_6 = -1.0025$

- Okada et al. (1999) used the GEMS/MD all atom model to develop a new set of force fields parameters for an amorphous PTFE perfluoro-n-butane. The computational ab initio calculations were performed at HF/6-31G level using GAUSSIAN94. The charges were estimated experimentally using dipole moment. The authors tested their parameters by performing MD simulations to compute the heat of vaporization and density. The results were in good agreement with the experimental values. The unknown GEMS/MD force field includes a unique term called VDW1-5. This term refers to PTFE chain helicity due to fluorine atoms in position 1-5. This claim was contradicted by (Jang et al., 2003) who developed a new set of parameters that predict PTFE helical conformation due to the fluorine atoms electrostatic forces. Okada et al. (1999) set of force field parameters is shown in Table 2.
- Watkins and Jorgensen (2001) explore the force fields parameters using Optimized Potentials for Liquid Simulations (OPLS) all atom classic model at (LMP2/cc-pVTZ(-f)//HF/6-31G*) Møller-Plesset perturbation second level of theory, which had consider the electron correlation contribution, using the correlation consistent basis set (Hehre and Huang, 1995) . The calculated densities and heat of vaporization provide significant values comparing them to the experimental results. The full set of force field parameters is shown in Table 3.
- Borodin et al. (2002) developed perfluoroalkanes and PTFE force fields using a united atom classical force field model for variety of oligomers (C_4F_{10} to $C_{20}F_{42}$) using ab initio calculations at (MP2/aug-cc-pvDz//B3LYP/D95+*) level. The Lennard Jones force field shows 2.2% error of the predicted densities and 10% higher values of the heat of vaporization experimental data. The force fields parameters are shown in Table 4

Table 2: PTFE GEM/MD all atom force fields adopted from Okada et al. (1999)

Bond Stretching

Atom A	*Atom B*	$R_0(\AA)$	$V_B(kcal/mol/\AA^2)$
CF3	CF2	1.5304	357.0
CF2	CF2	1.5302	344.0
CF3	F3	1.3494	508.0
CF2	F2	1.3653	391.0

Angle Bending

Atom A	*Atom B*	*Atom C*	$\theta_0(rad)$	$V_A(kcal/mol/rad^2)$
F3	CF3	F3	108.79	104.4
F3	CF3	CF2	110.14	80.2
F2	CF2	CF3	107.20	84.7
F2	CF2	F2	108.84	106.3
F2	CF2	CF3	108.45	79.5
CF2	CF2	CF3	116.51	97.9
CF2	CF2	CF2	116.51	97.9

Torsion

				V_k (*kcal/mol*)					
Atom A	*Atom B*	*Atom C*	*Atom D*	V_1	V_2	V_3	V_4	V_5	V_6
CF2	CF2	CF3	F3	0.0	0.0	0.5908	0.0	0.0	0.0
CF2	CF2	CF2	CF3	17.70	3.253	1.748	0.525	−0.020	−0.462
CF2	CF2	CF2	CF2	17.70	3.253	1.748	0.525	−0.020	−0.462

van der Waals

Atom A	*Atom B*	V_{12} $(kcal/mol/\AA^{12})$	V_6 $(kcal/mol/\AA^6)$
CF2	CF2	83394	230.00
CF3	CF3	39955	56.64
F2	F2	50487	138.51
F3	F3	54473	179.45

1 – 5 Nonbonding

Atom A	*Atom B*	$V_{nb12}(kcal/mol/\AA^{12})$	$V_{nb6}(kcal/mol/\AA^6)$
F2	F3	1300000	0
F2	F2	1300000	0

Partial Charges and Masses

Atom	*Charge* (*e*)	*Mass* (*a.u.*)
CF2	0.48	12.0
CF3	0.63	12.0
F2	−0.24	19.0
F3	−0.21	19.0

Table 3: PTFE OPLS-AA force field parameters adopted from Watkins and Jorgensen (2001)

bond	k_b (kcal mol^{-1} Å^{-2})	r_0 (Å)
CT−F[a]	367.0	1.332
CT−CT[b]	268.0	1.529

angle	k_θ (kcal mol^{-1} rad^{-2})	θ_0 (deg)
F−CT−F[a]	77.00	109.10
CT−CT−F[b]	50.00	109.50
CT−CT−CT[c]	58.35	112.70

dihedral angle	V_1	V_2	V_3	V_4
		General		
F−CT-CT-F	−2.500	0.000	0.250	0.000
CT-CT-CT-F	0.300	0.000	0.400	0.000
CT-CT-CT-CT	6.622	0.948	−1.388	−2.118
		n-C_4F_{10} Specific		
CT-CT-CT-CT	7.219	−0.484	−1.105	−0.990
		n-C_5F_{12} Specific		
CT-CT-CT-CT	5.829	−0.453	−1.266	−1.052
		$(CF_3)_2CFCF_2CF_3$ Specific		
CT-CT-CT-CT	8.227	−0.106	−0.435	−1.676

atom type	atom or group	q (e$^-$)	σ (Å)	ϵ (kcal mol^{-1})
F	F	−0.12	2.95	0.053
CT	CF_4	0.48	3.50	0.097
CT	CF_3 group	0.36	3.50	0.066
CT	CF_2 group	0.24	3.50	0.066
CT	CF group	0.12	3.50	0.066

Table 4: PTFE united atom classical force fields adopted from Borodin et al. (2002)

Nonbonded Force Field Parameters for PTFE

atom pair	A (kcal/mol)	B ($Å^{-1}$)	C [(kcal $Å^{-6}$)/mol]
F−F	63635.0	4.261	124.3
F−C	6923.2	3.084	315.8
C−C	14976.0	3.09	640.8

Valence Force Field Parameters for PTFE[a]

bond type	K^{BOND} (kcal mol^{-1} $Å^{-2}$)	r_0 (Å)
$F-C_m$	722.0	1.3391
$F-C_e$	722.0	1.3510
C_m-C_e	617.8	1.5658
C_e-C_e	617.8	1.5725

bend type	K^{BEND} (kcal mol^{-1} rad^{-2})	θ_0 (deg)
$F-C_m-F$	240.0	108.54
F−C−C	180.0	109.46
C−C−C	160.6	115.55
$F-C_e-F$	240.0	110.13

Torsional Force Field Parameters for PTFE

(kcal/mol)

type	K_1	K_2	K_3	K_4	K_5	K_6	K_7
C−C−C−C	−0.925	0.07	1.427	−0.540	−0.207	0.0	0.676
F−C−C−F	0.0	0.0	−0.380	0.0	0.0	0.0	0.0

- Jang et al. (2003) computed the force field for Perfluorinated Alkanes using the Dreiding untied atom model at B3LYP/DFT accuracy level and with the Mulliken charges (CF2 carbon = +0.52, CF3 carbon= +0.72, CF2 fluorine= -0.26, and CF3 fluorine= -0.24). These parameters were tested in a subsequent study (Jang et al., 2005) to reaffirm their accuracy as the best parameters of PTFE united model atoms. The full set of parameters is shown in Table 5. In addition to their accuracy, Jang et al. (2003) findings contradict the claim of previous studies about the source of perfluoroalkanes helicity. Contrary to the previous view that the helical conformation nature is due to the repulsive VDW interaction between the fluorine atoms, specifically at 1-5 locations (Okada et al., 1999),

Jang et al. (2003) study shows that it is the electrostatic interactions between the backbone and the fluorine atom that are the origin of twisting.

Table 5: PTFE Dreiding united atom force fields adopted from Jang et al. (2003)

	van der Waals parameters of exponential-6		
	ζ	D_{vdW}	R_{vdW}
C^h	12	0.084 40	3.8837
F	12	0.044 53	3.4985
	13	0.047 20	3.4480
	14	0.049 35	3.4112
	15	0.050 92	3.3825
	16	0.052 46	3.3589

(a) Dreiding Type Valence Force Field

bond stretching $E_r = {}^1/_2 K_r(R - R_0)^2$

valence angle bending $E_\theta = {}^1/_2[K_\theta/\sin^2\theta_0](\cos\theta - \cos\theta_0)^2$

dihedral angle torsion $E_\phi = {}^1/_2 V(1 - d\cos 3\phi)$

E_r	C−C	K_r	429.320	R_0	1.498
	C−F		605.260		1.336
E_θ	C−C−C	K_θ	106.274	θ_0	122.554
	F−C−C		100.337		118.320
	F−C−F		108.240		121.502
E_ϕ	C−C−C−C	V	6.434	d	1
	F−C−C−C		8.244		1
	F−C−C−F		8.085		−1

(b) Fourier Multicomponent Torsion

dihedral angle torsion $E_\phi = {}^1/_2\sum_{n=1}^{m} V_n(1 - d_n\cos n\phi)$

E_ϕ	C−C−C−C	V_1	86.4305	d_1	1
		V_2	9.2812	d_2	1
		V_3	18.2580	d_3	1
		V_4	9.8535	d_4	1
		V_5	9.7520	d_5	1
		V_6	0.8151	d_6	−1
	F−C−C−C	V_3	2.0000	d_3	−1
	F−C−C−F	V_3	2.0000	d_3	−1

- Paulechka et al. (2012) derived an OPLS-AA force fields for hydrofluorocarbons at the HF/6-31G(d) level along with CHarges from Electrostatic Potentials using a Grid based method (CHELPG) atomic charges (Breneman and Wiberg, 2004). CHELPG charges are premium than Mulliken and closer to the Restrained Electrostatic Potential (RESP) charges (Byrd and Rice, 2008), which make them more sensitive to predicting accurate properties. A downside of CHELPG charges, however, is their unsuitability when dealing with big systems; specifically because the inner atoms do not contribute significantly in

the molecular electrostatics potential. Nevertheless, the main contribution of this study is presenting a new mathematical method to predict the force field parameters based on mapping criteria. The parameters derived were successful in calculating many properties such as enthalpies of vaporization and densities with values that were in agreement with the experimental findings, the parameters are shown in Table 6, Table 7, Table 8, Table 9 and Table 10

Table 6: OPLS-AA bond parameters adopted from Paulechka et al. (2012)

Bond	Force constant $k_r \cdot k_B^{-1}$ / K [a]	$r_0 \cdot 10^{10}$ / m
CM–CT, CMf–CTf, CM–CTf	159519.7	1.510
CT–HC-1	171093.6	1.090
CT–CT, CTf–CTf	134682.0	1.529
CM–HC-2, CMf–HC-2	171093.6	1.080
CM–CM, CM–CMf	276265.9	1.340
CTf–Fpf	184680.5	1.332
CMf–Fcm	211325.0	1.340

[a] k_B refers to the Boltzmann constant

Table 7: OPLS-AA angle parameters adopted from Paulechka et al. (2012)

Angle	Force constant $k_\vartheta \cdot k_B^{-1}$ / K	Θ_0 / deg
CM–CM–HC-2, CMf–CM–HC-2, CM–CMf–HC-2	17612.6	120.0
CTf–CTf–Fpf	25160.8	109.5
CM–CT–HC-1	17612.6	120.0
HC-1–CT–HC-1	16606.1	107.8
HC-1–CT–CT	18870.6	110.7
CT–CT–CT	29362.7	112.7
CM–CM–CT, CMf–CM–CTf, CM–CMf–CTf	35225.2	124.0
CT–CM–HC-2, HC–CM–HC, CTf–CM–HC-2	17612.6	117.0
CM–CTf–Fpf, CMf–CTf–Fpf	25161.0	109.5
Fpf–CTf–Fpf	38747.9	109.1
CM–CMf–Fcm	40257.5	121.5
CTf–CMf–Fcm [a]	35225.3	110.6
HC-2–CMf–Fcm	25161.0	112.0

[a] Force constant is equal to that of CM–CM–CT angle, Θ_0 is estimated from equilibrium geometry of 2,3,3,3-tetrafluoropropene at HF/6-31+G(d,p) theory level

Table 8: OPLS-AA torsional parameters adopted from Paulechka et al. (2012)

Torsion	$k_1 \cdot k_B^{-1}$ / K	$k_2 \cdot k_B^{-1}$ / K	$k_3 \cdot k_B^{-1}$ / K
HC-1–CT–CT–HC-1, HC-2–CM-CM–HC-2, HC-1–CT–CT–CT	0.0	0.0	75.5
HC-2–CM–CT–HC-1	0.0	0.0	80.0
HC-1–CT–CM–CM	0.0	0.0	-93.6
CTf–CTf–CTf–Fpf	75.5	0.0	100.6
Fpf–CTf–CTf–Fpf	-629.0	0.0	62.9
CT–CM–CM–HC-2	0.0	3522.5	0.0
HC-2–CM–CMf–HC-2, HC–CM–CMf–Fcm, HC-2–CM–CMf–CTf, HC-2–CMf–CM–CTf, Fcm–CMf–CM–CTf	0.0	3522.5	0.0
CM–CM–CTf–Fpf, CM–CMf–CTf–Fpf, CMf–CM–CTf–Fpf	0.0	0.0	-209.0
HC-2–CM–CTf–Fpf	0.0	0.0	101.0
Improper torsions			
HC-2–CM–CM–HC-2, CM–CM–CT–HC-2, CMf–CM–HC-2–HC-2, CM–CMf–CTf–Fcm, CM–CMf–Fcm–HC-2, CMf–CM–CTf–HC-2	0.0	7548.0	0.0

Table 9: OPLS-AA torsional VDW parameters adopted from Paulechka et al. (2012)

Atomic Type	$\varepsilon \cdot k_B^{-1}$ / K [a]	$\sigma \cdot 10^{10}$ / m
CT	33.35	3.38
HC-1	19.50	2.60
CM	38.15	3.52
HC-2	16.37	2.60
CTf	30.50	3.43
Fpf	30.70	2.97
CMf	36.98	3.53
Fcm	23.17	2.98

[a] if atoms are separated by three bonds (1-4 interaction), this parameter is decreased by a factor of two

Table 10: OPLS-AA electrostatic parameters adopted from Paulechka et al. (2012)

No.	Atomic type	Atomic charge / *e*	Connected to atoms
1	CTf	0.694	2 4 5 6
2	CTf	0.092	1 3 7 8
3	CTf	0.694	2 9 10 11
4	Fpf	-0.201	1
5	Fpf	-0.201	1
6	Fpf	-0.201	1
7	Fpf	-0.137	2
8	Fpf	-0.137	2
9	Fpf	-0.201	3
10	Fpf	-0.201	3
11	Fpf	-0.201	3

In conclusion, PTFE is a bit tricky to describe in a force-field approach. This is evident in the number of studies that have attempted to develop new force-fields altogether but more importantly in the inconsistencies surrounding PTFE parameterizations in these studies as pointed out in the preceding discussion. In fact, it's not an overstatement that developing and validating an accurate set of new force field parameters is a full research project in its own right. For the purposes of this research, the PTFE OPLS-AA force fields from Watkins and Jorgensen (2001) will be utilized in the glassy state analysis, I used also the parameters that I generated to test density and solubility parameter.

2.3.3 **Molecular Dynamics Simulations Approach**

As an emerging field of research, MD approach takes advantage of specialized software packages to study and predict the dynamics (i.e. position, velocity, etc.) of the macroscopic states for polymers chain conformations and the mechanical or physical properties at the microscopic level. There have been a few studies on PTFE simulations but with limited successful simulations, due to the erratic treatment of this polymer in most force field parameterizations (e.g., Borodin et al., 2002, Hariharan and Harris, 1994). The impact of PTFE parameterizations inconsistencies could be serious on some of the calculated properties that are sensitive to the VDW parameters which, in turn, could significantly increase the possibility of the simulation to return incorrect results. This may explain why there is a scarcity in molecular dynamics simulations of this widely-used material. Listed below are examples of PTFE MD simulations studies:

- Holt and Farmer (1999b) used molecular dynamic simulation to test PTFE's solid state conformations and thermal changes (helix reversal) at different temperatures. Their study found that these changes resulted from the derangements of the PTFE's chains which increased with temperature starting at 248K. In light of this finding, Holt and Farmer (1999b) brought to an end the disagreement between (a) the x-ray data which suggested a significant degree of order on Teflon structure below 292K and (b) the NMR and Raman scattering techniques which suggested a disorder in structure even at very low temperatures.
- Vishnyakov and Neimark (2000) employs molecular dynamic simulation to study the Nafion polymer in two different solvent: water and methanol using Cerius2 software package. According to the study, the Nafion skeleton, which contains polytetrafluoroethylene, showed more folding pattern in water than in methanol as shown in Figure 5, and more specifically "the structure of the oligomer in water turned out to be substantially more folded compared to that in methanol. In average, every third CCCC torsion was found in gauche conformation in water, while in methanol the ratio of the number of gauche and trans CCCC torsions was roughly 1:6, i.e., the oligomer exhibits more stretched structure in methanol" (Vishnyakov and Neimark, 2000) . This behavior assured PTFE's insolubility (i.e., hydrophobic nature) in inorganic solvents such as water and it's solubility in organic solvents as methanol.
- The four phases of PTFE have been simulated by Sprik et al. (1997) and Sprik et al. (1999) as shown in Figure 6 and Figure 7, respectively. The researchers found that the partially disordered phase started at 625K and the melting points started at 725K. These two values are higher than the corresponding experimental ones; it is found that PTFE

starts entering the disorder region at 553 K and the melting point is about 600K experimentally (Hanford and Joyce, 1946).

In conclusion, while an abundance of experimental and force fields studies have been conducted to investigate the properties of PTFE, the research to examine these properties using molecular dynamics simulations remains in its infancy (Rae and Dattelbaum, 2004). The current work will utilize molecular dynamic simulation to achieve two objectives: (a) model and predict the PTFE glassy transition temperature, and (b) examine the impact of the different molecular weights simulation cells on the glassy transition temperature range. Here, the data extracted from studying the crystal structure (the experimental approach) and the force field parameters (the computational chemistry approach) is utilized in the advanced algorithm for the MD approach. Next, the MD simulations results at the molecular level usually are compared to the macroscopic properties that have been extracted from the experiments. The next section provides a review of PTFE macroscopic properties.

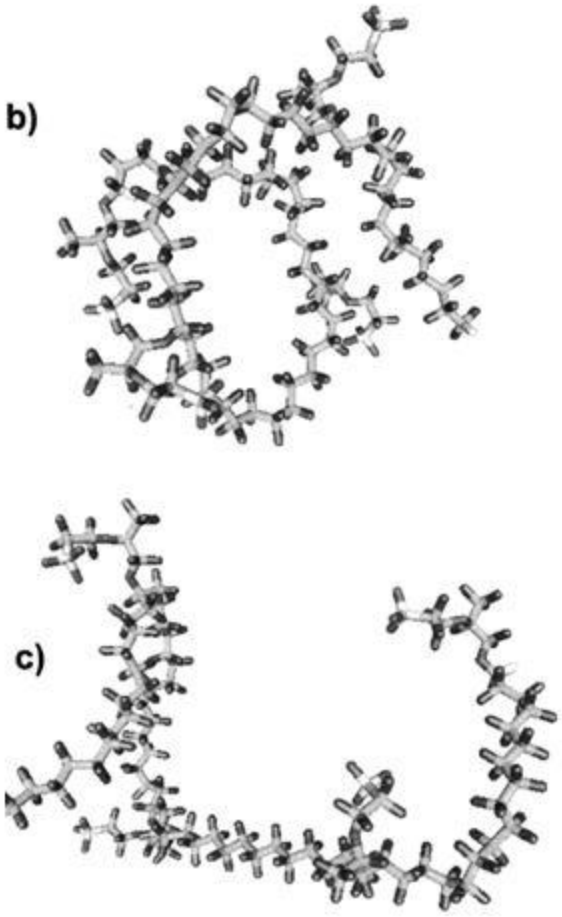

Figure 5: Nafion behavior in two solvents: (b) water where Nafion skeleton conformation is strongly folded and (c) methanol where PTFE shows less folding structure, adopted from Vishnyakov and Neimark (2000)

.

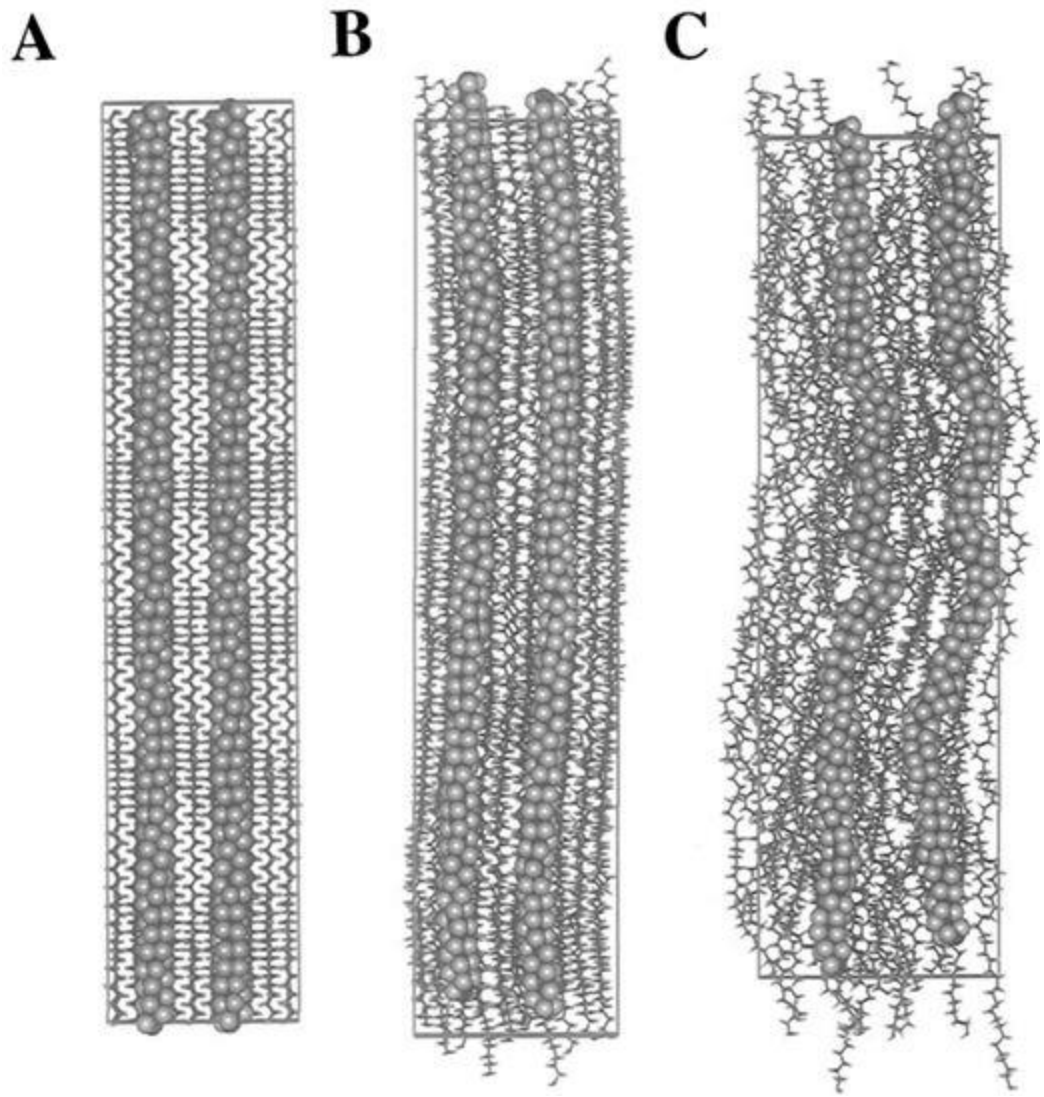

Figure 6: PTFE solid phase simulations: (a) represents the cryogenic temperature phase of PTFE structure, (b) shows PTFE chain structure at phase I, and (c) PTFE conformation at superheated temperatures adopted from Sprik et al. (1997)

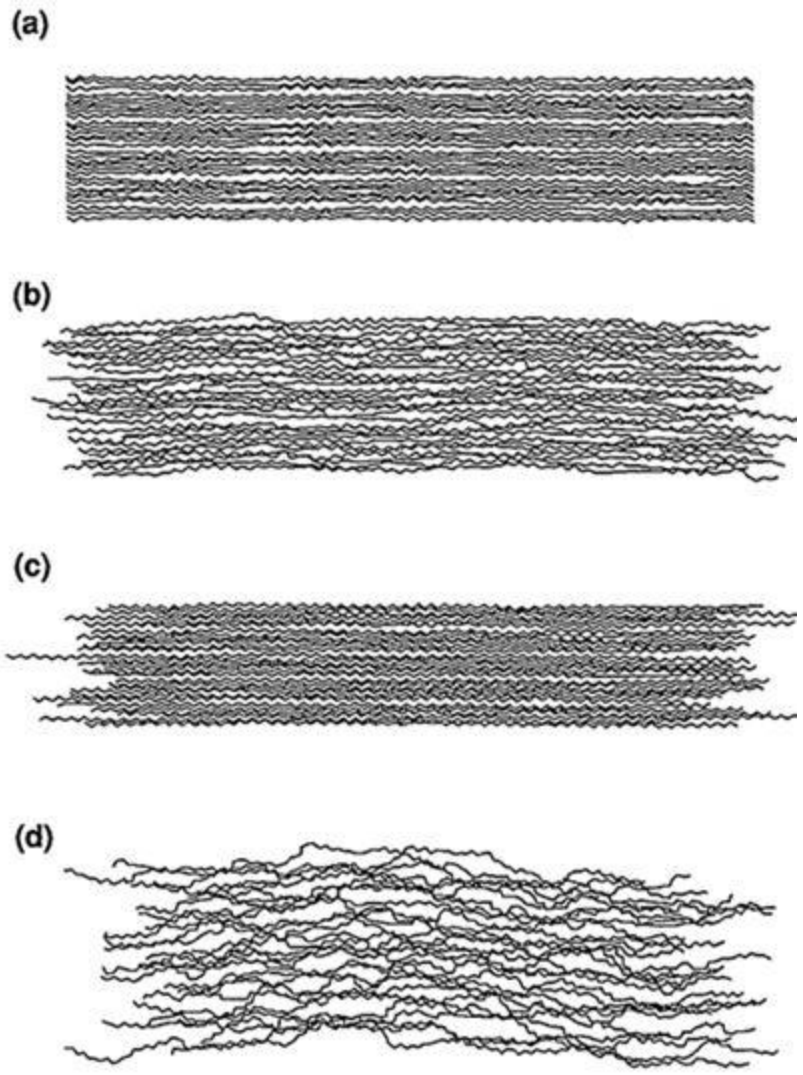

Figure 7: PTFE phases configurations: (a) chain structure at low temperature phase, (b) conformation of PTFE chains at phase I, (c) the high pressure phase structure, and (d) the structure at very high temperatures adopted from Sprik et al. (1999)

2.4 Macroscopic Properties

As pointed out earlier, the MD simulations results will be compared to published measurments of a variety of PTFE experimental macroscopic properties such as the mechanical and thermal properties. Such properties depend on molecular weight of the PTFE chains.

One way to measure the molecular size is by measuring the molecular weight which is defined as the sum of the atomic weights of all atoms setting up a molecule. Polymer molecular weight is vital because it controls many properties such as mechanical and thermal properties. For example, the molecular weight has a great impact on determining many physical properties which are related to the cohesive forces between molecules, primary valence bonds entanglement degree, and consequently the free rotation of the polymer around its backbone. The increase in the molecular size results in increasing the cohesive forces, the amount of entanglement, and the restriction of the atomic motion which affects the molecular conformation. The molecular size could be measured using different ways such as the degree of polymerization, the number average molecular weight and the weight average molecular weight. The degree of polymerization is defined as the number of the structural repeating units in addition to the first and last units. The degree of polymerization (DP) is expressed by equation 2.1 (Hearle, 1982):

$$DP = L/a = MW/MW_o \quad 2.1$$

where L is the chain length, a is the monomer unit length, MW is the chain molecular weight and MW_o is the monomer unit molecular weight. The number average molecular weight is defined as the total weight of polymer divided by the number of polymer molecules and the weight average molecular weight is defined as the total weight of polymer divided by the molecular weight of polymer molecules.

2.4.1 **Mechanical Properties**

The mechanical properties of polymers are those properties that show a response to an applied force. In other words, these properties are not constant but rather variable. They vary with conditions such as the applied load, the temperature, and the molecular weight. They reflect the effectiveness and the usage of the polymers and different materials. The mechanical

properties such as the tensile strength, modulus and toughness are affected by molecular weight. For example, the mechanical characteristics start to appear on the polymer oligomer at DP of 30 (also known as the critical degree of polymerization) and until the degree of polymerization reaches to 600. For long chain polymers (i.e. DP=600 or more), the mechanical behavior is nearly constant (the chains are not sliding) because of the chain entanglement and the intermolecular forces (Kaufman and Falcetta, 1977). The relation between the mechanical behavior of polymers and their molecular weight is nearly proportional. For example, the tensile strength increases with increasing the molecular weight as shown in Figure 8 (Carraher, 1996). This proportional relationship makes the polymer useful, robust and sufficient to bear forces and loads. The mechanical properties of PTFE have been widely studied; mostly using the experimental approach. Below are examples of such studies:

- The PTFE fatigue behavior and mechanical damage features (Koo et al., 1967)
- The temperature effect on hardness, friction and the shear strength (King and Tabor, 2002)
- Creep and deformation (Speerschneider and Li, 1962, Khan and Zhang, 2001)
- PTFE low friction and wear behavior based on speed, load and humidity (Unal et al., 2004)
- PTFE stress-strain behavior under compression (Rae and Dattelbaum, 2004) and tension (Rae and Brown, 2005)

PTFE has tensile strength in range of (21-35) MPa, Elongation in range of (300%-500%) and modulus of elasticity about 0.49 GPa (Lenntech, 1998)

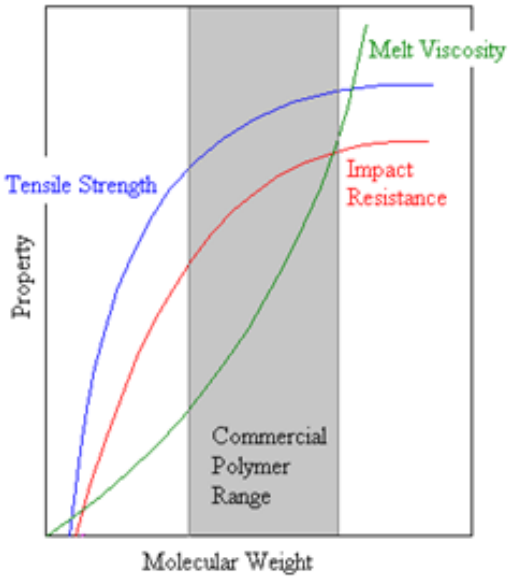

Figure 8: Molecular weight versus mechanical properties adopted from Carraher (1996)

2.4.2 **Thermal Properties**

Thermal properties of polymers are those characteristics that are affected by temperature. PTFE is considered a thermoplastic polymer because its thermal stability is affected by the temperature. Specifically, it becomes soft when heated and hard-finished when cooled. Examples of thermal bulk properties that are related to temperature include: (a) the melting temperature T_m, and (b) the glassy transition temperature T_g. Those properties are affected by the molecular weight of the material.

2.4.2.1 Melting Temperature

The melting temperature is defined as the temperature at which the solid state of a material transforms to the liquid state. It is influenced by the molecular weight, and the relation between the chain length and the melting. As shown in Figure 9 (Billmeyer, 1957), high molecular weight polymers have both high melting and glassy transition temperatures.

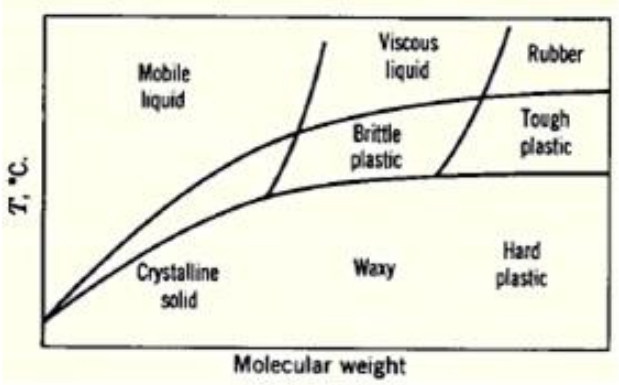

Figure 9: Molecular weight versus the melting and glassy transition temperatures adopted from Billmeyer (1957)

The melting temperature is expressed by equation 2.2 below:

$$1/T_m = a + b/n \tag{2.2}$$

where T_m is the melting point, n is the chain length, and a and b are constants (Stille, 1962). Experimental data show that PTFE has a melting point of 327 °C under atmospheric pressure. This temperature becomes higher if PTFE is subjected to higher pressure. One experimental study found that PTFE melting point increases by 0.154 °C per atm (Sperati and Starkweather, 1961).

2.4.2.2 Glassy Transition Temperature

Mark (1970) defines the glassy transition temperature as "the temperature at which the forces holding the distinct components of an amorphous solid together are overcome by thermally induced motions within the time scale of the experiment, so that these components are able to undergo large-scale molecular motions on this time scale, limited mainly by the inherent resistance of each component to such flow". The chain backbone degree of rotation plays a vital

role in deciding the glassy transition temperature where the macromolecule backbone movements are governed by the molecular weight and the non-bonded interaction forces. To this end, as the molecular weight and the intermolecular forces increase, the degree of molecular movements becomes more limited which results in higher glassy transition temperature.

The occurrence of the glassy transition temperature causes many changes in polymers properties such as their stiffness, thermal conductivity, and specific volume. Research evidence indicates that the behavior of thermoplastics above the glassy transition temperature is elastic. This is due to the intermolecular forces being overcome by the thermally induced molecular motions for polymer segments. More specifically, as temperature increases, thermoplastics gradually soften and lose their rigidity (i.e. hardness) until they eventually melt.

Several experimental studies have computed the glassy transition temperature (Lau et al., 1984, Durrell et al., 1965). Listed below are examples of such studies

- Sauer and Kline (1955) found PTFE glassy transition temperature to be around 200K.
- Nicholson (2011) found PTFE glassy transition temperature to be around 388K.
- Sperati and Starkweather (1961) found tetrafluoroethylene glassy transition temperature to be around 160K.
- Rae and Dattelbaum (2004) found PTFE glassy transition temperature to be around 173K.

Interestingly, while increasing PTFE molecular weight was found to yield higher glassy transition temperature values relative to other polymers, experimental research found that in fluorine polymer composites, the value of the glassy transition temperature is inversely related to

the percentage of fluorine in these composites. As Figure 10 (Hougham, 1999), shows, glassy transition T_g decreases with increasing the fluorine amount.

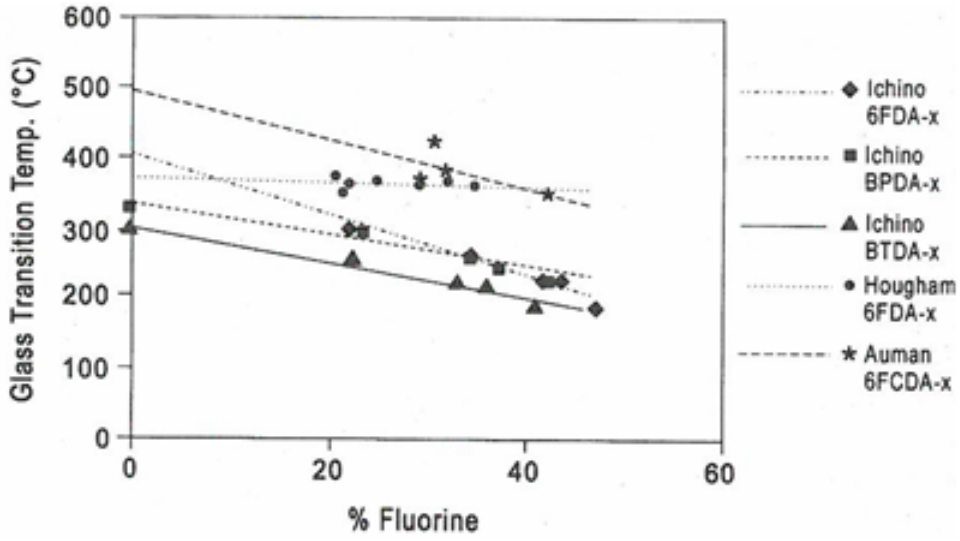

Figure 10: Glass transition temperature versus % fluorine where 6FDA-x refer to 2,2'-bis(3,4 dicarboxyphenyl)hexafluoropropane-dianhydride, BPDA-x to 3,3′,4,4′-biphenylene-tetracarboxylic-dianhydride, BTDA-x to Benzophenone tetracarboxylic-dianhydride, and 6FCDA-x refer to hexafluoroisopropylidene diaryl-dianhydride adopted from Hougham (1999)

3 Approach

3.1 Definition

Molecular Dynamics Simulations (MD) is a tool used for modeling and analyzing bio-molecular and polymeric systems through computational methods to solve Newton's second law of motion in order to predict equilibrium and dynamic properties. The computational methods translate and align information from several fields (multidisciplinary) such as biology, chemistry, physics, mathematics, computer science and engineering. Further, the computational method adopts an algorithm based on the molecular, classical and statistical mechanics to create the atomic positions and trajectories of a system of particles under specific conditions.

3.2 Why Molecular Dynamics?

There are many goals underlying the molecular dynamics simulations approach. Computer simulations act as a bridge between the microscopic details, via computational simulations, and macroscopic scale, via lab experiments. This connection allows predicting the molecular system behavior at the atomic level accurately when there is a lack of measurements in the experimental data or when these measurements are hidden. On other hand, molecular modeling enhances proofing tests for the experimental data and vice versa. This comparison between measurements of both theoretical and experimental approaches is hoped to promote scientific research.

3.3 History

Molecular dynamics simulations approach has its roots in the history of molecular modeling that dates back to 1800 when John Dalton introduced the atomic theory, which posited that atoms vary in shape (Dalton, 1805). In 1811, Avogadro distinguished between atoms and molecules,

which helped him to determine the atomic weight and introduce Avogadro's law (Mauskopf, 1969). Later in 1860, a clear chemical definition for the chemical structural formula has been made. In 1864, Wichelhaus-Foster developed the valency concept (Acharya, 2010). In 1865, the most important idea of the crystallographic structure representation in 2D was proposed by Loschmidt, the founder of the nano-world and Loschmidt number (Bader and Parker, 2001). Then, the 3D crystal structure of tetrahedral carbon was introduced by Jacobus Hoff in 1874 to describe the molecular models (Walker, 1913). The discovery and development of x-ray diffraction gave a hand to Linus Pauling in modeling the L- and D-isomers of Alanine in 1950 and helped in promoting understanding of the crystallographic structure. In 1953, the principle of conformational analysis was introduced by Barton (Barton and Cookson, 1956).

The modern molecular dynamic simulation era started in 1957 when Alder and Wainwright (1957a) studied the phase transition of hard spheres, particularly the molecular dynamic motion of hard spheres using the classical equation of motion and calculating some equilibrium properties using periodic boundary conditions (Alder and Wainwright, 1957b). In 1959, the myoglobin protein 3D structure was determined for the first time by Perutz & Kendrew (Etten, 2004). This was followed in 1964 by A. Rahman who simulated, using a computer, a system of particles applying the classical equations of motion (Rahman, 1964), then he ran a water simulation in 1974 using the molecular dynamics (Stillinger and Rahman, 1974). The availability of powerful computers in addition to the internet over the past few decades has increased the rapid prosperity of the MD simulations field. Therefore, many computer programs have been created for this purpose (i.e., MD) such as AMBER (Cardelli, 1986), CHARMM (Brooks et al., 1983), GROningen MOlecular Simulation (GROMOS) (Scott et al., 1999) and NAMD (Nelson et al., 1996).

3.4 Molecular Dynamics Basics

The MD approach is based on four important fields: molecular mechanics, classical mechanics, statistical mechanics, and design optimization.

3.4.1 **Molecular Mechanics**

Molecular mechanics is also known as the force field which describes all types of atom interactions empirically at the microscopic state in a specific and implicit expression using the potential energy function. The potential function evaluates the bonded (intramolecular) and non-bonded interactions between atoms in energy terms as shown in Figure 11

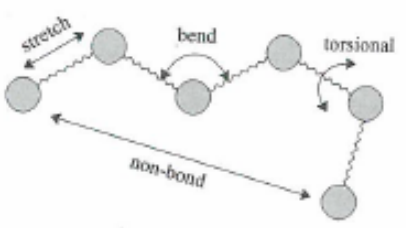

Figure 11: Force fields energy terms adopted from Jensen (2007)

$$E_{Total} = E_{bonded} + E_{nonbonded} \quad (3.1)$$

The bonded interactions represent the interaction between two connected atoms (represented by a bond). The bond energy results from the compression or expansion deformation modes; it is expressed using Hooke's Law by considering the atoms as sphere particles connected via a spring. In addition, there are three connected atoms (represented by an angle), the energy from the bending in angles, and four connected atoms (represented by dihedrals or improper); the torsional energy.

$$E_{bonded} = E_{bonds} + E_{angles} + E_{torsional\ angles} \quad (3.2)$$

The bond potential term states the equilibrium position b_o as a reference, the deviation distance $(b - b_o)$ from the reference and k_b the bond force constant.

$$E_{bonds} = \sum_{bonds} k_b (b - b_o)^2 \quad (3.3)$$

The angle potential term states the equilibrium angle reference θ_o, the deviation from the reference angle $(\theta - \theta_o)$ and k_θ the angle force constant.

$$E_{angles} = \sum_{angles} k_\theta (\theta - \theta_o)^2 \quad (3.4)$$

The torsional potential term includes the dihedral and the improper angles. The dihedral potential term states n as the multiciplity of the function, ϕ the dihedral angle, δ the phase shift and k_ϕ the dihedral force constant. The improper potential term clarify the out-plane reference angle ω_o, the out-plane deviation angle $(\omega - \omega_o)$ and k_ω the force constant.

$$E_{torsional\ angles} = E_{dihedrals} + E_{impropers} \quad (3.5)$$

$$E_{dihedrals} = \sum_{dihedrals} k_\phi [1 + cos(n\phi - \delta)] \quad (3.6)$$

$$E_{impropers} = \sum_{impropers} k_\omega (\omega - \omega_o)^2 \quad (3.7)$$

The non-bonded interactions represent the Lennard-Jones potential, also known as Van der Waals (VDW) and the electrostatic energy.

$$E_{nonbonded} = E_{vdw} + E_{elect} \quad (3.8)$$

The L-J potential explains the attraction and repulsion between the atom pair where Ɛ is the potential well depth, R_{min} is the distance where L-J potential is zero or the minimum, r_{ij} is the distance between i and j atoms. The electrostatic (Coulomb) potential explains the repulsive or attractive forces between the atomic electrical charges pair $q_i q_j$, where r_{ij} is the distance between the pair and ε is the dielectric constant.

$$E_{vdw} = \sum_{vdw} \varepsilon \left[\left(\frac{Rmin_{ij}}{r_{ij}} \right)^{12} - \left(\frac{Rmin_{ij}}{r_{ij}} \right)^{6} \right] \quad (3.9)$$

$$E_{elect} = \sum_{electrostatic} \frac{q_i q_j}{\varepsilon r_{ij}} \quad (3.10)$$

The last term is called Urey – Bradley which expresses the angle bending using 1,3 non bonded atoms, cross interaction atoms or H-bonding atoms, where u_o is the reference distance between the 1,3 atoms, deviation distance $(u - u_o)$ and k_u is the force constant.

$$E_{Urey-Bradley} = \sum_{Urey-Bradley} k_u (u - u_o)^2 \quad (3.11)$$

The force field full term is (Amaro et al., 2007)

$$E_{total} = \sum_{bonds} kb(b\text{-}b_o)^2 + \sum_{angles} k_\theta (\theta\text{-}\theta_o)^2 + \sum_{dihedrals} k\phi[1 + \cos(n\phi\text{-}\delta)] + \sum_{impropers} k\omega(\omega\text{-}\omega_o)^2 + \sum_{Urey\text{-}Bradley} k_u(u\text{-}u_o)^2 + \sum_{vdw} \varepsilon \left[\left(\frac{Rmin_{ij}}{r_{ij}}\right)^{12} - \left(\frac{Rmin_{ij}}{r_{ij}}\right)^{6}\right] + \sum_{electostatic} \frac{q_i q_j}{\varepsilon r_{ij}} \quad (3.12)$$

The force field is an important model in calculating and predicting many properties based on the force field parameterization which contains a large number of parameters (Leach and Kier, 1997). OPLS, CHARMM, AMBER and GROMOS are example of the force fields molecular mechanics models.

3.4.2 **Classical Mechanics**

Classical mechanics describes the motion of a system of particles at the microscopic state under certain forces based on Newton's second law of motion, where $\vec{F}$ is the exerted force on the particle, m is the particle mass and $\vec{a}$ is the acceleration.

$$\vec{F} = m\vec{a} \quad (3.13)$$

The above equation could be written by replacing two terms by other equivalent expressions: the acceleration by the second derivative of the position vector and the force by the gradient of the potential energy function.

$$\vec{F} = -\nabla E = m\,\frac{d^2\vec{x}}{dt^2} \tag{3.14}$$

For MD simulations algorithms, the needed elements for calculating the trajectories are the mass, initial position and the initial velocity. The atomic mass is available information for all the atoms. The initial positions (i.e. initial conditions) is predicted experimentally from the NMR spectroscopy analysis or the x-ray diffraction technique, the initial position characterizes the topology and the 3D structure and stores information in files such as the PDB's (protein data bank). The initial velocity is calculated using a mathematical distribution such as Maxwell-Boltzmann. Classical mechanics specifies Newton's second law for the body motion using other expressions in order to link the microscopic details to the macroscopic scale such as the phase space, the Lagrangian and the Hamiltonian.

3.4.2.1 Phase Space

The phase space for a particle can be defined as the group of conditions for a particle in the 3-dimensions that is determined by the particle position and velocity or what is known by the momenta, each particle is verified by 6 points; three for the position in the 3D space $\vec{r}(\vec{r}_i, \vec{r}_j, \vec{r}_k)$ and three for the velocity $\vec{v}(\vec{v}_i, \vec{v}_j, \vec{v}_k)$. The momenta equation is as follows:

$$\vec{p} = m\,\vec{v} = m\,\dot{\vec{r}} \tag{3.15}$$

where $\vec{p}$ is the momenta, m is the mass, $\vec{v}$ or $\dot{\vec{r}}$ is the velocity.

Newton's second law could be rewritten using the momenta expression

$$\vec{F} = m\vec{a} = m\frac{d\vec{v}}{dt} = m\frac{d\vec{r}}{dt} = \frac{d\vec{p}}{dt} \tag{3.16}$$

3.4.2.2 Lagrangian Expression

Newton's second law of body motion is reconsidered using the Euler- Lagrange equation in order to find an expression that elucidates the conservative forces or, in other words, the conservative momenta and energies in terms of position and velocity. Therefore, the Lagrangian is defined as " the difference between the kinetic and potential energies as a function of positions and velocities" (Tuckerman, 2009)

The Lagrangian is expressed for a particle in the following equation

$$L(\vec{r}, \dot{\vec{r}}) = K\left(\dot{\vec{r}}\right) - E(\vec{r}) \tag{3.17}$$

where L is the Lagrangian, K is the kinetic energy and E is the potential energy.

The Euler- Lagrange equation for the same system is stated as

$$\frac{d}{dt}\left(\frac{\partial L}{\partial \dot{\vec{r}}}\right) - \frac{\partial L}{\partial \vec{r}} = 0 \tag{3.18}$$

3.4.2.3 Hamiltonian Expression

The Hamiltonian is another operator that clarifies the conservative system. In this formula, the total energy (i.e. the kinetic and the potential) is observed in terms of position and momenta. The Hamiltonian for a particle is:

$$H(\vec{r}, \vec{p}) = \frac{\vec{p}^2}{2m} + E(\vec{r}) \tag{3.19}$$

3.4.3 **Statistical Mechanics**

Statistical mechanics is the branch of mechanics that basically deals with the macroscopic and thermodynamic conditions of actual system. Statistical mechanics translates the data from the microscopic category of each particle in a system in order to predict the macroscopic state and properties using the mathematical analysis from classical mechanics, molecular theory from molecular mechanics and thermodynamics concepts.

3.4.3.1 Statistical mechanics principles

The statistical principles rely on the thermodynamic three laws and the ensemble idea. The three laws of thermodynamics are correlated to the macroscopic scale where the macroscopic state could be determined by thermodynamic variables such as the entropy S, pressure P, energy E, number of particles N, total mass M, total volume V, temperature T, etc.

The ensemble is related to the microscopic scale; it is generally defined as a group of components that shared in a specific outcome. In statistical mechanics, the set of points in a system contribute to macroscopic state .The macroscopic state is determined by calculating the average of the microscopic states. For example, calculating the phase space for all the ensemble atoms at the microscopic scale for a specific property will predict the system average property at the macroscopic state.

3.4.3.2 Ensemble types

There are different types of ensembles in the molecular dynamics simulations based on the thermodynamic variables that lead the ensemble and determine its state properties; these variables are constant and conserved in the ensemble. The most popular ensembles are: the

micro-canonical (NVE), the grand-canonical (μVT), the canonical (NVT) and the isothermal-isobaric (NPT). However, in the modern molecular dynamics simulations the most used ensembles are (NPT) and (NVT). In the micro-canonical ensemble (NVE), the number of particles, the volume and the energies are constant where the system is isolated from its surrounding and the subsystems have the same energies. The grand-canonical (μVT), the chemical potential, the volume and the temperature are constant. The canonical ensemble (NVT), the number of particles, the volume and the temperature are constant. The isothermal-isobaric (NPT), the number of particles, the pressure and the temperature are constant.

3.4.4 **Design Optimization**

Optimization in molecular simulations is defined as the process of seeking the lowest energy level of the force field mathematical model using the gradient energy expression that was explained in (3.12) and (3.14).

3.4.4.1 Optimization Process Requirement

There is a set of preparations that need to be taken into consideration to define the design optimization problem. According to (Arora, 2004), the optimization process requirements are:

- Define the problem (finding the minimum energy level of a system of atoms)
- Collect the needed input data (PDB the atoms initial coordinates and initial velocities)
- Define the design variables and parameters (the deviated distance from equilibrium bond, angle, distance between atomic charges etc.)
- Decide the optimization criteria (minimization)
- Define the problem constraints

Having the above ingredients, the mathematical model in (3.12) would be ready for the optimization process. There are two criteria for the optimization process: minimization or maximization. The optimization criterion in the molecular dynamic simulation is the minimization one. This is due to searching for the local minima for the atoms force fields energy levels. In the end, the constraint is added to the mathematical model in the following equation

$$m\ddot{\vec{r}} = \vec{F}(\vec{r}) + \lambda \nabla\sigma \tag{3.20}$$

where $\nabla\sigma . \dot{\vec{r}} = 0$

where m is the mass, $\ddot{\vec{r}}$ is the position second derivative (acceleration), $\vec{F}$ is the net forces in the systems (i.e. perpendicular and parallel forces), λ is the Lagrange multiplier and $\nabla\sigma$ expresses the constraints. The constraints represent the rigid bonds for example for a molecule of two atoms a_1 at position $\overrightarrow{r_1}$ and a_2 at position $\overrightarrow{r_2}$ with a fixed bond length d, the constraint is

$$\sigma(\overrightarrow{r_1}, \overrightarrow{r_2}) = (\overrightarrow{r_1} - \overrightarrow{r_2})^2 - d^2 = 0 \tag{3.21}$$

where $\nabla\sigma = 2(\overrightarrow{r_1} - \overrightarrow{r_2})$ for each pair of atoms

3.4.4.2 Optimization Approaches

There are two approaches in energy minimization according to (Leach and Kier, 1997): the non-derivative and the derivative. The non-derivative approach has two methods: the simplex method and the sequential univariate method (Schlegel, 1987). The derivative approach includes the first order derivative and the second order derivative. The first order derivative methods are: steepest descents method (Averill and Painter, 1992), the conjugate gradient method (Štich et al., 1989), line search in one dimension and arbitrary step approach (Leach and Kier, 1997). The second order derivative method is the Newton-Raphson method (Boyd et al., 1973). In the

molecular dynamic simulation, the most popular methods are the steepest descents and conjugate gradient.

3.5 General Algorithms

The molecular dynamics simulation algorithms are based on solving Newton's equation of motion by calculating the forces using the potential energy function gradient for the simulation cell system as described in equation (3.14). These calculations are made at every timestep where the real time duration of the simulations is determined according to the computational language capability and the size of the simulation cell. The simulation cell is determined by dimensions in x, y and z. The initial conditions of the simulation cell are divided into two groups: the initial coordinates and the initial velocities. The periodic boundary conditions (PBC's) are applied to the simulation cell. The PBC's mean that when an atom passes into the simulation cell boundary another atom goes out from the other boundary at the same time. The algorithms take into consideration the importance of reducing the cost in terms of time and computers resources especially for large systems. Therefore, the spherical cutoff technique is used for the non-bonded computations. The cutoff technique limits the local interaction distance to both VDW and the electrostatic calculations. Moreover, the Particle Mesh Ewald (PME) method is used for the electrostatic potential computations. PME is the most known method to simulate systems in periodic boundary conditions (Petersen, 1995), it calculates the electrostatic energies for short and long range interactions. The PME in the simulation algorithms is defined by the PME grid cell. The dimensions of this cell are equal to or greater than the dimensions of the simulated cell boundary conditions.

4 Methodology

The purpose of this chapter is to present the methodology that I used in the following major tasks: (1) generating PTFE force-fields parameters, (2) building NAMD input files, (3) building the polymer configuration, (4) testing PTFE new residue, (5) obtaining the amorphous structure for PTFE polymer, and (6) performing MD simulations to calculate PTFE glassy transition temperature. The parameterization task involved using the OPLS-AA potential energy model to obtain the PTFE intermolecular and intramolecular force-field parameters. The MD simulations task involved: (a) using PTFE OPLS-AA force field parameters which will be used in the simulation work, (b) performing MD simulations to measure the glassy transition temperature and comparing it with experimental values, (c) measuring different properties that are affected by the glassy transition temperature and comparing them with experimental values, and (d) determining the glassy transition temperature governing forces at the molecular level. These tasks will be delineated in the subsequent sections

4.1 Force-Field Parameterization

Molecular mechanics models (i.e., force fields) are important ways to investigate the structure, vibration frequencies, and the conformational energy via bonding and non-bonding interactions. A good force field model should handle the electrostatic and torsional parameters which affect the accuracy of describing the inter-molecular energy and the molecular geometry, respectively. Furthermore, a robust force field model should have a detailed functional form which includes a description of such terms as the anharmonic stretching and bending vibrations terms.

OPLS-AA force field model is one of the most accurate and complicated energy potential functions and which encompasses all the terms that are needed to obtain a complete and comprehensive MD process. In addition, it offers transferability from smaller oligomer to the bigger ones (Borodin et al., 2002). Having reasonable parameters will predict a logical geometry and therefore allow for predicting different sensible properties and functions. Jorgensen and Tirado-Rives (1988) developed one of the most popular OPLS models which is widely-used in molecular dynamics simulations. In a subsequent study, Jorgensen et al. (1996) developed and tested a data bank for OPLS force fields for the united and all atoms models. The functional form of their OPLS model is presented in equation 4.1:

$$\mathrm{E_{total}} = \sum_{\mathrm{bonds}} k_r\left(r - r_{eq}\right)^2 + \sum_{\mathrm{angles}} \mathrm{k}_\theta\left(\theta - \theta_{eq}\right)^2 + \sum_{\mathrm{dihedrals}} V_1/2\ \left[1 + \cos\left(\phi_i + f_i 1\right)\right] + V_2/2\ \left[1 + \cos\left(2\phi_i + f_i 2\right)\right] + V_3/2\ \left[1 + \cos\left(3\phi_i + f_i 3\right)\right] + f_{ij}\ \left(\sum_{\mathrm{vdw}} 4\varepsilon_{ij}\left[\left(\frac{\sigma_{ij}}{\mathrm{rij}}\right)^{12} - \left(\frac{\sigma_{ij}}{\mathrm{rij}}\right)^{6}\right] + \sum_{\mathrm{electostatic}} \frac{\mathrm{q_i q_j}}{4\pi\varepsilon_\circ \mathrm{r_{ij}}}\right) \quad (4.1)$$

where k_r, refers to the bond constant, k_θ refers to the angle constant, r_{eq} refers to the equilibrium bond value, θ_{eq} refers to the equilibrium angle value, ϕ_i refers to the dihedral angle, V_1, V_2, and V_3 refer to the dihedral coefficients, $f_1, f_2,$ and f_3 refer to the phase angles, f_{ij} refers to the fudge factor with a default value of 1.0, $\mathrm{q_i}$ and $\mathrm{q_j}$ refer to the electrostatic charges for pair of atoms, $\varepsilon_\circ$ refers to the dielectric constant of vacuum, $\varepsilon_{ij} = \sqrt{\varepsilon_{ii}\varepsilon_{jj}}$ and refers to the potential well depth, $\sigma_{ij} = \sqrt{\sigma_{ii}\sigma_{jj}}$ and refers to the distance where L-J potential is zero or the minimum, and $\mathrm{r_{ij}}$ refers to the distance between the pair of atoms.

The OPLS-AA model is more usable and applicable than the united atom model. Unfortunately, the bank of parameters which was developed by Jorgensen et al. (1996) did not consider

perfluoroalkanes oligomers. A few subsequent studies developed PTFE OPLS-AA force field parameters (Watkins and Jorgensen, 2001, Paulechka et al., 2012). Parameters from these studies provide more accurate description of different perfluoroalkanes properties such as the thermodynamic and the structural properties. In this work, we present a new set of force-field parameters for PTFE using OPLS-AA model. To the best of our knowledge, this study is the first to consider PTFE all-atom model at DFT and MP2 levels which should allow for obtaining a higher level of force-fields accuracy and using new method (i.e., AFMM) instead of the old and tedious parameterization methods. This, in turn, should allow for more reliable and accurate simulations. The parameterization strategy for this research is presented in Figure 12

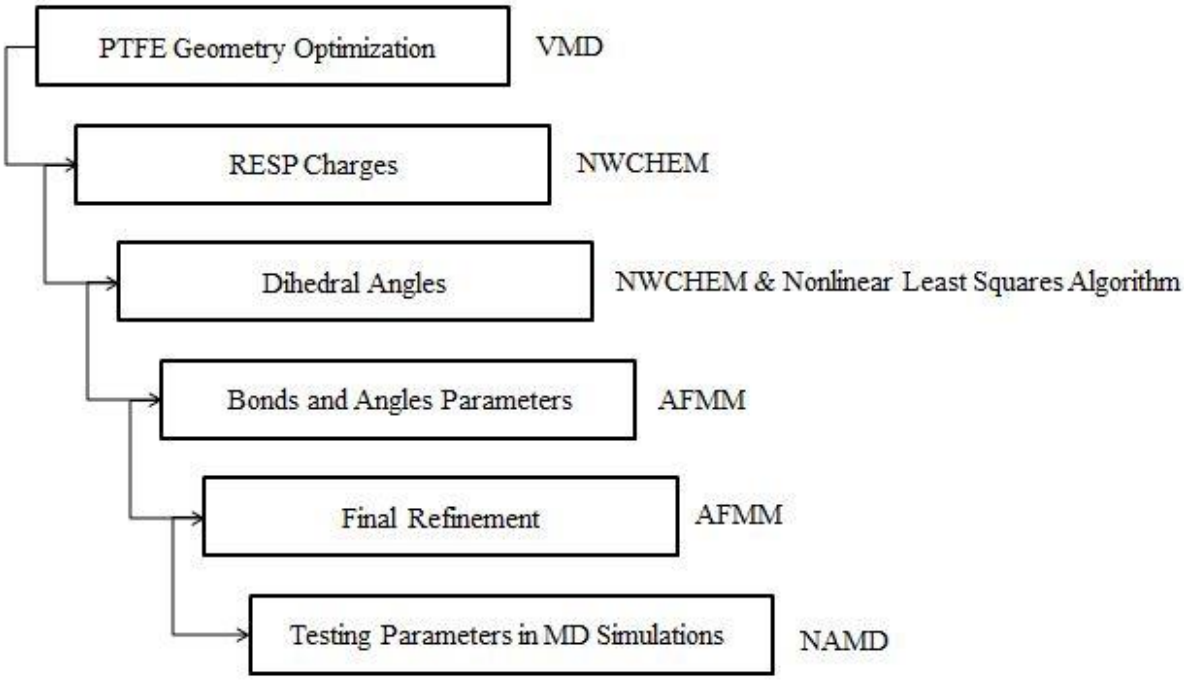

Figure 12: PTFE force fields parameterization scheme

4.1.1 **Intermolecular Interactions**

Intermolecular refers to the non-bonding interactions of the VDW and the electrostatic potentials. VDW parameters were copied from the initial parameter set (Watkins and Jorgensen, 2001) without modification due to their stability in response to molecular changes (Vaiana et al., 2005). The atomic charges could be calculated using many software packages such as ORCA (Neese, 2009) and NWCHEM (Kendall et al., 2000). These computational modeling tools provide unique detailed level of any model electronic structure. In this work, electrostatic potentials were derived based on ab initio calculations for perfluorobutane using North West Computational Chemistry (NWCHEM) package (Bylaska et al., 2007) at two levels of theory: DFT at (B3LYP/6-31G*) and (MP2/6-31G*). Then, the electrostatic charges were fitted to the restrained electrostatic potential (RESP) model (Bayly et al., 1993).

All quantum mechanics calculations were performed using NWCHEM. It is freely accessed computational chemistry software with high potential for different molecular simulations, geometry optimization, force fields and energy calculations. NWCHEM adopts different ab initio quantum chemistry models such as Hartree-Fock (also known as self-consistent method) and Density Functional Method (DFT) (Bylaska et al., 2007) for molecular structure modeling and gradient approximations (Kendall et al., 2000, Valiev et al., 2010).

As for PTFE model, NWCHEM needs to define the model explicitly by defining its geometry (i.e. Cartesian coordinates), these coordinates are the starting point to run NWCHEM input file. Usually the input files describe the system, the basis set and the level of theory.

The PTFE geometry models were built from scratch using VMD Visual Molecular Dynamics (Humphrey et al., 1996) starting from one carbon atom , then ending with 11 carbon atoms.

NWCHEM performs geometry optimization by calculating the first derivative of the energy with respect to the nuclear coordinates to determine if the system is at a local minimum at (MP2/6-13G*) level, also generates restrained electrostatic potential fitting (RESP) for PTFE charges after computing the electrostatic charges. The above optimization is applied first on small PTFE model made of one carbon and four fluorine atoms, after that it was repeated 10 times, each time by increasing one carbon atom to have bigger model with more constant charges for the internal segments (i.e. CF2 segments), the final chain consists of 11 carbon atoms and 24 fluorine atoms.

4.1.2 **Intramolecular Interactions**

Intramolecular refers to the interactions of dihedrals, bonds, and angles potentials. In the current work, the rotational energy barrier for dihedral is calculated using NWCHEM at DFT (B3LYP/6-13G*) level of theory to denote the reference quantum mechanics data. These calculations were performed through fixing the dihedral angle of interest and scanning the potential energy surface along a full profile (i.e., from 0° to 360°) with increments of 5°. After that, the OPLS-AA molecular mechanics dihedral energy term was fitted to the reference data using nonlinear least squares fitting criteria (Marquardt, 1963).

4.1.2.1 Nonlinear Least Square Fitting

Nonlinear least square fitting is a method of modeling that is designed to fit data to a linear or nonlinear mathematical function. However, most of the real problems are fitted to nonlinear functions. Such regression could be performed using software as MATLAB. In this research I used the nonlinear least square fitting to fit the quantum mechanics data for the dihedral angles to the molecular mechanic dihedral function in order to compute the torsional parameters.

4.1.2.2 AFMM

The equilibrium values in the molecular mechanics model can be obtained in two ways: X-ray diffraction experiments and ab initio calculations. The spring constant values could be determined using (a) Infrared absorption spectroscopy (Nakanishi, 1962), (b) Raman spectroscopy (Long and Long, 1977), and (c) ab initio calculations. AFMM generates the bonded force fields parameters based on the quantum calculations of normal modes (i.e., frequencies). The reference quantum mechanical normal modes should be calculated at specific level of theory such as DFT or HF. The vibrational frequencies and infrared intensities are computed to get the numerical hessian and the projected Hessian by analytical method (i.e., DFT). Figure 13 (Vaiana et al., 2005) represents the parameters optimization process that is used in AFMM algorithm. The algorithm shows the matches between the normal modes analysis from molecular mechanics and the reference frequencies from quantum mechanics.

In this work, I utilized AFMM (Automated Frequency Matching Method); an efficient package for parameterization (Vaiana et al., 2005) that is based on fitting the molecular mechanics potential energy function on normal modes, which in turn, are obtained from quantum mechanics tools such as NWCHEM and GAUSSIAN (Frisch et al., 1995). The molecular mechanics normal modes and the corresponding eigenvectors are calculated using a molecular mechanics tool such as CHARMM (Brooks et al., 1983). AFMM program includes Monte-Carlo algorithm that generates the missing molecular mechanics parameters by periodically changing them until find the best force-field set.

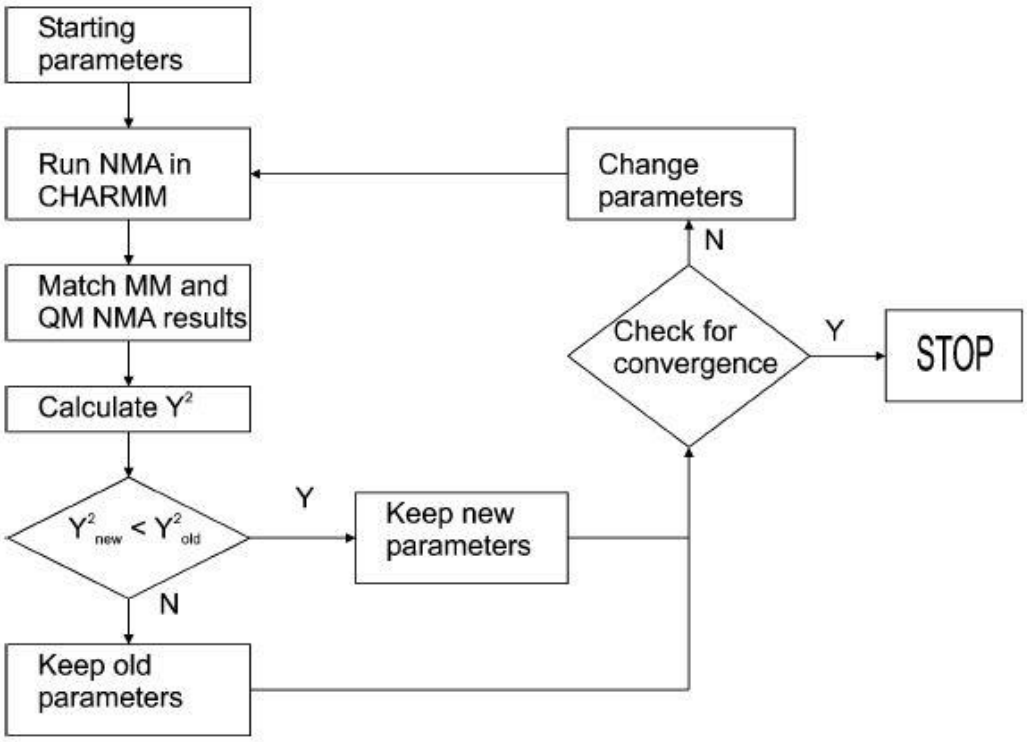

Figure 13: Parameters optimization process in AFMM adopted from (Vaiana et al., 2005)

However, and as a prerequisite to using AFMM, the following input files had to be built first: geometry, topology, structure, parameter and AFMM configuration files. I built the geometry PTFE chain using VMD, these data were utilized as geometry input file which were optimized using NWCHEM, then the optimized geometry was implemented CHARMM for further optimization, after that the optimized geometry again will be implemented in NWCHEM for further optimization and vibrational frequency calculations. Finally, the NWCHEM output geometry was used as an input for the AFMM normal modes fitting. It should be noted that atoms order in CHARMM optimization should be the same as in NWCHEM.

The topology file has force fields information which includes the internal coordinates, the mass, the atomic charges and the covalent bonds. I built this file by defining the PTFE residue RESP

charges information, the mass and the intramolecular covalent bonds. After that, I generated the structure file using the topology file in CHARMM.

AFMM configuration file contains of two parts: the parameters and the general commands. The parameters part includes defining the missing molecular mechanics parameter and range values. The missing parameter takes an initial value for the force constant; this value could be experimental or theoretical. The range values define the minimum and maximum values that could be taken in the optimization process. The general part includes group of commands to control the maximum number of optimization steps, the maximum number of steps if convergence occurs, CHARMM program path, CHARMM input file path, NWCHEM vibration frequencies output file, empirical scaling factor if the missing parameter initial guess was experimental value and it is equal to one if it is theoretical, the name of the matching frequencies output file, and the way of normal modes matching to be weighted (i.e., projection, frequency or nothing).

In order to evaluate AFMM parameterization, the computing of the non-weighted sigma is used (Vaiana et al., 2005)

$$\sigma = \sqrt{\frac{\sum_{3N-6}(\nu_i - \nu_j^{max})^2}{3N-6}} \tag{4.2}$$

where N is the number of atoms in a molecule and 3N-6 are the independent vibrational frequency, ν_j^{max} is the frequency that is corresponding to the highest projection, and ν_i is the corresponding frequency. The good parameterization has σ value between 0 to 100 cm^{-1}

4.2 NAMD Input Files

This task involves building NAMD input files which are needed to run the molecular simulations process. NAMD refers to “NAnoscale Molecular Dynamics program” simulation (Nelson et al., 1996). It uses CHARMM force field model to represent the potential function that illustrates the classical motion equations at the molecular level as explained in Chapter 3. Fortunately, NAMD adopts other force fields models such as AMBER, OPLS-AA, and any force field model that has a compatible potential function formula like CHARMM. As any research tool, NAMD has specific input and output files.

This part demonstrates the NAMD input files along with building PTFE single chain. Running simulation in NAMD needs four files: (a) the PDB file, (b) the PSF file, (c) the parameter file, and (d) the configuration file. Figure 14 illustrates these files (Isgro et al., 2003).

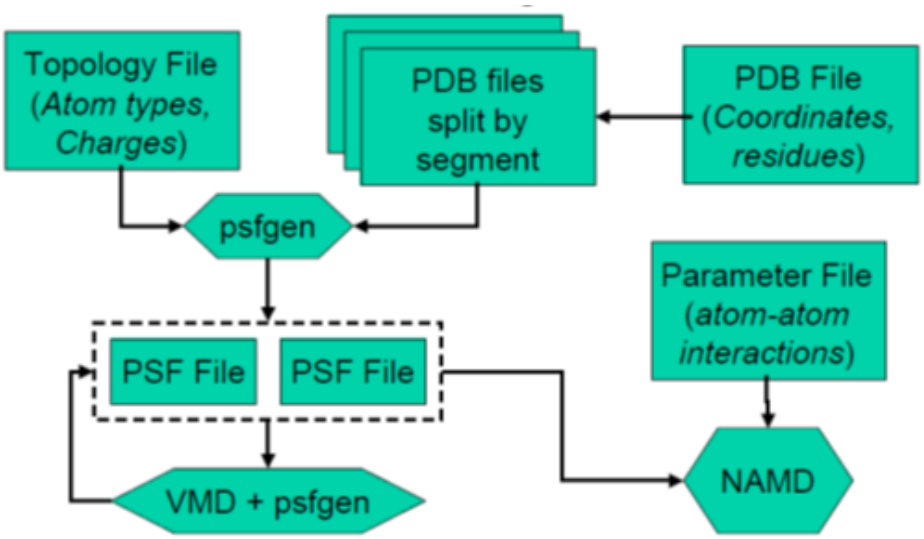

Figure 14: NAMD Input files adopted from Isgro et al. (2003)

4.2.1 **Protein Data Bank File and Single Chain File**

The PDB refers to Protein Data Bank file (Westbrook et al., 2003). The PDB demonstrates the crystal structure data at the molecular level such as the three dimensional structure for the oligomer (i.e., x, y, z coordinates), the residue (i.e., sequence) name, the residue ID, the segment ID, the occupancy and temperature factor.

The PDB information can be built by hand or extracted using different tools such as NMR spectroscopy, X-ray crystallography, and electron microscopy. In addition, the PDB file can be visualized using visual molecular tools such as the VMD. Usually, the original PDB is a mere copy which requires manual refinement (i.e., by hand) to create new atom names that do not conflict with any other atoms names in the topology or in the parameter files. Moreover, unique names should be created for the residues and segments. It should be noted that the PDB file is case sensitive to the atom and residue names. The PTFE *original* PDB that I built by hand is partially shown in Figure 15.

```
ATOM   1  C    0      39.351  -0.419  -0.000  0.00  0.00       C
ATOM   2  C    0      38.102   0.464   0.000  0.00  0.00       C
ATOM   3  C    0      36.853  -0.420  -0.000  0.00  0.00       C
ATOM   4  C    0      35.603   0.463   0.000  0.00  0.00       C
```

Figure 15: PTFE original PDB

Figure 16 below presents a portion of the PTFE *final* PDB which I built by hand using VMD for a single chain of 64 carbon atoms and 130 fluorine atoms. In this figure, the PDB shows the atom serial number, the atom name (e.g., CQ1), the residue name (i.e., YZN), the atom position in the

three coordinates, the atom occupancy and the segment name (i.e., U). The chain is shown in Figure 17.

```
ATOM 1   CQ1 YZN X    0    0.419   39.351    0.000   1.00   0.00   U    C
ATOM 2   CQV YZN X    0   -0.419  -39.351    0.000   1.00   0.00   U    C
ATOM 3   FQ1 YZN X    0   -0.211   40.241    0.000   1.00   0.00   U    F
ATOM 4   FQ2 YZN X    0    1.048   39.352    0.890   1.00   0.00   U    F
ATOM 5   FQ3 YZN X    0    1.048   39.352   -0.890   1.00   0.00   U    F
ATOM 6   FR1 YZN X    0    0.211  -40.241    0.000   1.00   0.00   U    F
```

Figure 16: PTFE final PDB

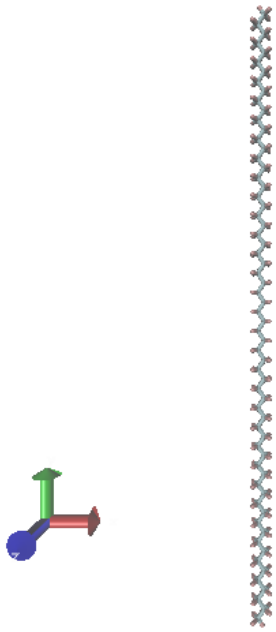

Figure 17: PTFE single chain

4.2.2 **Protein Structure File**

The PSF refers to the Protein Structure File; it includes atoms data such as atom name, type, residue name, atomic mass, and atomic partial charge. It also shows the atom connectivity to bonds, angles, dihedrals and impropers. PSF is built using the PSFGN software package 1.6 edition (Gullingsrud et al., 2006) in VMD 1.9 edition. Before a PSF can be built, another file, called the topology file, must be built. The topology file has CHARMM force fields information which includes the internal coordinates, the mass, the atomic charges and the covalent bonds. In addition, the topology file includes information for patches which are important for connecting or terminating protein segments. The PTFE chain PSF is partially shown in Figure 18 below; in this figure PSF shows the atom serial number, segment name, residue name, atom name, atom type, atomic partial charge and the atomic mass:

```
190 U    0    YZN  FN5  FPF   -0.137000      18.9980    0
191 U    0    YZN  FN6  FPF   -0.137000      18.9980    0
192 U    0    YZN  FN7  FPF   -0.137000      18.9980    0
193 U    0    YZN  FN8  FPF   -0.137000      18.9980    0
194 U    0    YZN  FN9  FPF   -0.137000      18.9980    0
193 !NBOND: bonds
1       3       1       4       1       5       1       9
2       6       2       7       2       8       2      70
9      71       9      72       9      10      10      11
```

Figure 18: PTFE PSF file

4.2.3 **Parameter File**

The parameter file has all the parameters that will be used in the simulation process. The parameters contain VDW parameters, the constant and the equilibrium values for the bonds, angles, dihedrals and impropers. In this research, the PTFE OPLS-AA force fields parameters were written in CHARMM parameter file format.

4.2.4 **Configuration File**

The configuration file encompasses all the information and commands that are needed to run the simulation process. It includes information from the PDB, PSF, and the parameter files. The conditions which should be defined in the configuration file: coordinates from the PDB file, structure from PSF file, the parameter file, the output and input name, the simulation temperature, the periodic boundary conditions by defining the cell dimensions and the center of the cell, the non-bonding interactions parameters by defining the VDW cutoff and PME parameters, the dynamics parameters by defining time step size and number of steps. There are many other conditions that can be defined based on the ensemble type (i.e., NVT or NPT) and the goal of the simulation so that the configuration file could be customized with specific commands.

4.3 Polymer Configuration

After obtaining the parameters and building the PTFE single chain, the next task is to build a polymer simulation cell of multiple chains. The idea of building a cubic PTFE simulation cell was inspired from the membrane lipid configuration tutorial (Freddolino and Shih, 2006) and the polypropylene MD simulation (Dai et al., 2011). Under this configuration, the simulation cell

took the shape of an orthogonal monolayer which was created from the parallel arrangement of a number of $C_{64}F_{130}$ single chains using VMD/TCL scripting language. Figure 19 illustrates PTFE cubic cell top view whereas Figure 20 shows the side view. By the completion of this task, the PTFE simulation cell consisted of 196 chains, the size of the periodic cell is 79*81*79 $A°^3$, and the distance between the neighboring chains is approximately 5.88 A°. This distance was calculated based on the density of PTFE (i.e., 2.2 gm/cm^3). In addition, the PSF file for the polymer configuration (196 chains membrane) was created with 196 segments. At this point, the PDB, the PSF, the parameter, and the configuration files are ready for the simulation process.

4.4 New Residue Test

In NAMD, the new residues that are built with new set of parameters should be tested before they can be used in the simulations. This test is carried out by performing water simulation for the new residues. A water box was built around one PTFE chain using the solvate plugin package in VMD (edition 1.5). The simulation cell periodic boundary conditions size is 54*131*52 A°, the NPT simulation has been performed at 298K for one nanosecond, the water simulation test succeeded and with no missing parameters. It should be noted that I did this water simulation to examine the force-field parameters and not to study PTFE properties in water, however, studying PTFE hydrophobicity needs enough simulation time to detect this important behavior. Figure 21 and Figure 22 below show PTFE water box simulation cell.

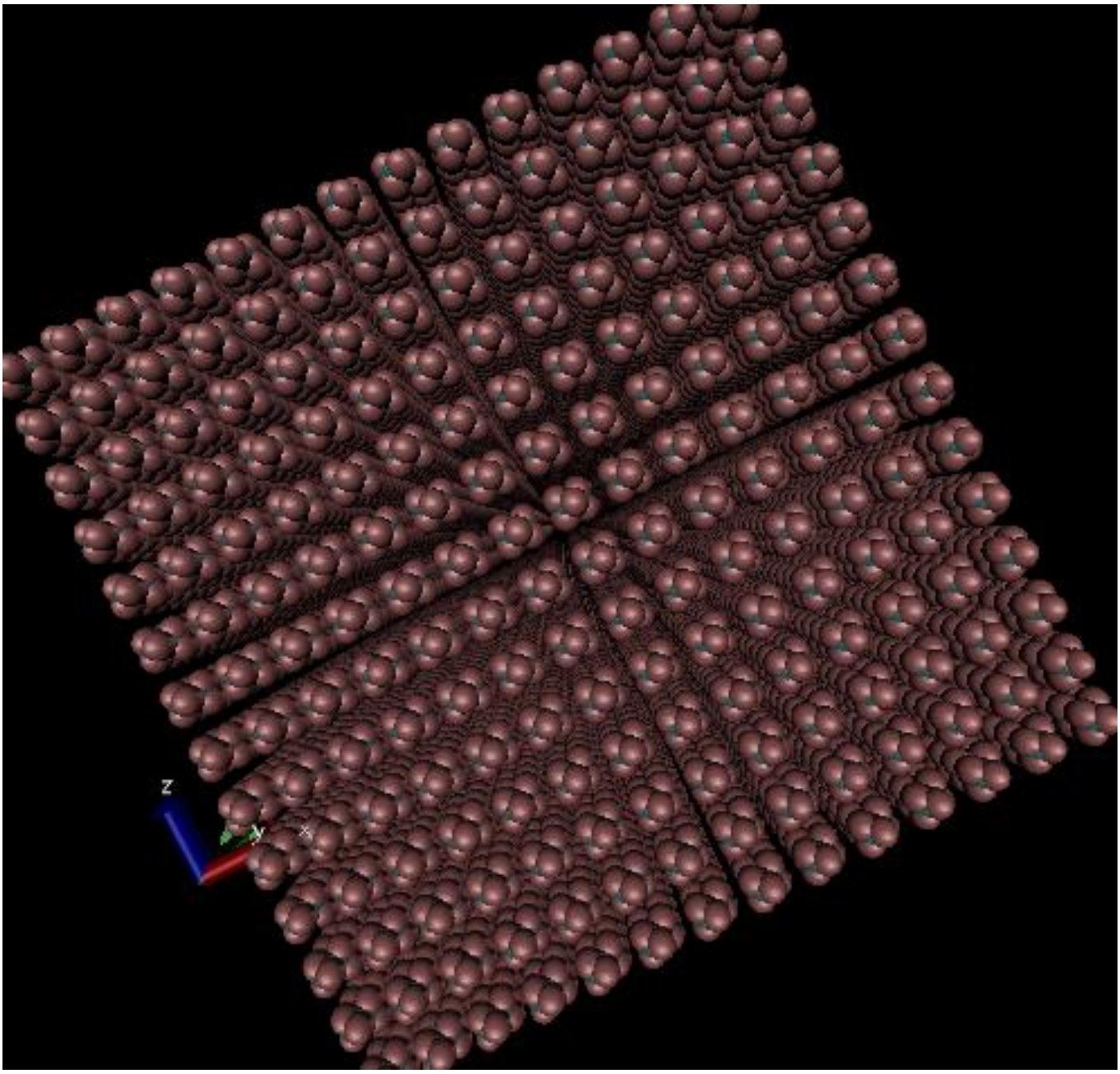

Figure 19: PTFE model top view

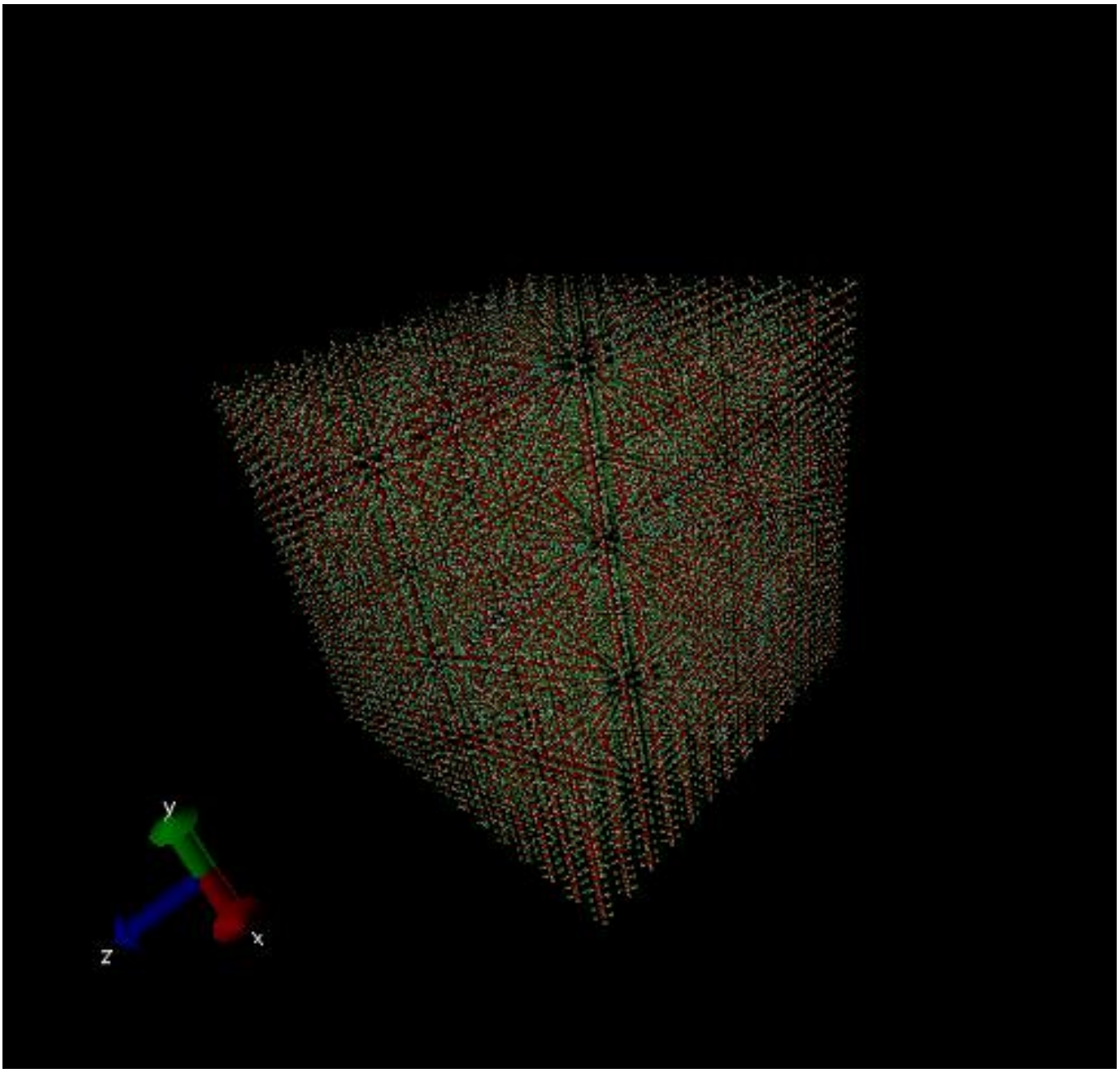

Figure 20: PTFE model side view

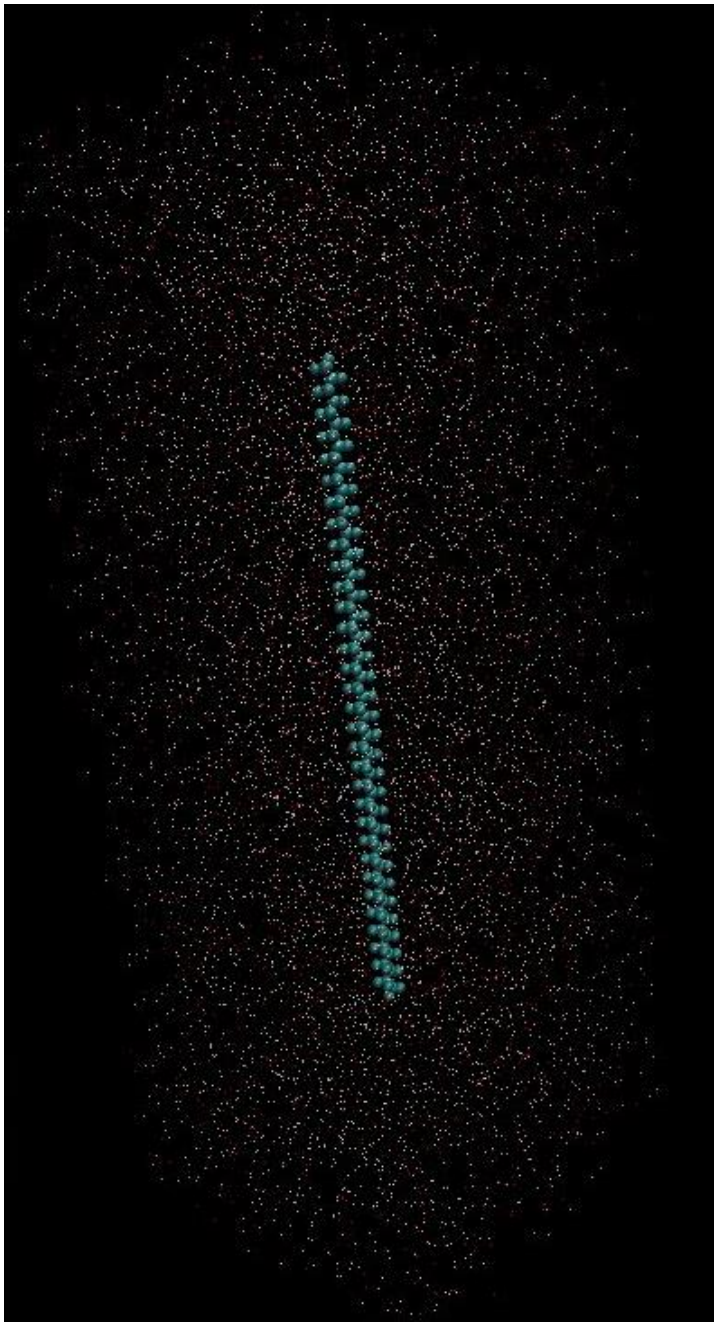

Figure 21: PTFE water box simulation cell

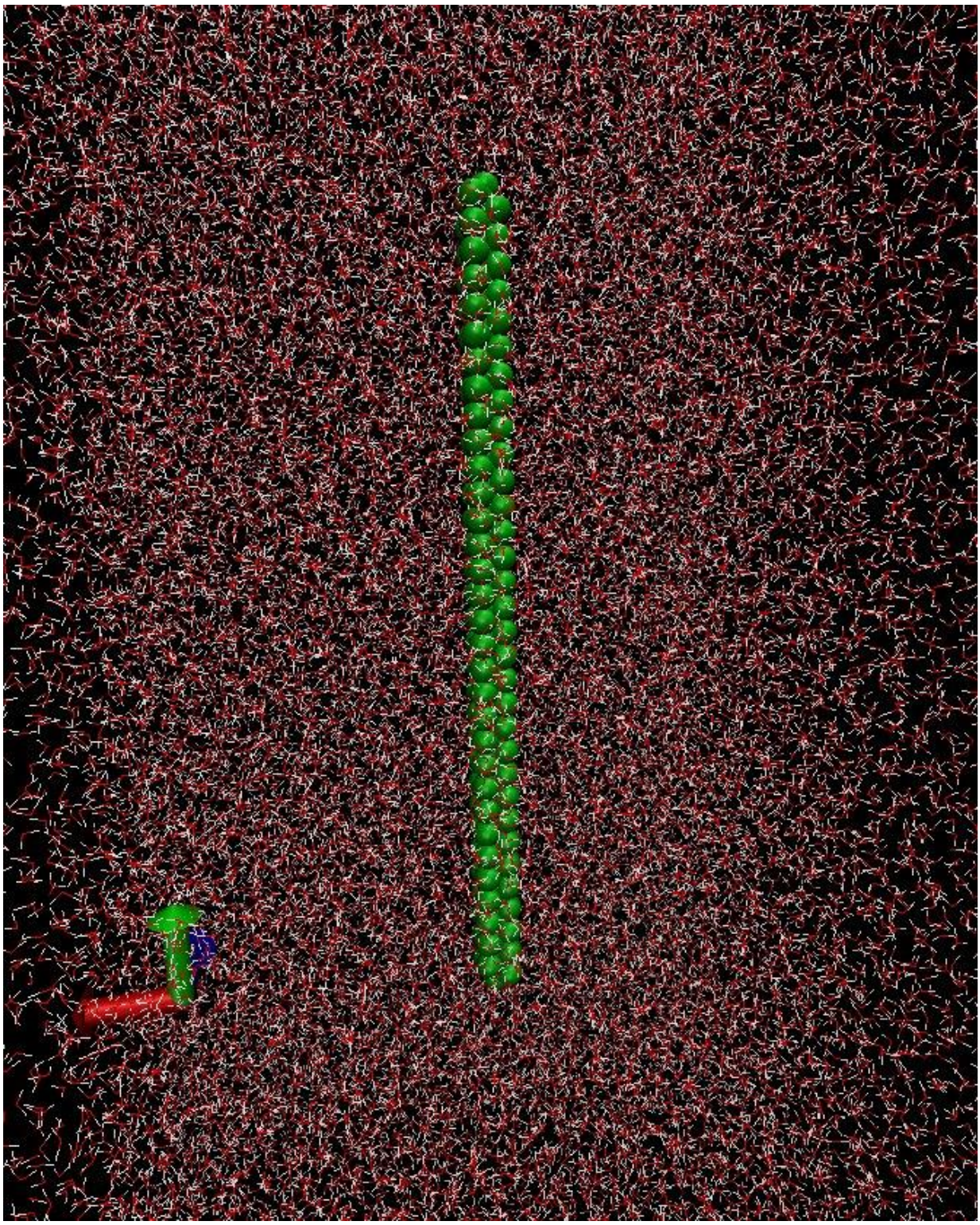

Figure 22: PTFE water box simulation cell

4.5 Amorphous Structure

The amorphous structure refers to the disarrangements of the molecules where the carbon chains are disordered due to the absence of crystallinity. In MD simulations studies, studying the glassy transition temperature is contingent on obtaining the amorphous configuration. Research evidence reveals that polymer properties such as the specific volume will differ as the polymer passes the glassy transition when it is in the amorphous phase structure. However, no variation in the specific volume will occur when the polymer passes the glassy transition while it is in the crystalline structure. This is because the polymer melt and the polymer glass for an amorphous structure are related to the same thermodynamic state at the glassy transition. As noted by Turnbull and Cohen (1961), at this state "the free energy of the amorphous phase should be a minimum when this free volume is distributed at random. Such a random distribution of free volume can occur in the amorphous but not in the crystalline phase". The relationship between the specific volume change in the amorphous and crystalline phases is shows in Figure 23.

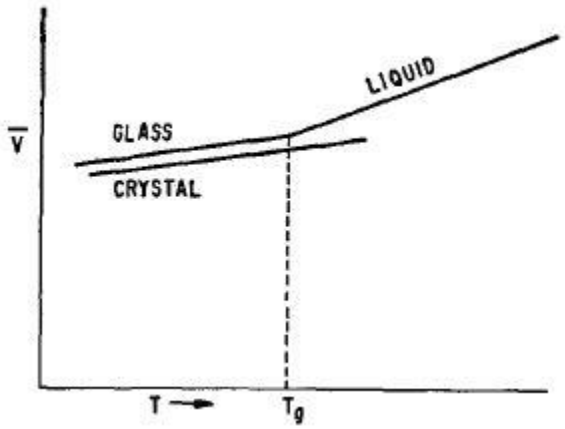

Figure 23: specific volume changes in the amorphous structure where $\bar{v}$ is the specific volume and T is the temperature adopted from Turnbull and Cohen (1961)

The polymer MD simulations literature offers three ways to obtain the amorphous structure as follows:

- Cerius2 (Accelrys) amorphous builder. This tool as shown in Figure 24 has been used by several researchers for PTFE simulation related work (e.g., Holt and Farmer, 1999a, Holt and Farmer, 1999b, Jang et al., 2005). Cerius2 Amorphous builder is based on Monte Carlo algorithm which reduces the atoms VDW radii by at least 70% to prevent the VDW repulsive interactions between atoms. In addition, it should be noted that when using Cerius2, the Monte Carlo algorithm ensures that the dihedral angels will not overlap but rather follow the Boltzmann distribution.

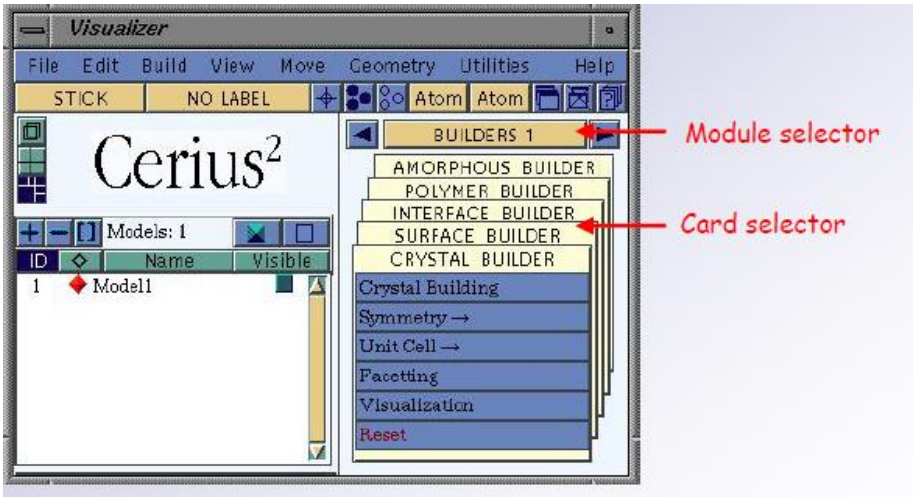

Figure 24: Material Studio/Cerius 2

- The gradual compression of the simulation cell box (i.e. increasing the pressure) until it reaches the gaseous phase. Okada et al. (1999) and Jang et al. (2003) used this approach to obtain the amorphous structure for PTFE.
- The simulated annealing (SA) criteria. This method has been used by many researchers in condensed phase simulations. For example, Dai et al. (2011) obtain the

amorphous configuration for polypropylene using SA in NAMD. The annealing process is initiated by the gradual heating of the crystalline polymer to a high temperature where all atoms are randomly softened to the melt phase. This step is followed by a slow cooling process to relax the polymer configuration from the internal stresses after being heated to high temperatures. In MD simulations, the heating and cooling cycle is consistently repeated over time in order for the molecular segments to overcome the high energy barriers in the crystalline polymer and until the amorphous structure is obtained (Van Laarhoven and Aarts, 1987). Figure 25 shows PTFE amorphous structure which was obtained using the SA experimentally (Bunn et al., 1958). In the experiment, the specimen was cooled after it was heated to 500 °C. The corresponding amorphous structure to be obtained from the MD simulations should have discorded and random chains as shown in Figure 26.

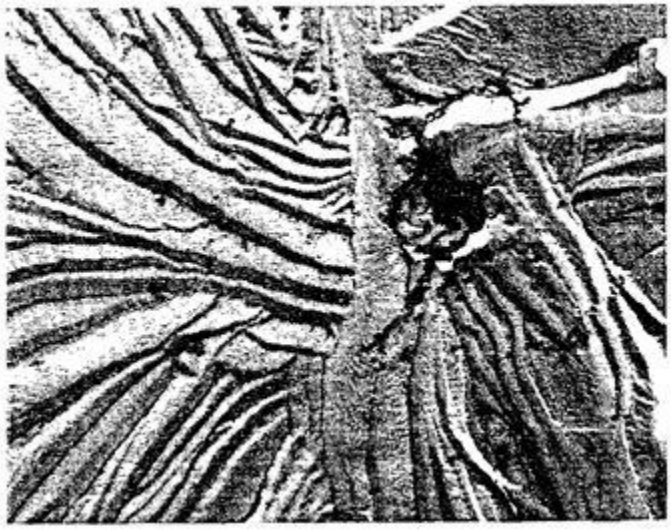

Figure 25: PTFE amorphous structure heated to 500 °C and slowly cooled obtained from experiments using electron micrograph adopted from Bunn et al. (1958)

Figure 26: Polymer amorphous structure obtained from MD adopted from Tangram (2012)

4.6 Computing Glassy Transition Temperature

Once an amorphous structure has been obtained, the glass transition temperature can be computed by performing a relaxation process. The relaxation procedure is demonstrated in Figure 27 and is further explained in the following steps:

1. NVT MD simulations at high temperature (600K for PTFE): the MD runs will start first by using the NVT ensemble where the macroscopic boundary conditions are kept constant. Two tasks will be performed under this ensemble, minimization and equilibration. In NAMD, the conjugate gradients approach using the first order derivative minimization method will be used. This method is efficient, accurate and less expensive especially for large systems because it collects the results from previous iterations and passes them on to the next iteration. The decrease in the gradient tolerance should be monitored along the course of the simulation. A gradient tolerance value of or below of 10^{-5} indicates a good structure quality (NAMD,

2004). The equilibration is performed to allow the simulated cell to develop and evolve from the initial configuration to the equilibrium state at 600K (Leach, 1996).

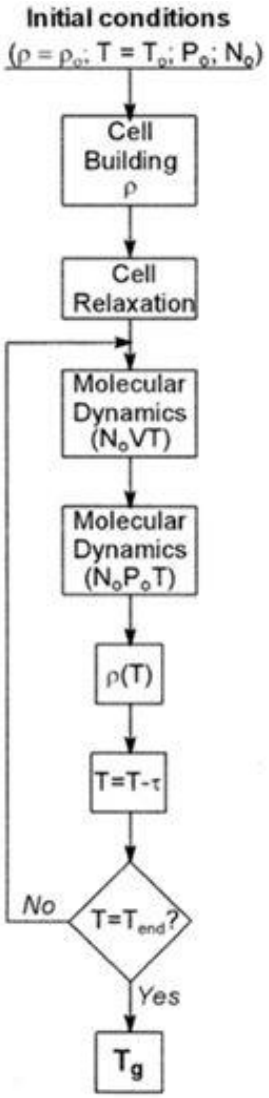

Figure 27: Algorithm to compute glassy transition temperature using MD simulations adopted from SOLDERA (2000)

2. NPT MD simulations at high temperature (600K): as the system moves from one equilibrated state to another, it will be minimized and equilibrated using NPT macroscopic boundary conditions. In this ensemble, the simulation cell size will

expand due to the high internal stresses in the system. These internal stresses are due to: (a) the high system temperature that is defined by the kinetic energy of all the system atoms, and (b) the pressure of the simulation cell which relies on the position and the forces of all the atoms (Tieleman et al., 1997). It should be noted that the equilibration time should be enough for the system to reach to the equilibrium state. The equilibration state will be tested using different MD simulations measurements such as the RMSD (Root Mean Square Deviation) which computes the difference between two frames. If the system is equilibrated for enough time, the RMSD chart will have a steady state line with small fluctuations. As Figure 28 shows, the longer the simulation time, the smaller the fluctuations.

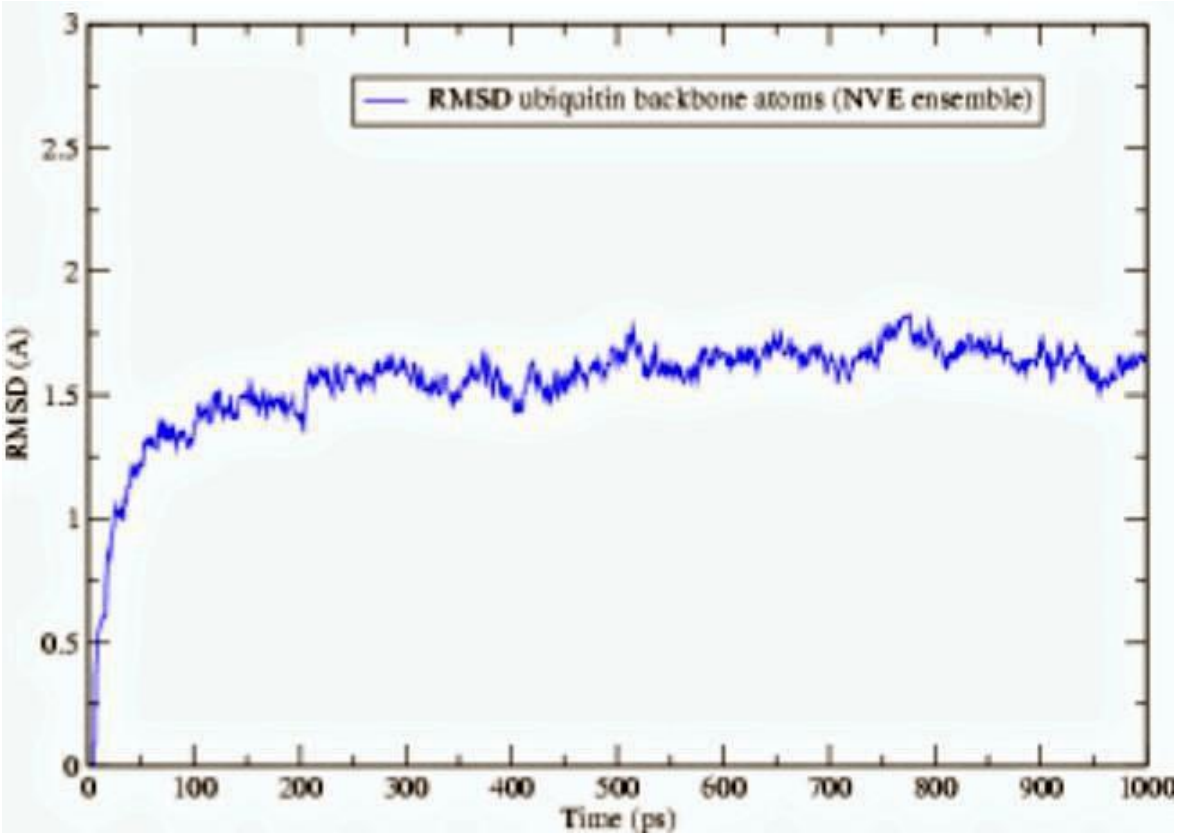

Figure 28: Root mean square versus time adopted from Isgro et al. (2003)

3. NPT annealing to the desired temperature and for long enough time to reach the thermodynamic equilibrium. After having a disordered polymer at high temperature, a slowly cooling process will be performed. This process should be very slow to allow any needed transformations to occur. Otherwise, the system would be quenched, deformed and tricked to unfavorable minimum local energy.
4. Repeat the annealing process to different target temperatures. Three target temperatures will be used as follows: low temperature, temperature around the Tg, and temperature higher than the Tg. It should be noted that high cooling rates will be used for the high temperature targets and low cooling rates for low temperature targets. for example the cooling rate was for PE about 0.8K/ps for lower targets and higher for the high desired temperatures (Hossain et al., 2010)

As mentioned earlier, this research will compare the PTFE glassy transition temperature value from the MD simulations with the glassy transition temperature value from the experimental approach. The comparison will be depicted in a chart similar to Figure 29 from Han et al. (1994) who computed the PE (Polyethylene) glassy transition temperature and compared it to the corresponding experimental values. As shown in the figure, the simulated values were not far from the experimental ones, for example the experimental Tg for polyisobutylene (PIB) is 150K while the MD value is 165K. It is worth mentioning that the calculated Tg value from MD simulations will most likely be higher than the experimental values as shown in Figure 30. The variance in values is due to the difference in time scale between the experimental and MD approaches. Specifically, the experiments are usually performed to measure Tg and the change in many properties using real time scale of seconds or minutes while the MD uses shorter scale such as nanosecond (Han et al., 1994).

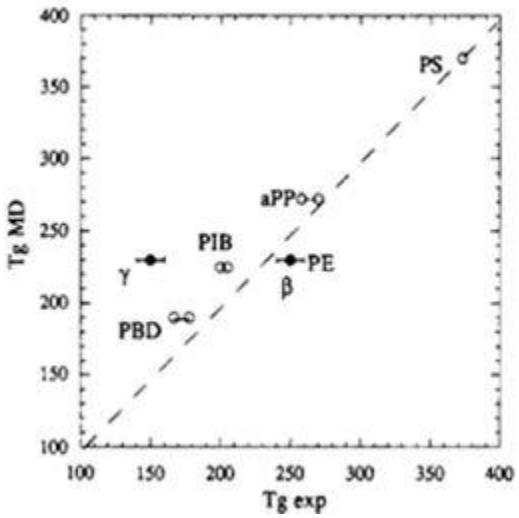

Figure 29: Experimental glassy transition temperature values versus molecular dynamic simulations values, the dashed line represent the ideal case where Tg MD = Tg exp. This figure shows Tg for different polymers, polyethylene (PE), atactic polystyrene (PS), polyisobutylene (PIB), atactic polypropylene (aPP) and cis-poly(1,3-butadiene) (cis-PBD) adopted from Han et al. (1994)

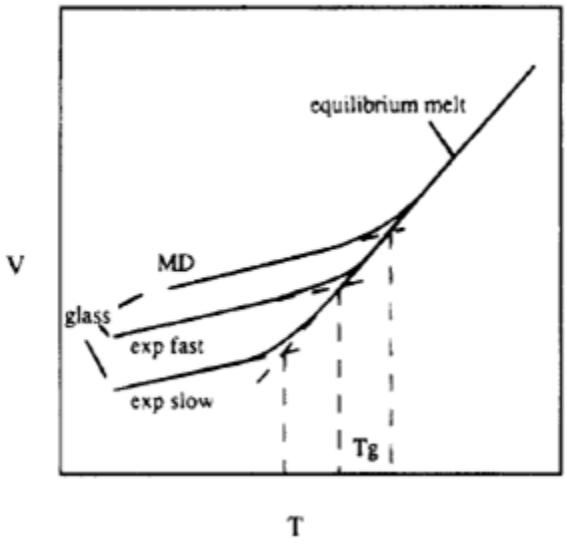

Figure 30: Experimental and molecular simulations values general representation adopted from Han et al. (1994)

4.7 Measuring Properties Affected by Glassy Transition Temperature

The process of measuring the glassy transition temperature is based on identifying changes in some of the properties that are affected by this transition such as the volumetric thermal expansion, the specific volume, and the bulk modulus.

4.7.1 Volumetric Coefficient of Thermal Expansion

The glassy transition temperature can be measured at the phase transition; that is when a change in the volumetric thermal expansion occurs due to the system passing the glassy transition temperature. At the point of transition, changes in the volume due to the annealing process can be drawn versus the temperature as shown in Figure 31. The intersection between the high cooling rate line and the low cooling rate line determines the Tg. The PTFE experimental research studied two types of thermal expansion coefficient, PTFE linear coefficient of thermal expansion, and PTFE volumetric coefficient of thermal expansion. The linear coefficient of thermal expansion refers to the ratio of the strain in material length to the change in temperature (Tipler and Mosca, 2007) as shown in equation (4.3).

$$\alpha = \frac{\Delta L / L}{\Delta T} \tag{4.3}$$

where α is linear coefficient of thermal expansion, ΔL is the change in length, L is the original length, and ΔT is the change in temperature.

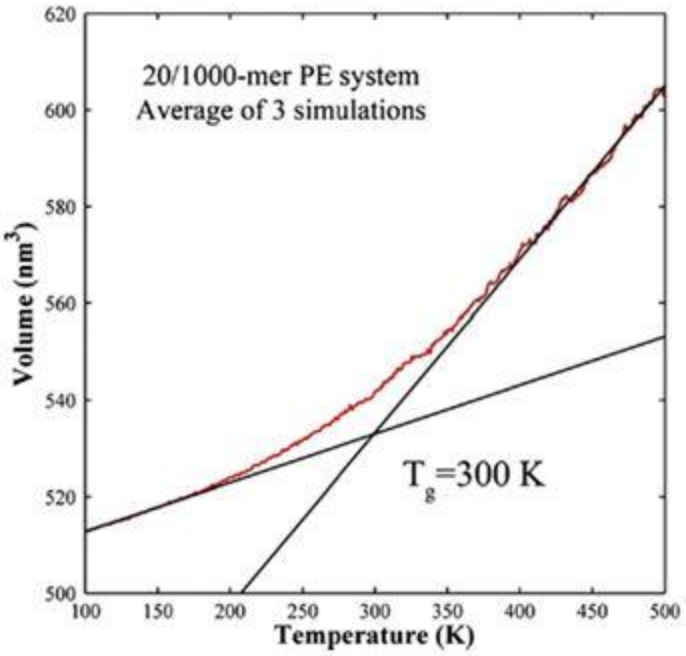

Figure 31: Volume versus temperature to compute Tg of PE adopted from Hossain et al. (2010)

Kirby (1956) and Araki (1965) computed PTFE linear coefficient of thermal expansion experimentally. Specifically, Araki (1965) investigated the glassy transition temperature for PTFE specimen rods as shown in Figure 32 and found that it occurs at 400K in the amorphous region and the Tg mean value for different PTFE specimens is about 365K. In, addition, PTFE linear coefficient of thermal expansion has changed due to Tg. Two cases taken into consideration when the coefficients of linear thermal expansion were computed based on the amorphous fraction A: first, below the glassy transition temperature $\alpha 1$, and second above the glassy transition temperature $\alpha 2$. The amorphous fraction A increases with increasing amorphicity. It is found that at A=0 where $\alpha 1$ and $\alpha 2$ are equal to $6* 10^{-4}$ / °C, and at A=1, $\alpha 1=2* 10^{-4}$ /°C and $\alpha 2=3* 10^{-4}$ /°C. Araki (1965) experimental results are shown in details in Table 11

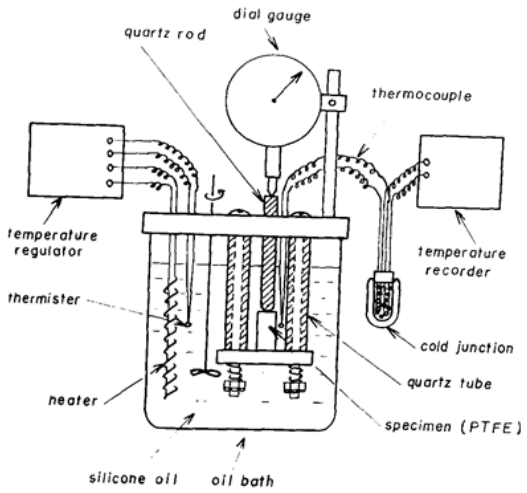

Fig. 1. Schematic diagram of the apparatus.

Figure 32: PTFE rod experiment to compute Tg adopted from Araki (1965)

Table 11: Tg and linear coefficient of thermal expansion results adopted from Araki (1965)

Thermal Expansion of PTFE

No.	Molded sample	Specific gravity (25°C./25°C.)	Amorphous fraction	T_g, °K.	$\alpha_1 \times 10^{-4}$ deg.$^{-1}$	$\alpha_2 \times 10^{-4}$ deg.$^{-1}$	$T_g\ \Delta\beta$[a]	$T_g\ \Delta\beta/A$
1	Polyflon M-11A	2.1530	0.48	400	1.30	1.87	0.0684	0.143
2	Polyflon M-11	2.1624	0.45	397	1.24	1.62	0.0453	0.101
3	Fluon G1	2.1748	0.41	402	1.12	1.59	0.0567	0.138
4	Teflon 1	2.1763	0.41	398	1.22	1.57	0.0418	0.102
5	Teflon 7	2.1799	0.40	394	1.16	1.51	0.0414	0.103
6	Teflon 6C	2.1984	0.34	392	1.08	1.42	0.0400	0.118
7	Fluon CD1	2.2068	0.31	388	1.03	1.34	0.0361	0.116
8	Polyflon Fine	2.2258	0.26	397	0.93	1.11	0.0214	0.082
9	Teflon 6	2.2320	0.24	394	0.98	1.26	0.0331	0.138
			Mean	396			Mean	0.116

[a] $\Delta\beta = 3(\alpha_2 - \alpha_1)$.

The volumetric coefficient of thermal expansion refers to ratio of the strain in material volume to the change in temperature (Tipler and Mosca, 2007) as shown in equation (4.4).

$$\beta = \frac{\Delta V / V_{cell}}{\Delta T} \quad (4.4)$$

where β is the volumetric coefficient of thermal expansion, ΔV is the change in volume, V is the cell size, and ΔT is the change in temperature.

Experimentally, Eby and Sinnott (1961) suggested two glassy transitions based on studying the changes in the volumetric coefficient of thermal expansion: the first is at 263K where the volumetric coefficient of thermal expansion is about 0.243 $*10^{-3}$ / °C, and the second transition temperature around 400K where the volumetric coefficient of thermal expansion is about 0.5 $*10^{-3}$ / °C. Another experimental and important finding in this regard is by Quinn et al. (1951) as shown in Table 12. Quinn et al. (1951) was interested in studying the PTFE volume-temperature relation, he calculated the volumetric coefficient of thermal expansion in details at wide range of temperatures.

Table 12: PTFE volumetric coefficients of thermal expansion adopted from Quinn et al. (1951) and DuPont (1996)

***Teflon*® PTFE Resins**
Cubical Coefficients of Expansion

Temperature Range, °C (°F)	$cm^3/cm^3.°C$	$in^3/in^3.°F$
–40 to 15(–40 to 59)	2.6×10^{-4}	1.5×10^{-4}
15 to 35 (59* to 95)	1.7%	
35 to 140 (95 to 284)	3.1×10^{-4}	1.7×10^{-4}
140 to 200 (284 to 392)	6.3×10^{-4}	3.5×10^{-4}
200 to 250 (392 to 482)	8.0×10^{-4}	4.4×10^{-4}
250 to 300 (482 to 572)	1.0×10^{-3}	5.7×10^{-4}

*Quinn et al., *J. Applied Phys.* 22, 1085 (1951)

This research is interested in studying PTFE volume – temperature relation and the change in the volumetric coefficient of thermal expansion.

4.7.2 **Specific Volume**

Specific volume is defined by the volume that is filled by a definite quantity of a material (Cengel et al., 2011). It is the inverse of density as shown in equation (4.5)

$$\nu = \frac{1}{\rho} = \frac{V}{m} \tag{4.5}$$

where ν is the specific volume, ρ is the density, V is the volume, and m is the mass.

The change in the specific volume for a material will predict the glassy transition temperature as shown in Figure 33. In addition, the specific volume values will vary due to change in temperature values along with the simulation time as shown in Figure 34.

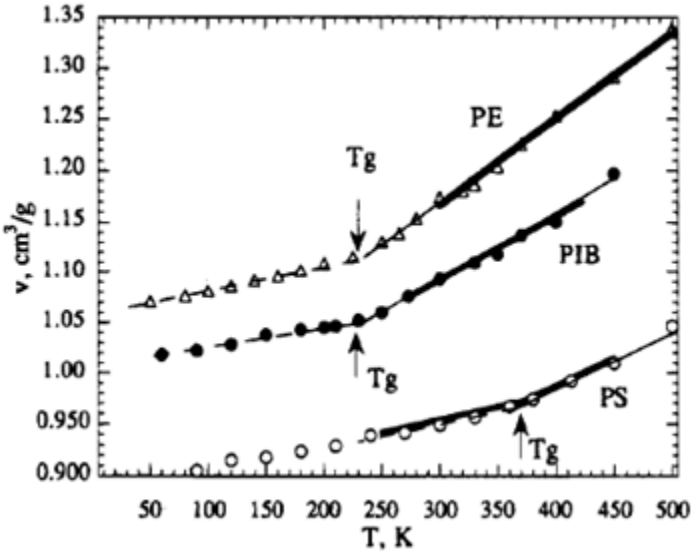

Figure 33: Specific volume versus temperature to compute polyethylene (PE), atactic polystyrene (PS), polyisobutylene (PIB) glassy transition temperature adopted from Han et al. (1994)

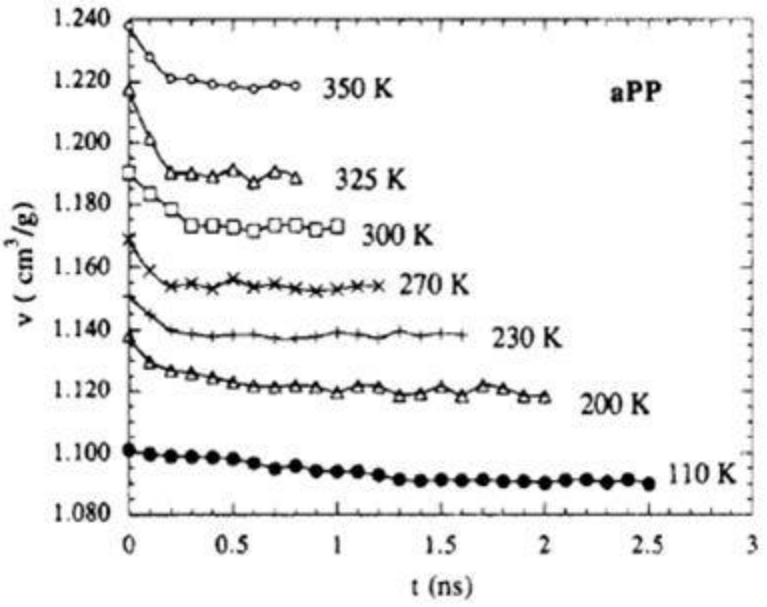

Figure 34: Specific volume versus time for PE at different temperatures, where the points are 100ps interval averages from MD runs adopted from Han et al. (1994)

As mentioned previously, the specific volume is the inverse of the density so we could compute the density from MD simulations and compare it with the experimental density values. Sperati and Starkweather (1961) found that the density for non- crystalline PTFE is equal to 2.00 g/cm^3 and the density for PTFE in perfect crystalline phase is equal to 2.3 g/cm^3 so the obtained values should fall in this density range. In Table 13, density values has been listed for PTFE specimen that is cooled from 380°C at four different cooling rates, the structure of this specimen structure is shown in Figure 35

4.7.3 **Bulk Modulus**

Bulk modulus property is an important elastic measurement which refers to the resistance of a material to compression (Anderson, 1995). The bulk modulus values that will be computed from MD will be compared to the experimental bulk modulus values. Warfield et al. (1970) found that

PTFE bulk modulus values vary from 2.1 GPa to 2.8 GPa. In addition, Chabrier et al. (1999) found that PTFE bulk modulus was about 1.61 GPa.

Table 13: Four PTFE specimens A, B, C and D density values adopted from Natarajan (1973)

Results of Cooling Rate Experiments

Cooling rate deg C/min.	Mean lamellar thickness (Å)	Standard deviation (Å)	Standard error of the mean (Å)	Density g/cc	Percent crystallinity
Quench	1110	329	52	2.138	45
2	1600	493	78	2.146	53
0.48	1440	501	79	2.156	58
0.12	1850	839	132	2.192	65
0.02	2590	2037	322	2.205	68

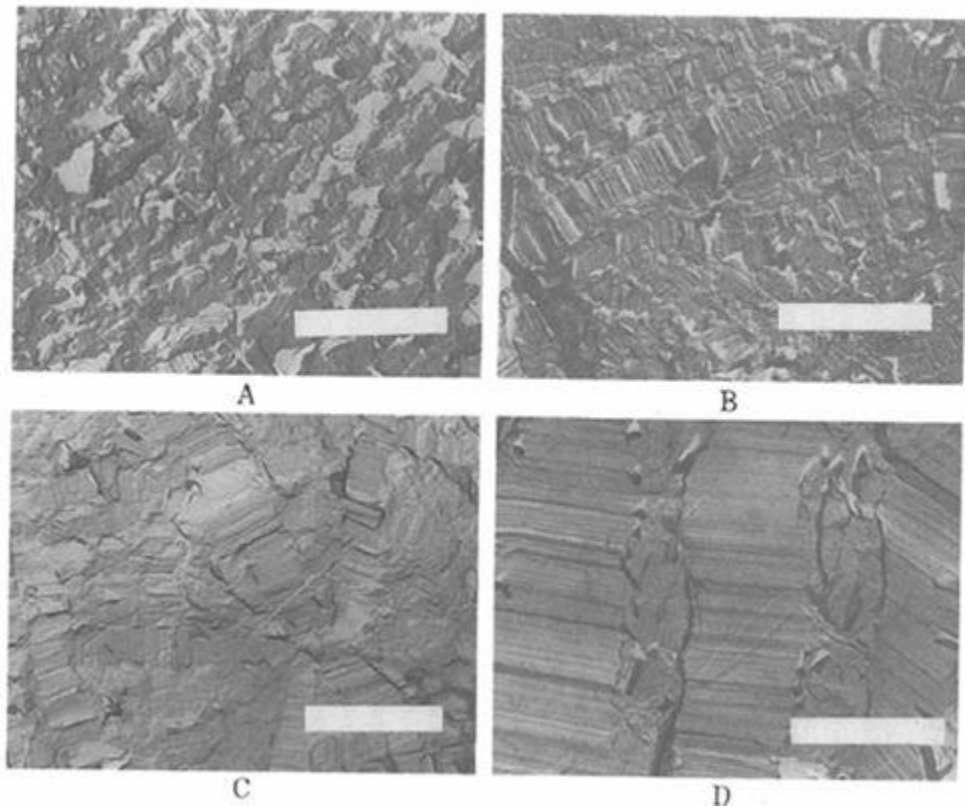

Figure 35: Four PTFE electron micrographs specimens structure at different cooling rates: A at 2.0, B at 0.48, C at 0.12, and D at 0.02 deg/min adopted from Natarajan (1973)

4.8 Glassy Transition Temperature Governing Forces at Molecular Level

The effect of the glassy transition on the bonding and non-bonding energies has been investigated in many MD simulations studies. For example, Li et al. (2009) computed polyimide glassy transition temperature and its influence on the inter and intra-molecular energies. The researchers noticed that the bonding energy values for the simulated system have the same linear trend while the non-bonding energy values have a kink in the trend line as shown in Figure 36. These results assure the significant role of the intermolecular energy in polyimide thermal properties. However, Yu et al. (2001) found that both the intermolecular and the dihedral energies had a sudden change when passing the glassy transition point as shown in Figure 37 . This research will study the glassy transition temperature and its impact on both the intrarmolecular and intermolecular energies. Specifically, investigating the impact of the non-bonding and the dihedral forces on the occurring the PTFE glassy transition temperature.

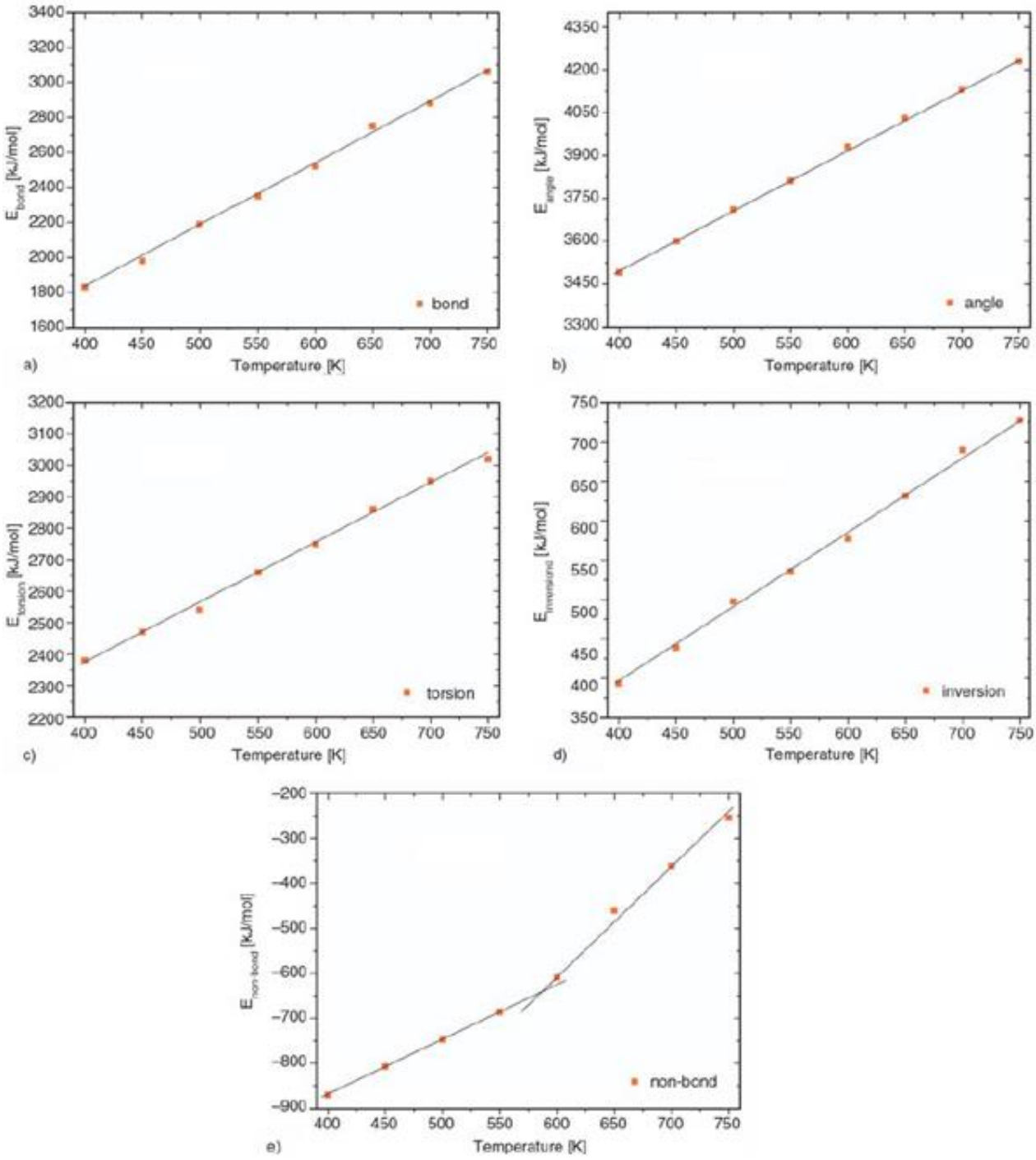

Figure 36: Polyimide glassy transition temperature governing forces: (a) bond energies versus temperature, (b) angle energies versus temperature, (c) torsion energies versus temperature, (d) inversion energies versus temperature, and (e) non-bond energies versus temperature adopted from Li et al. (2009)

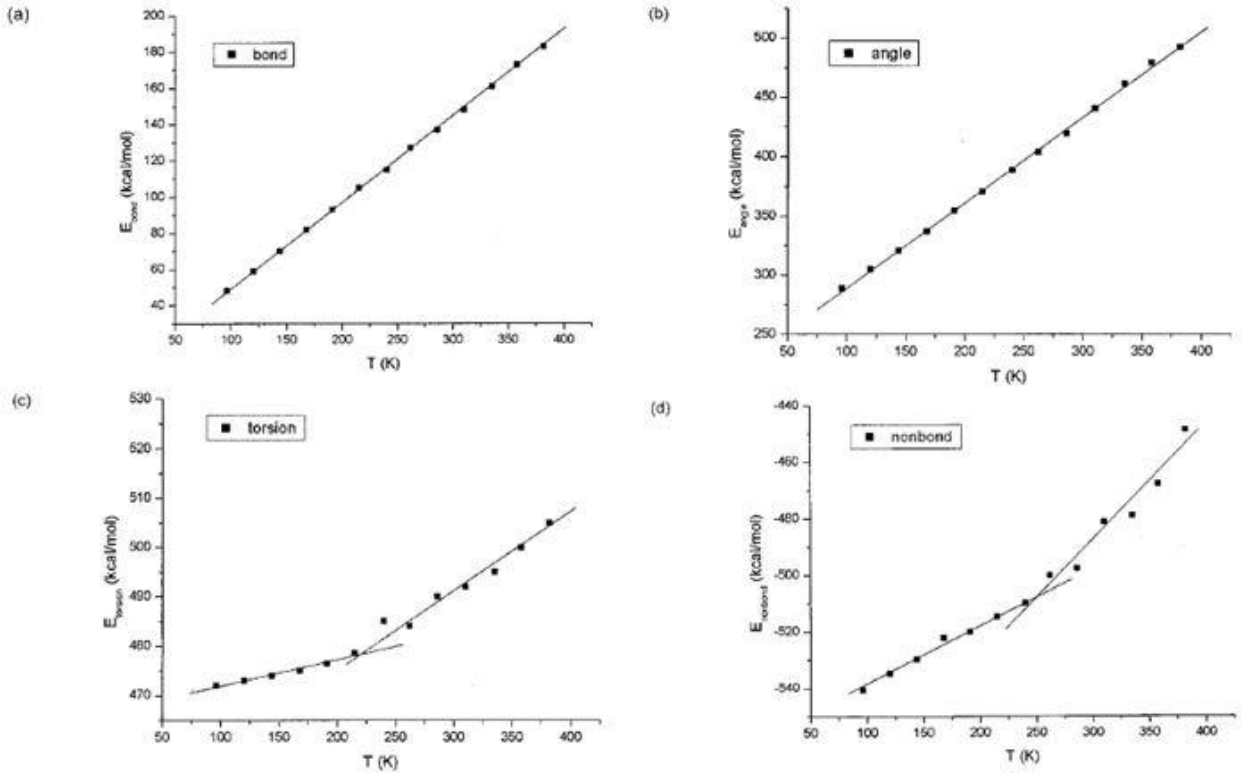

Figure 37: Polyoxymethylene glassy transition temperature governing forces: (a) bond energies versus temperature, (b) angle energies versus temperature, (c) torsion energies versus temperature, and (d) non-bond energies versus temperature adopted from Yu et al. (2001)

5 Discussion & Results

The purpose of this chapter is to present the results of this project along with the discussion for the following: (1) PTFE force-field parameters, (2) building NAMD input files, (3) building the polymer configuration, (4) testing PTFE new residue, (5) obtaining the amorphous structure for PTFE polymer, and (6) performing MD simulations to calculate PTFE glassy transition temperature. The parameterization task involved using the OPLS-AA potential energy model to obtain the PTFE intermolecular and intramolecular force-field parameters. The MD simulations task involved: (a) using PTFE OPLS-AA force field parameters which will be used in the simulation work, (b) performing MD simulations to measure the glassy transition temperature and comparing it with experimental values, (c) measuring different properties that are affected by the glassy transition temperature and comparing them with experimental values, and (d) determining the glassy transition temperature governing forces at the molecular level. These tasks will be delineated in the subsequent sections

5.1 The Force-Field Parameters

In this project I obtained two sets of PTFE parameters: (1) PTFE OPLS-AA parameters with RESP charges and three dihedral coefficients at DFT (B3LYP/6-31G*) level of theory, and (2) PTFE OPLS-AA parameters with RESP at MP2/6-31G* level of theory charges and six dihedral coefficients at DFT (B3LYP/6-31G*) level of theory.

5.1.1 **B3LYP Derived Parameters**

The first set is presented in Table 16 Four unique atom types are used for the RESP point charges: CF2, CF3, F2, and F3. The atomic charges for the electrostatic potentials were derived based on ab initio calculations for perfluorobutane in NWCHEM package (Bylaska et al., 2007) at (B3LYP/6-31G*) DFT level of theory. Then, the electrostatic charges were fitted to the RESP model (Bayly et al., 1993). Table 14 shows the RESP charges for PTFE at different chain length. Due to their importance in determining polymer conformation and properties, the torsional angles were treated carefully by scanning the potential energy surface along a full profile with increments of 5°, in this set the dihedrals were fitted with three coefficients where the quantum data were calculated using NWCHEM at (B3LYP/6-13G*) DFT level of theory. Figure 38 and Figure 39 show the fitting for C-C-C-C (PTFE main backbone), and C-C-C-F dihedral angles, respectively. As for the bonds and angles parameters, we generated them using AFMM and refined them so as to achieve a frequency match between normal modes from molecular mechanics (MM) on one hand and quantum mechanics (QM) as a reference set, on the other hand. As I mentioned earlier, the acceptable parameterization in AFMM should have a value of σ between 0 to 100 cm^{-1}, where σ is the root mean square deviation from reference set (Vaiana et al., 2005). In the current work, σ values for all the parameters are presented in Table 15 . Hence, σ values fall within the acceptable range. The frequency matching for the parameters are presented in Figure 40, Figure 41, Figure 42, Figure 43, and Figure 44 . In addition, I test the solubility parameter by performing MD simulations on different PTFE oligomers at their boiling points. The solubility parameter is dependent on the concept of cohesive energy density (CED), which is defined as the energy needed to release the molecule from its adjacent molecules in the liquid phase. The solubility parameter (Grulke, 1999, Hildebrand and Scott, Hansen, 1969).

$$\delta = \sqrt{(CED)} = \sqrt{\frac{\Delta H_m - RT}{V_m}} \quad (5.1)$$

where δ is the solubility parameter, ΔH_m is the molar heat of vaporization, V_m is the molar volume, R is the ideal gas constant, and T is the temperature. Therefore, obtaining the solubility parameter is contingent on calculating the heat of vaporization.

The heat of vaporization is defined as the sufficient amount of heat that is absorbed by one mole of liquid to convert it to the gaseous phase at constant temperature. Experimentally, heat of vaporization is detected by measuring the liquid enthalpy of vaporization around the boiling point using calorimetry or by predicting it using Clausius-Clapeyron equation (Jenkins, 2008). In MD simulations, it is measured using the total intermolecular cohesive energy in the liquid phase plus the work done by volume variation or by the difference between the intramolecular and potential energies for the gaseous and liquid phase respectively(Watkins and Jorgensen, 2001, Wang and Hou, 2011).

$$\Delta H_{vap} = \Delta H_{gas} - \Delta H_{liq} = E(gas)_{intramolecular} - E(liq)_{total} + RT \quad (5.2)$$

where, ΔH_{vap} is the heat of vaporization, ΔH_{gas} is the enthalpy at the gaseous phase, ΔH_{liq} is the enthalpy at the liquid phase, $E(gas)_{intramolecular}$ is the intermolecular energy at the gaseous phase, $E(liq)_{total}$ is the total energy at the liquid phase, R is the ideal gas constant, and T is the temperature. The term RT is equal to the PV work term and it is negligible for liquids.

The solubility parameter values for PTFE different oligomers are presented in Table 17, the simulated values for the solubility parameter and the heat of vaporization are higher than their corresponding experimental values as obtained from the literature although this is to be expected due to the difference in scale between the MD simulations and the experimental approaches. Consistent with other studies (Wang and Hou, 2011), we further compared the simulated values for the heat of vaporization against experimental values from the CRC handbook. We noticed

that the CRC values were not only smaller than the simulated values but even smaller than the experimental values from the literature. For example, the heat of vaporization for C_6F_{14} in our research was 7.97 $kcal/mol$ compared to a CRC value of 7.1(Hougham, 1999) and experimental value of 7.51(Basařová and Svoboda, 1991).

Table 14: RESP charges for PTFE at B3LYP/6-31G* for different chain length

PTFE Model	CF2 group		CF3 group	
	C	F	C	F
C_4F_{10}	+0.33	-0.19	+0.60	-0.18
C_5F_{12}	+0.34	-0.18	+0.60	-0.18
C_6F_{14}	+0.34	-0.18	+0.60	-0.18
C_7F_{16}	+0.36	-0.19	+0.60	-0.18
C_8F_{18}	+0.36	-0.19	+0.60	-0.18
$C_{10}F_{22}$	+0.37	-0.19	+0.51	-0.17
$C_{11}F_{24}$	+0.35	-0.18	+0.60	-0.18

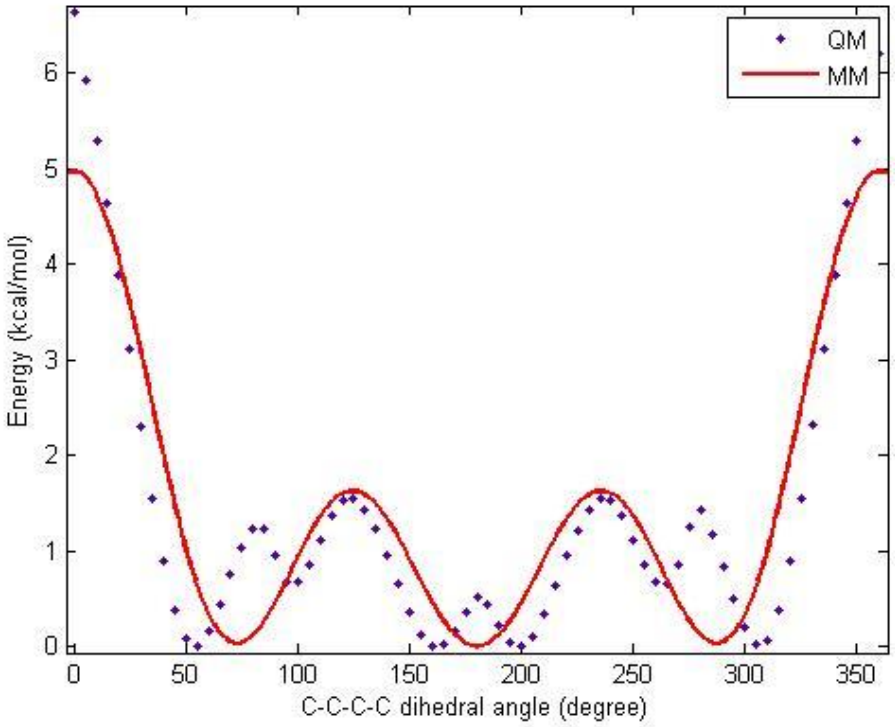

Figure 38: C-C-C-C dihedral angle fitting

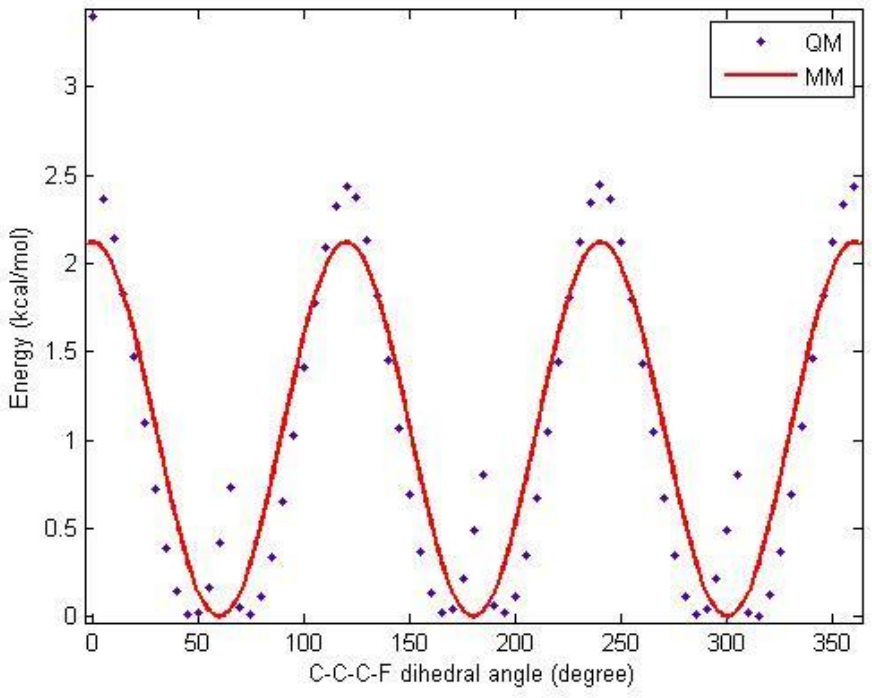

Figure 39: C-C-C-F dihedral angle fitting

Table 15: PTFE B3LYP derived parameters sigma values using AFMM

Parameter	σ values (cm^{-1})
C-C	79.90
C-F	81.50
F-C-F	80.70
C-C-F	81.50
C-C-C	81.90

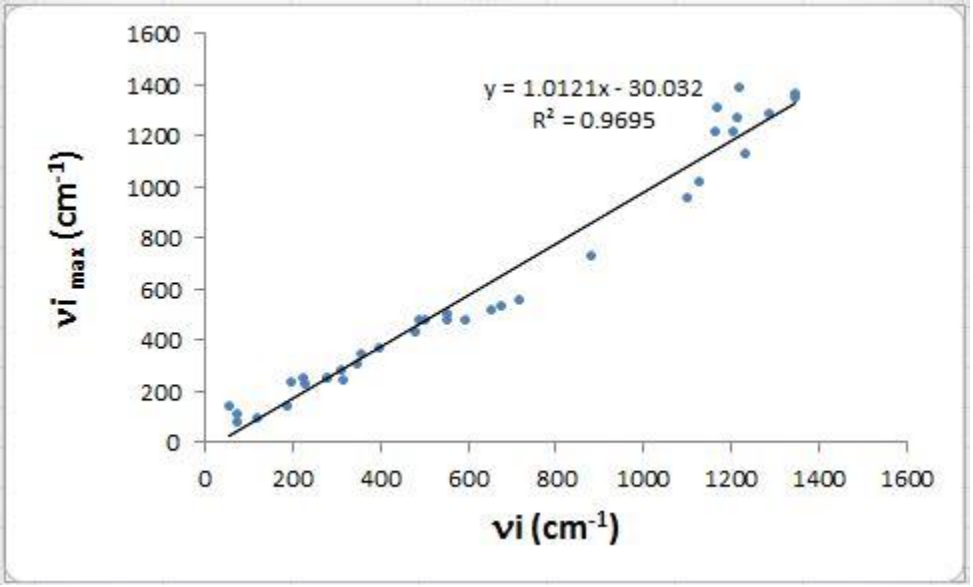

Figure 40: Normal modes frequency matching plot of C-C bond at B3LYP level. The line illustrates the ideal situation of optimal matching. The points represent the frequency matching of PTFE bond parameter for C-C where σ value equal to 79.9 cm^{-1}

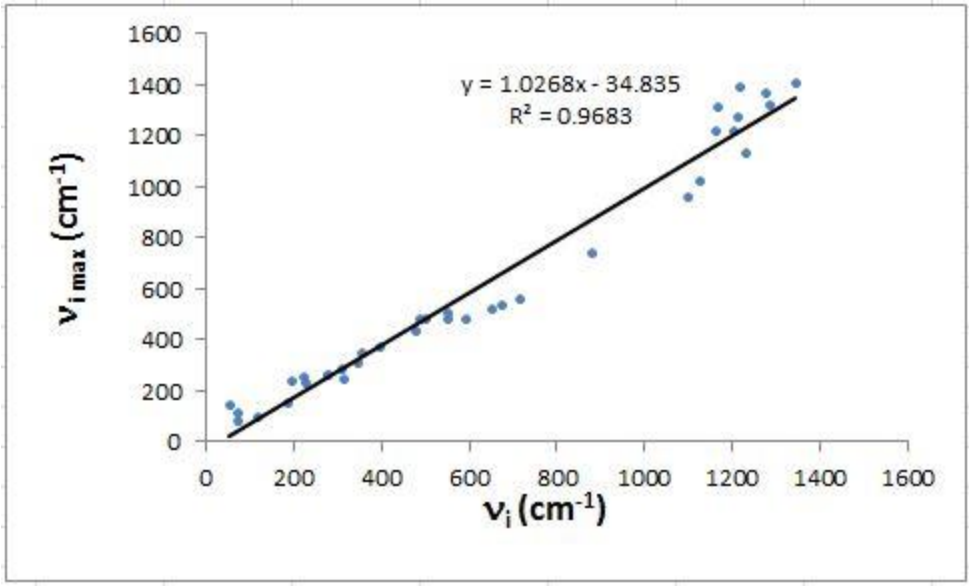

Figure 41: Normal modes frequency matching plot of C-F bond at B3LYP level. The line illustrates the ideal situation of optimal matching. The points represent the frequency matching of PTFE bond parameter for C-F where σ value equal to 81.5 cm^{-1}

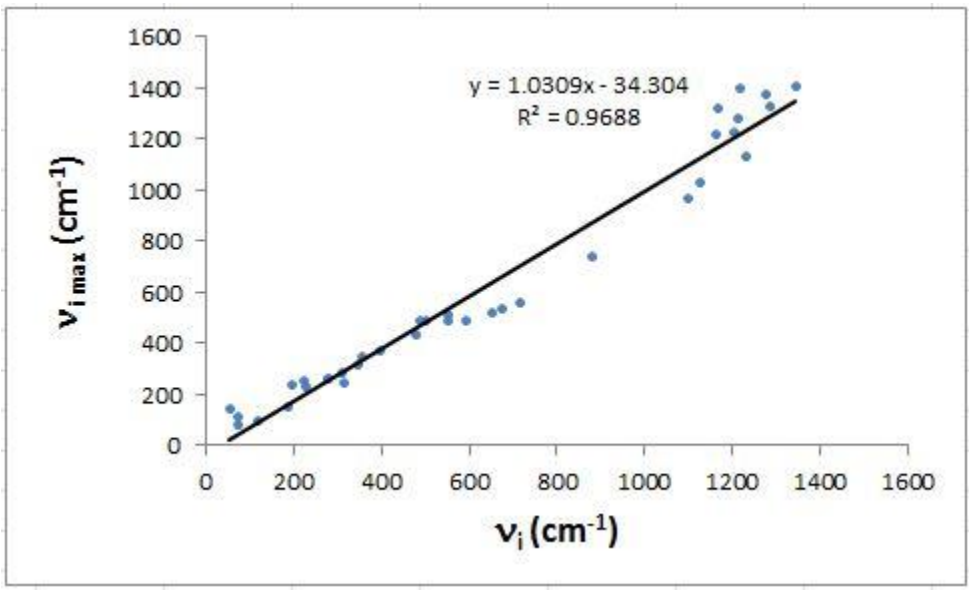

Figure 42: Normal modes frequency matching plot of F-C-F angle at B3LYP level. The line illustrates the ideal situation of optimal matching. The points represent the frequency matching of PTFE angle parameter for F-C-F where σ value equal to 80.7cm^{-1}

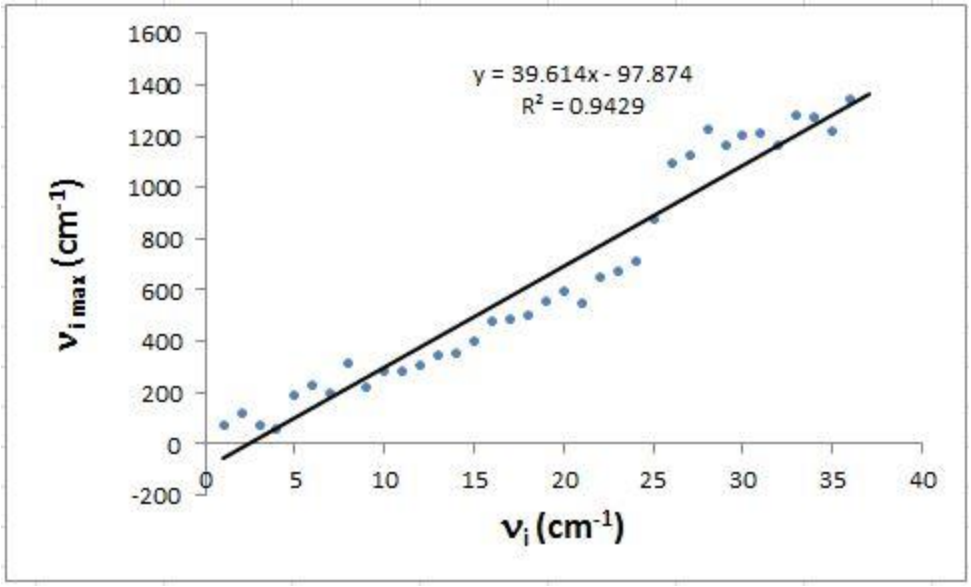

Figure 43: Normal modes frequency matching plot of C-C-F angle at B3LYP level. The line illustrates the ideal situation of optimal matching. The points represent the frequency matching of PTFE angle parameter for C-C-F where σ value equal to 81.5 cm^{-1}

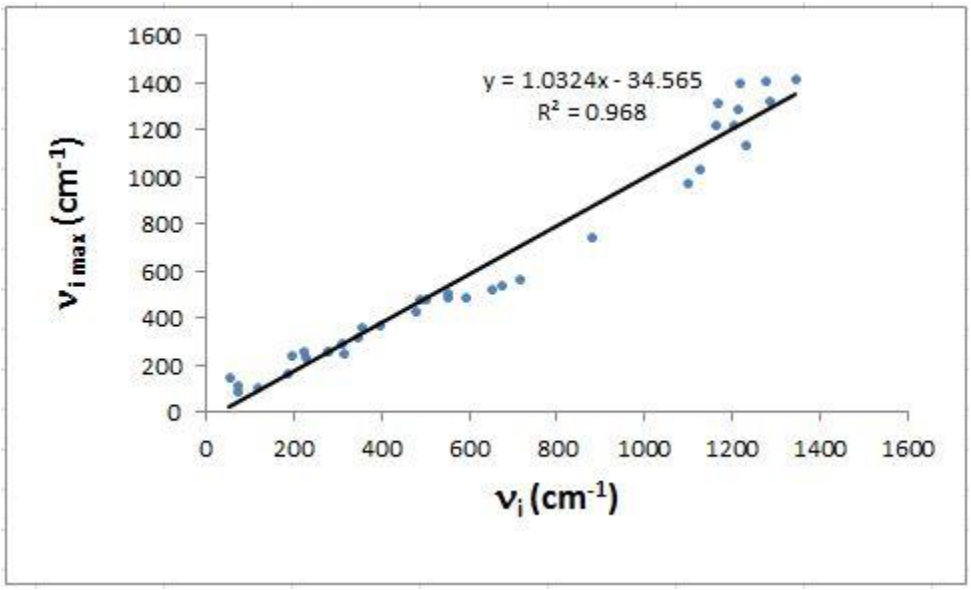

Figure 44: Normal modes frequency matching plot of C-C-C angle at B3LYP level. The line illustrates the ideal situation of optimal matching. The points represent the frequency matching of PTFE angle parameter for C-C-C where σ value equal to 81.9 cm^{-1}

Table 16: PTFE OPLS-AA (B3LYP/6-13G*) force-fields parameters

Bonds			
Bond	k_r(kcal/mol/A²)	r_o (A°)	
F—C	304.82	1.38	
C—C	259.93	1.54	
Angles			
Angles	k_θ(kcal/mol/A²)	θ_o (Degree)	
F—C—F	107.64	108.72	
C—C—C	57.553	116.31	
F—C—C	56.39	107.90	
Dihedrals			
Dihedral	V_1	V_2	V_3
C—C—C—F	0.00	0.00	1.06
C—C—C—C	1.24	-1.01	1.24
F—C—C—F	0.00	0.00	1.34
RESP Charges for C4F10			
Atom	Charges (e)		
CF2	+0.329		
CF3	+0.598		
F2	-0.189		
F3	-0.183		

Table 17: PTFE solubility parameter and heat of vaporization

Reference Molecule	Heat of Vaporization(kcal/mol)			Solubility Parameter $(cal/cm^3)^{1/2}$		
	MD (Other Research)	MD (This Research)	Experimental	T(K)	MD (This research)	Experimental
C_4F_{10}	5.54(Okada et al., 1999), 5.45±0.10(Watkins and Jorgensen, 2001)	5.60	5.47(Lide, 2004)	273	5.80	N/A
C_5F_{12}	6.37(Okada et al., 1999), 6.52±0.13(Watkins and Jorgensen, 2001)	6.70	6.05(Hougham, 1999)	298	5.82	5.5(Hougham, 1999)
C_6F_{14}	7.65(Okada et al., 1999), 7.86±.13(Watkins and Jorgensen, 2001)	7.97	7.1(Hougham, 1999), 7.51(Basařová and Svoboda, 1991)	298	6.02	5.6(Hougham, 1999)
C_7F_{16}	N/A	7.40	7.37(Hougham, 1999)	353	5.50	5.7(Hougham, 1999)
C_8F_{18}	N/A	9.13	7.97(Lide, 2004), 9.2(Hougham, 1999)	378	5.80	5.7(Hougham, 1999)

5.1.2 **MP2 Derived Parameters**

The second set is presented in Table 21, where four unique atom types are used for the RESP point charges: CF2, CF3, F2, and F3. The atomic charges for the electrostatic potentials were derived based on ab initio calculations for perfluorobutane in NWCHEM package (Bylaska et al., 2007) at (MP2/6-31G*) level of theory. Then, the electrostatic charges were fitted to the RESP model (Bayly et al., 1993). Table 18 shows the RESP charges at MP2 level of theory for PTFE different chain length.

The torsional angles were treated carefully by scanning the potential energy surface along a full profile with increments of 5°, in this set the dihedrals were fitted at different level of expansion as shown in Table 19, we choose the fitting with six terms to avoid the poor prediction or what is called by Overfitting, the expansion very clearly shows a convergence in the coefficients, the quantum data were calculated using NWCHEM at MP2 level of theory. The bonds and angles parameters, we generated them using AFMM and refined them so as to achieve a frequency match between normal modes from MM on one hand and QM as a reference set. In the current work, σ values for all the parameters are presented in Table 20. Hence, sigma values fall within the acceptable range. The frequency matching for the MP2 derived parameters are shown in Figure 45, Figure 46, Figure 47, Figure 48, and Figure 49

Table 18: RESP charges for PTFE at MP2/6-31G* for different chain length

PTFE Model	CF2 group		CF3 group	
	C	F	C	F
C_4F_{10}	+0.53	-0.32	+1.13	-0.34
C_5F_{12}	+0.62	-0.33	+1.03	-0.32
C_6F_{14}	+0.62	-0.33	+1.09	-0.34
C_7F_{16}	+0.61	-0.33	+1.09	-0.33
C_8F_{18}	+0.60	-0.33	+1.08	-0.33
$C_{10}F_{22}$	+0.63	-0.33	+1.103	-0.34
$C_{11}F_{24}$	+0.63	-0.33	+1.12	-0.34

Table 19: PTFE dihedral fitting at different level of expansions

Level of Expansion	R^2	Adjusted R^2	RMSE	V1	V2	V3	V4	V5	V6	V7	V8	V9	V10
3	0.85	0.85	0.66	1.24	-1.01	1.25							
4	0.93	0.93	0.45	1.39	-0.82	1.4	-0.59						
5	0.97	0.97	0.30	1.29	-0.90	1.30	-0.67	0.41					
6	0.98	0.98	0.24	1.32	-0.86	1.33	-0.62	0.45	-0.22				
7	0.99	0.98	0.18	1.36	-0.83	1.37	-0.60	0.49	-0.19	-0.21			
8	0.99	0.98	0.18	1.36	-0.83	1.37	-0.60	0.49	-0.19	-0.20	-0.02		
9	0.99	0.99	0.14	1.34	-0.84	1.35	-0.60	0.47	-0.21	-0.23	-0.03	0.15	
10	0.99	0.99	0.13	1.35	-0.84	1.36	-0.60	0.47	-0.20	-0.23	-0.02	0.15	-0.05

Table 20: PTFE MP2 derived parameters sigma values using AFMM

Parameter	σ values (cm^{-1})
C-C	77.0
C-F	79.1
F-C-F	79.3
C-C-F	79.6
C-C-C	79.5

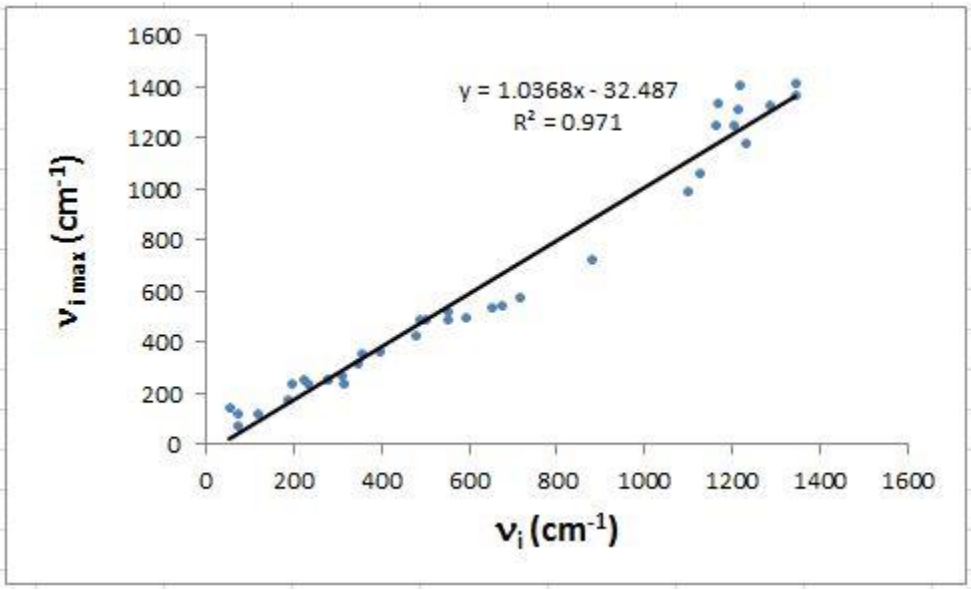

Figure 45: Normal modes frequency matching plot of C-F bond at MP2 level. The line illustrates the ideal situation of optimal matching. The points represent the frequency matching of PTFE bond parameter for C-F where σ value equal to 77.0 cm^{-1}

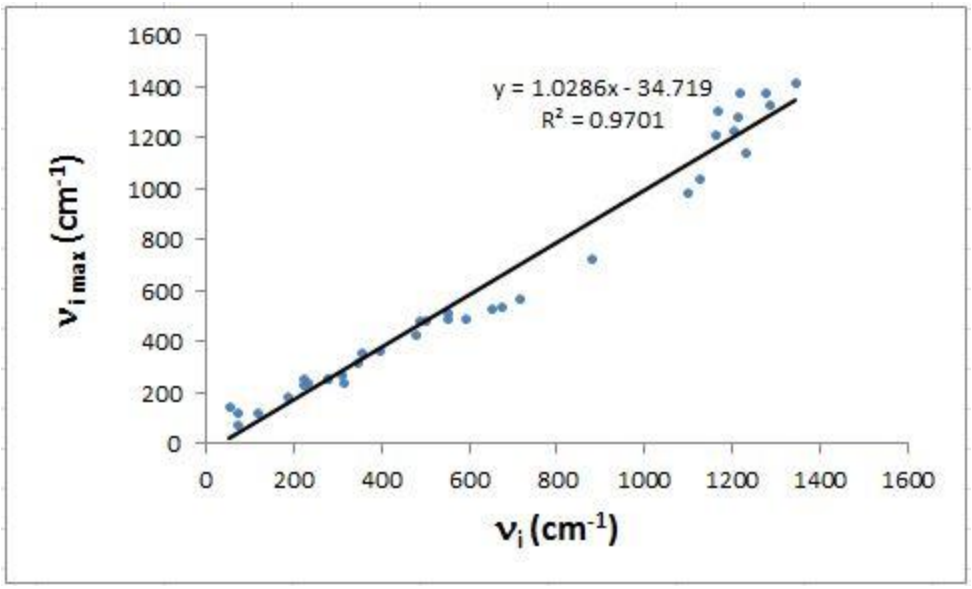

Figure 46: Normal modes frequency matching plot of C-C bond at MP2 level. The line illustrates the ideal situation of optimal matching. The points represent the frequency matching of PTFE bond parameter for C-C where σ value equal to 79.0 cm^{-1}

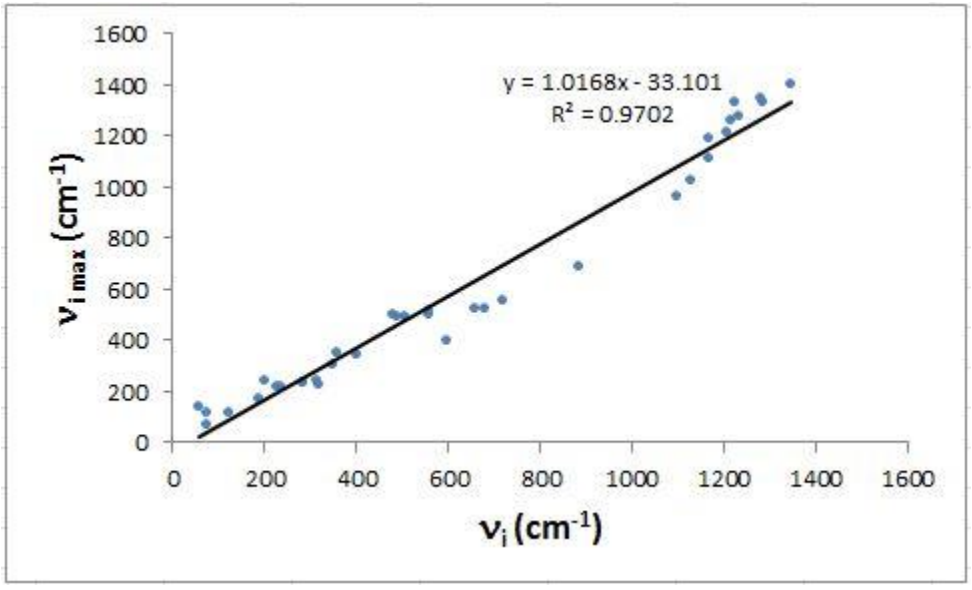

Figure 47: Normal modes frequency matching plot of F-C-F angle at MP2 level. The line illustrates the ideal situation of optimal matching. The points represent the frequency matching of PTFE angle parameter for F-C-F where σ value equal to 79.3 cm^{-1}

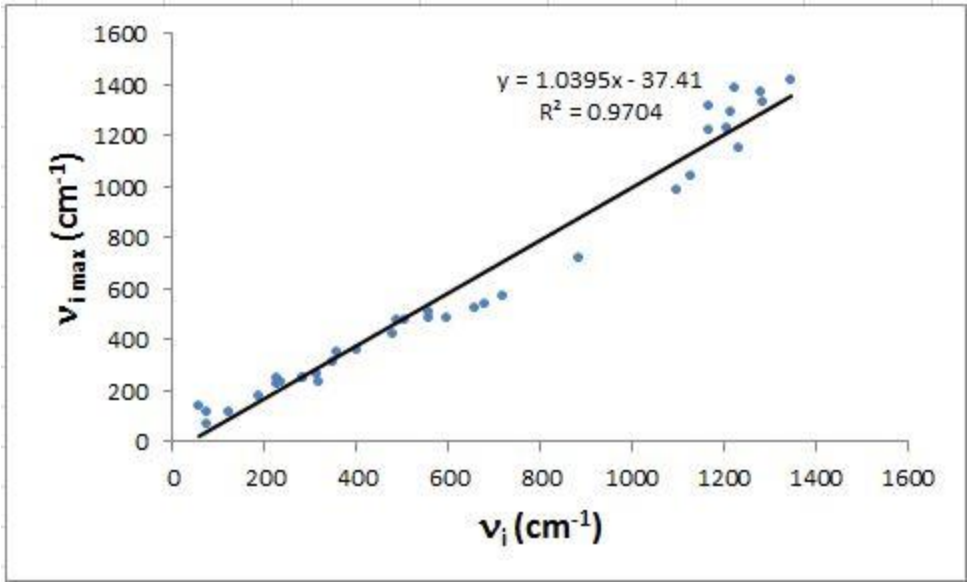

Figure 48: Normal modes frequency matching plot of C-C-F angle at MP2 level. The line illustrates the ideal situation of optimal matching. The points represent the frequency matching of PTFE angle parameter for C-C-F where σ value equal to 79.6 cm^{-1}

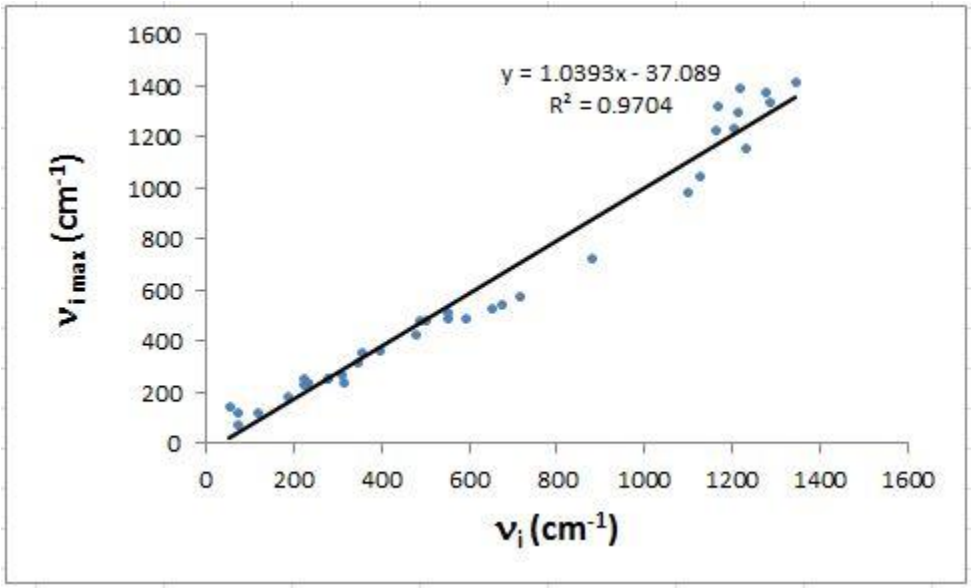

Figure 49: Normal modes frequency matching plot of C-C-C angle at MP2 level. The line illustrates the ideal situation of optimal matching. The points represent the frequency matching of PTFE angle parameter for C-C-C where σ value equal to 79.5 cm^{-1}

Table 21: PTFE final set of prameters with RESP at MP2 level

Bonds						
Bond	k_b(kcal/mol/A²)			b_o (A°)		
F-- C	333.63			1.38		
C-- C	263.41			1.54		
Angles						
Angles	k_θ(kcal/mol/A²)			θ_o (Degree)		
F—C—F	119.99			108.76		
C—C—C	41.77			116.31		
F—C—C	50.21			108.87		
Dihedrals						
Dihedral	V_1	V_2	V_3	V_4	V_5	V_6
C—C—C—F	0.00	0.00	1.06	0.00	0.00	0.00
C—C—C—C	1.35	-0.84	1.36	-0.60	0.47	-0.20
F—C—C—F	0.00	0.00	1.34	0.00	0.00	0.00
RESP Charges at MP2/6-31G*						
Atom	Charges (e)					
CF2	0.632					
CF3	1.080					
F2	-0.316					
F3	-0.360					

I tested the MP2 derived parameters by measuring the density as illustrated in Table 22 and PTFE density was 1.79 gm/cm^3 while the experimental density value for the melt is about 2.0 gm/cm^3, from this result we found that the MP2 parameters predicted density with 10% deviation from the reference value (i.e., PTFE experimental melt) which makes this result is acceptable agreement with the experimental finding.

Table 22: MP2 derived parameters density test

PTFE melt density (gm/cm^3)	This research	The experimental research
	1.79	2.0
Deviation (%)	10%	0.0%

5.2 Glassy Transition Temperature Analysis

As pointed out earlier, modeling the PTFE glassy transition temperature involved performing two major tasks. We began by building PTFE amorphous structure. To this end, we used a PTFE chain consisting of 64 carbon and 130 fluorine atoms. Next, we utilized Material Studio (Module, 2011) amorphous module to obtain the amorphous structure. Figure 50 displays the resulting amorphous structure with 10 chains where the total number of atoms equal to 1940. The amorphous builder is based on Monte Carlo algorithm which reduces the atoms VDW radii by at least 70% to prevent the VDW repulsive interactions between atoms. In addition, it should be noted that when using the Monte Carlo algorithm ensures that the dihedral angels will not overlap but rather follow the Boltzmann distribution, with the amorphous structure successfully built, the next task was to compute the glass transition temperature by performing a relaxation simulations. The relaxation procedure started

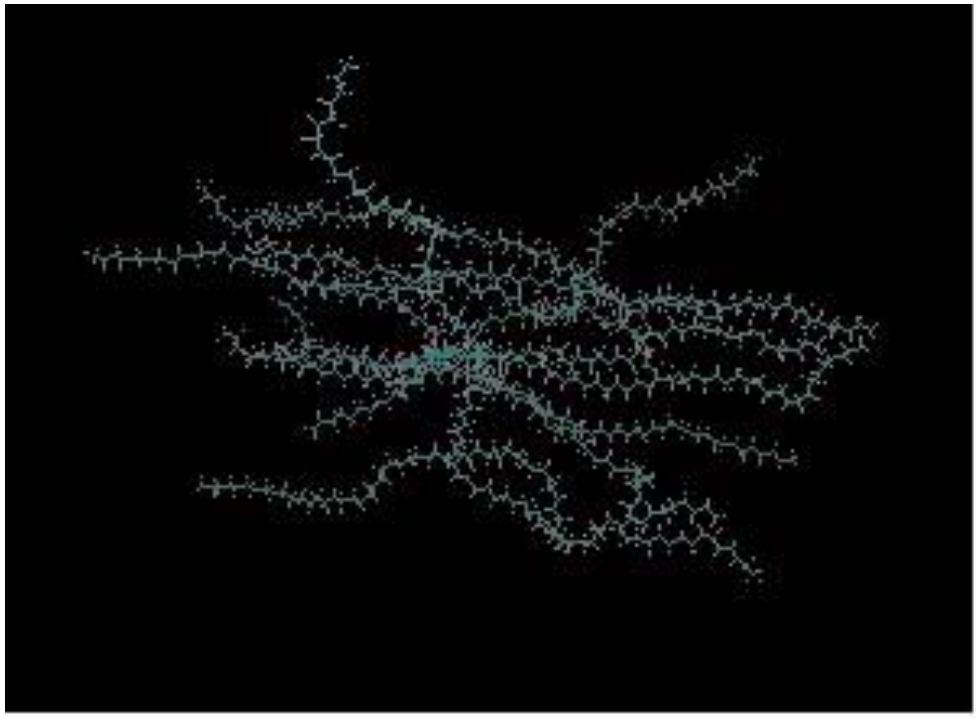

Figure 50: PTFE amorphous structure using Material Studio

with NVT MD simulations at high temperature (550K), where the macroscopic boundary conditions were kept constant. This step was followed by NPT MD simulations at high temperature (550K). As the system moved from one equilibrated state to another, it was minimized and equilibrated using NPT. Finally we performed NPT annealing to the desired temperature for enough time to reach the thermodynamic equilibrium. Three target temperatures were used in the annealing process as follows: a temperature lower than the glassy transition temperature (i.e, 150K), a temperature around the glassy transition temperature (i.e, 350K), and a temperature higher than the glassy transition temperature (i.e, 450K). The cooling process was performed gradually to allow any needed transformations to occur. Otherwise, the system would be quenched to unfavorable minimum local energy. For example, the relaxation to a temperature lower than PTFE glassy transition temperature takes 50000 fs with cooling rate of 1.0K/ps as

shown shown in Figure 51. It should be noted that high cooling rates were used for the high temperature targets and low cooling rates for low temperature targets, for example for the annealing to 450K and 350K we use the high rate while for the annealing to 150K we use the slow cooling rate. The relaxation simulations were performed with 1 femtosecond (fs) timestep. Nose-Hoover algorithm was used to control pressure (Martyna et al., 1994). Further, to control intermolecular interactions, a 12 A° cut-off radius and particle mesh Ewald method (Darden et al., 1993) were used.

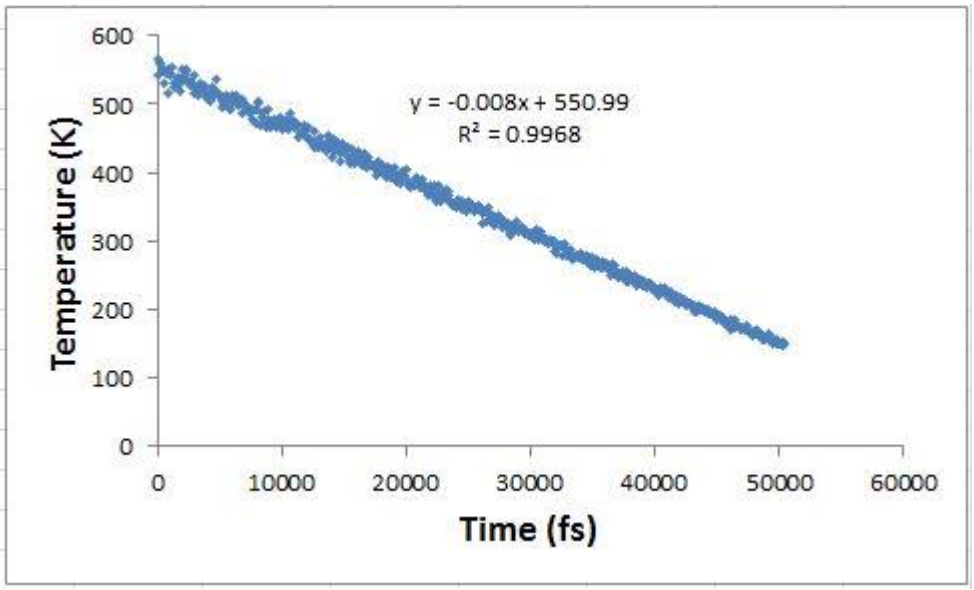

Figure 51: Low rate PTFE relaxation

The glassy transition temperature for PTFE is represented in Figure 52. The kink in the volume evolution as a function of temperature appears about 398K, which falls in the glassy transition temperature between 160K to 400K from the experimental approach findings, for example Sperati and Starkweather (1961)found that TFE glassy transition temperature to be around 160K, (Araki, 1965)found PTFE glassy transition temperature to be around 396K for

different PTFE mixture samples. This wide range would be due to the different in molecular weight between the TFE and PTFE.

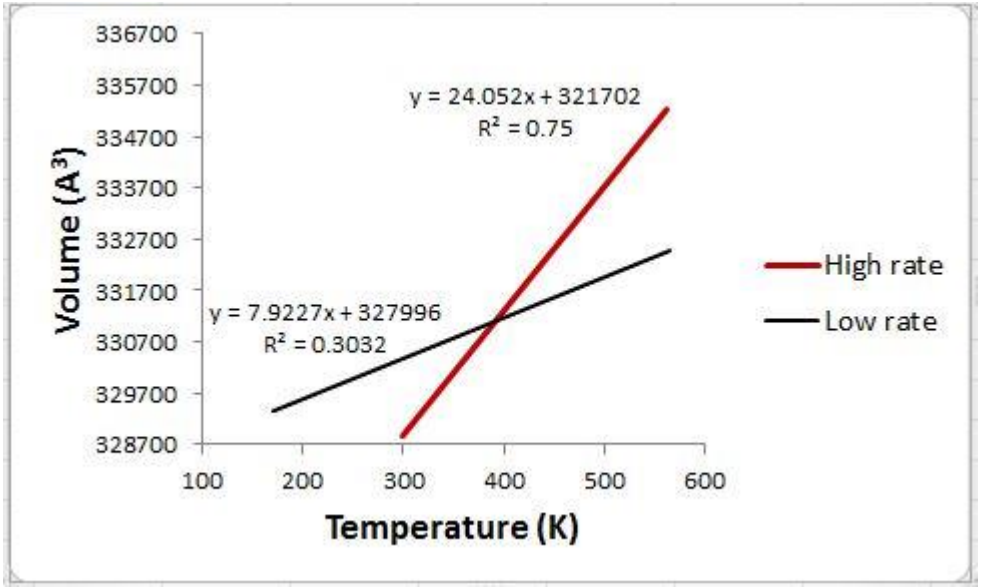

Figure 52: PTFE glassy transition temperature is computed from volume evolution as a function of temperature

6 Different PTFE Molecular Weight Cells Analysis

The purpose of this chapter is to present tasks which involved the following: first, building PTFE cells with different molecular weight (i.e., different chain lengths), specifically C_5F_{12}, C_8F_{18}, and $C_{11}F_{24}$. Second, generating the amorphous structure using molecular dynamics simulation, under periodic boundary conditions using NAMD package. Third, testing PTFE melt phase properties. Fourth, predicting the glassy transition temperature for the PTFE cells and analyzing properties that are affected by the glassy transition behavior.

6.1 PTFE Cells

I completed building all PTFE periodic cells, the simulation cells took the shape of an orthogonal monolayer which was created from the parallel arrangement of a number of single chains using VMD/TCL scripting language. Figure 53, Figure 54, and Figure 55 illustrate the cells. Table 23 below shows the cells information (i.e., number of chains and atoms). By the completion of this task, all the PTFE simulation cells consisted of 196 chains. As an example the size of the periodic cell of C5 is 92*8*92 $A^{\circ 3}$, and the distance between the neighboring chains is approximately 6.89 A°. This distance was calculated based on the density of PTFE (i.e., 1.6 gm/cm^3). In addition, the PSF file for the polymer configuration (196 chains membrane) was created with 196 segments. At this point, the PDB, the PSF, the parameter, and the configuration files are ready for the simulation process.

Table 23: PTFE Cells

Cell	# of chains	# of Atoms
C_5F_{12}	196	3,332
C_8F_{18}	196	5,096
$C_{11}F_{24}$	196	6,860

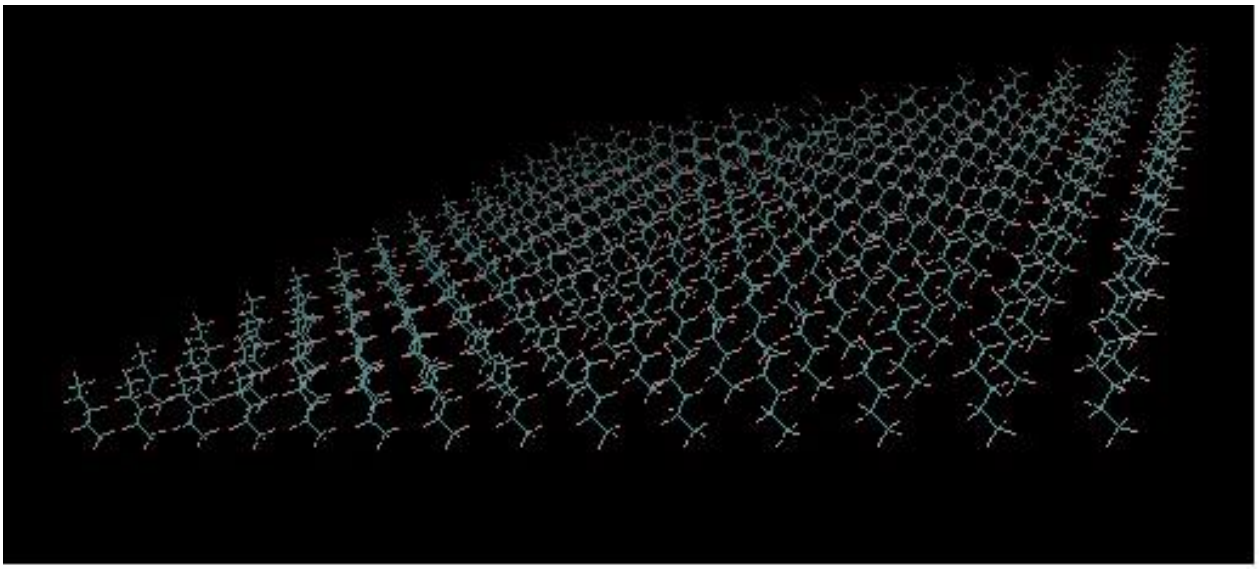

Figure 53: 196 PTFE chains of C_5F_{12}

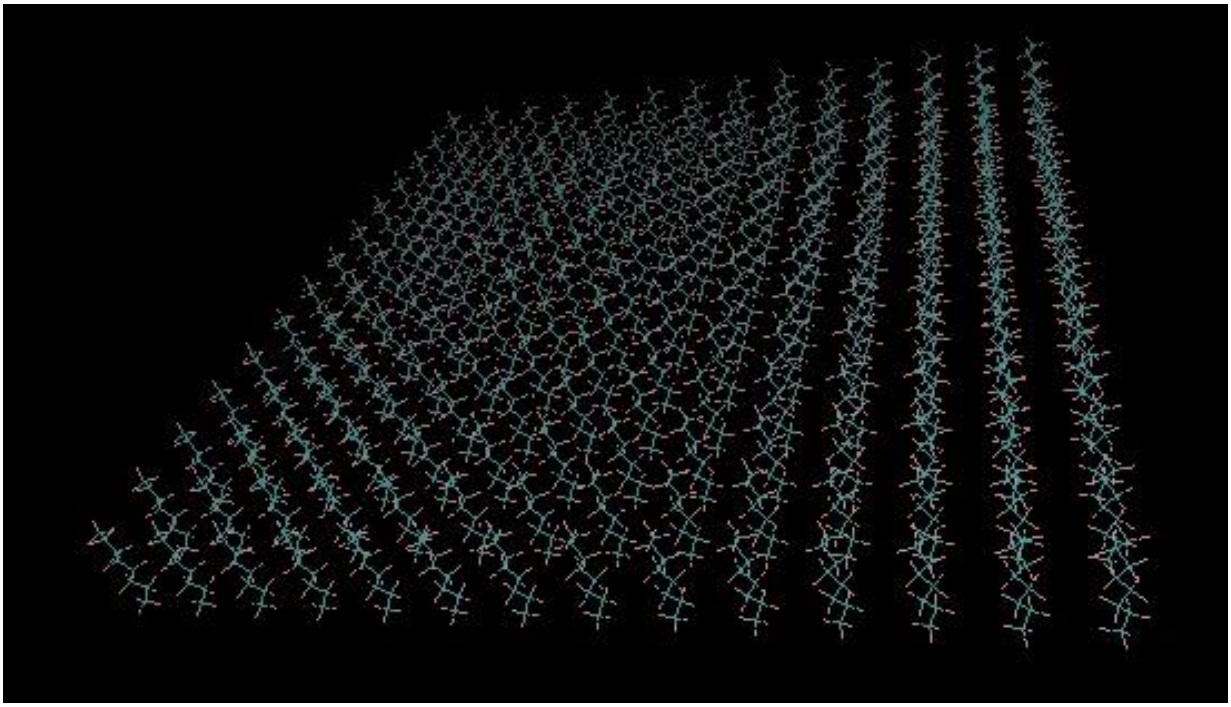

Figure 54: 196 PTFE chains of C_8F_{18}

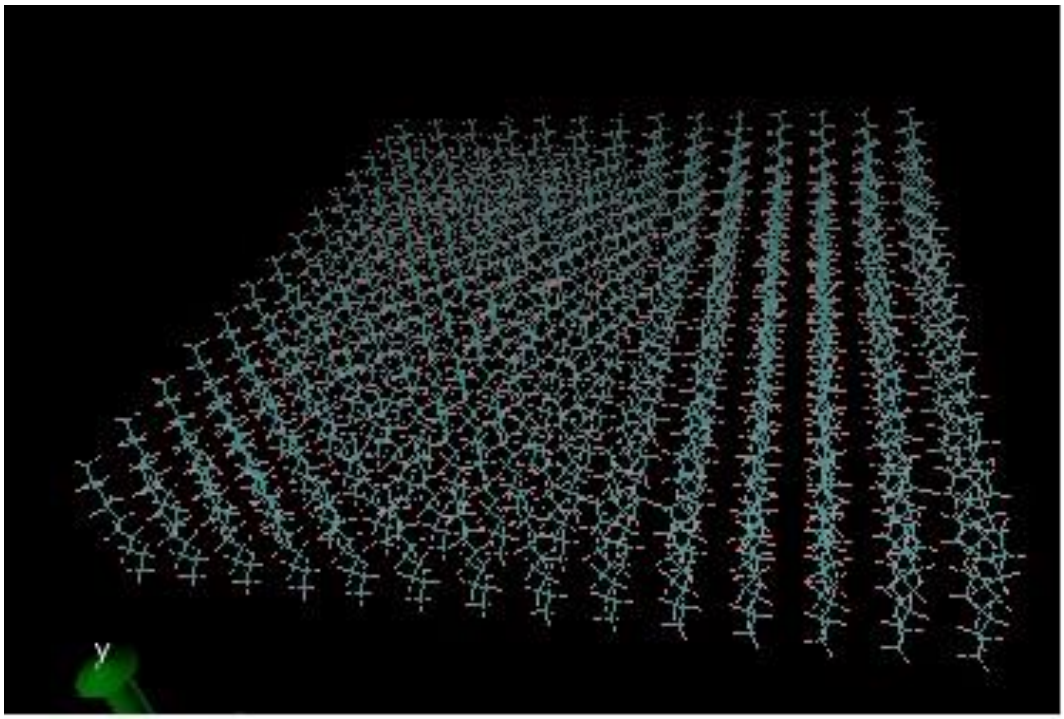

Figure 55: 196 PTFE chain of $C_{11}F_{24}$

6.2 Amorphous Phase

The amorphous structure refers to the disarrangements of the molecules where the carbon chains are disordered due to the absence of crystallinity. The glassy transition temperature is predicted with amorphous structure at melt phase, so I performed MD simulations at different temperatures for each cell to estimate where the liquid phase is.

6.2.1 C_5F_{12} Melt Phase

MD simulations were performed for the cell, which is tested under different temperatures to predict the phase, Table 24 shows in detail the phase at each temperature

Table 24: C_5F_{12} phases at different temperatures

Temperature (K)	Phase
295	Gas
290	Gas
280	Gas
270	Gas
260	Gas
250	Gas
240	Gas
230	Gas
220	Gas
210	Gas
200	Liquid

Figure 56 and Figure 57 show the gas phase at 230K and 260 respectively.

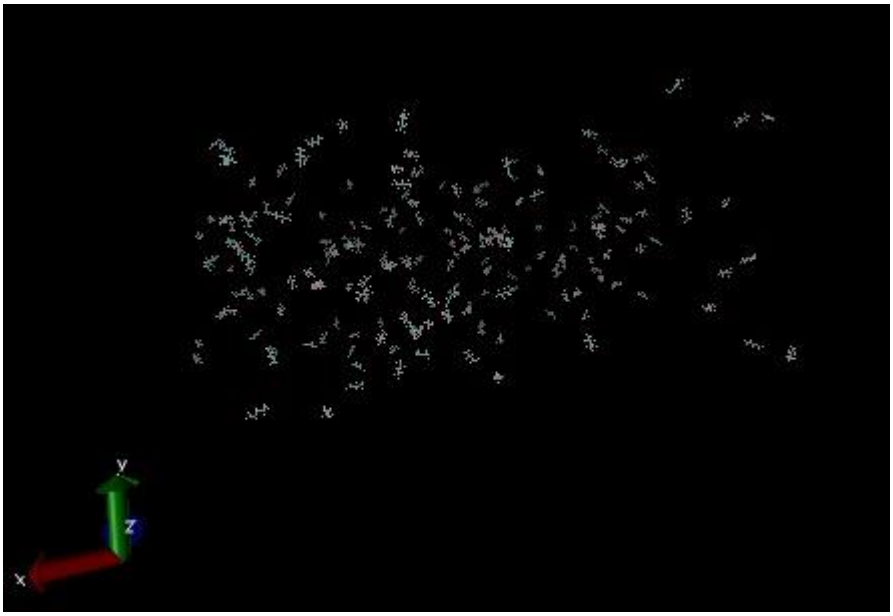

Figure 56: Gas phase of C_5F_{12} at 230K

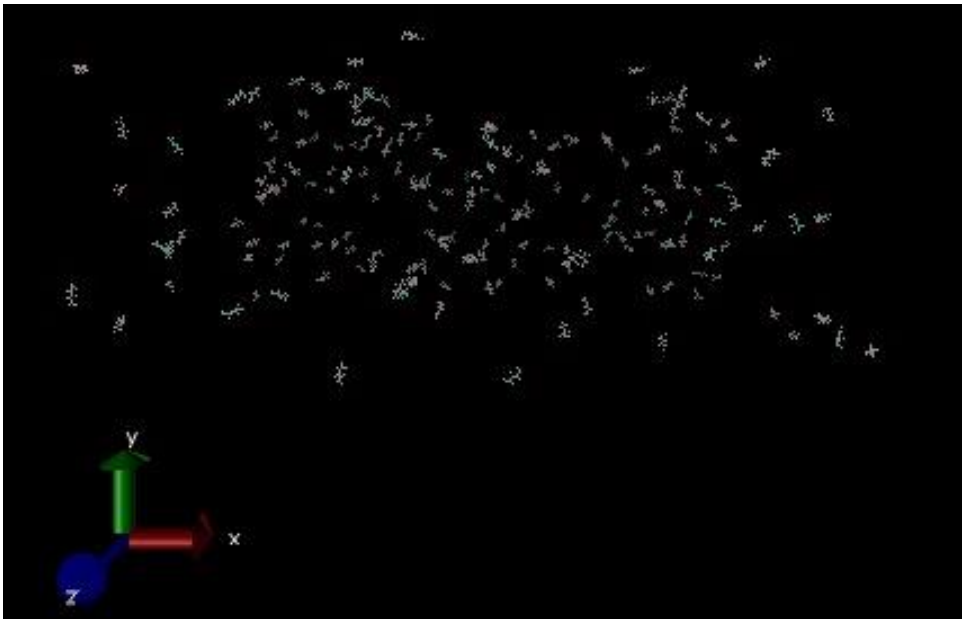

Figure 57: Gas phase of C_5F_{12} at 260K

The liquid phase starts to appear at 200K as shown in Figure 58 and Figure 59, the simulations time was 100 ns

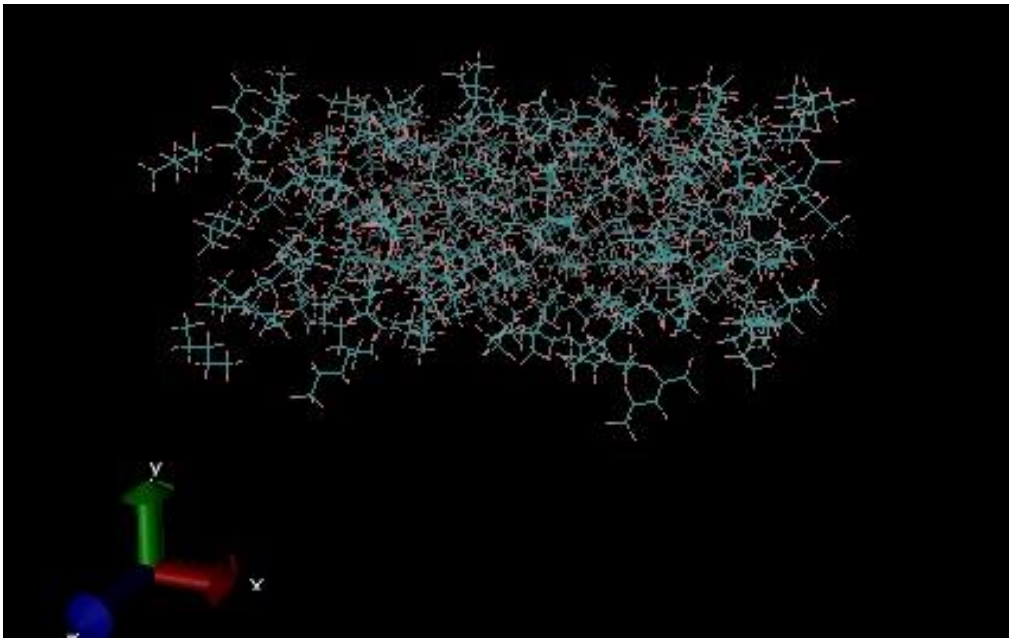

Figure 58: C_5F_{12} side view at 200K after 100 ns

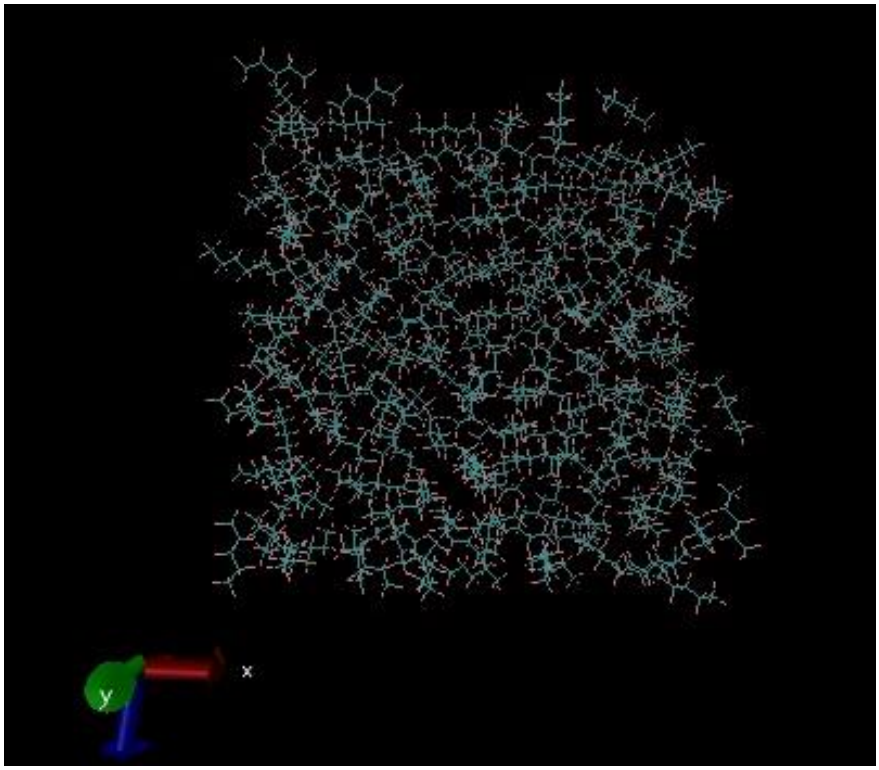

Figure 59: C_5F_{12} top view at 200K after 100 ns

6.2.2 C_8F_{18} Melt Phase

MD simulations were performed for the cell that is tested under different temperatures to predict the phase, Table 25 shows in detail the phase at each temperature

Table 25: C_8F_{18} phases at different temperatures

Temperature (K)	Phase
378	Gas
375	Gas
365	Gas
350	Gas
340	Gas
330	Liquid

Figure 61 show the gas phase at 350K and 340 correspondingly.

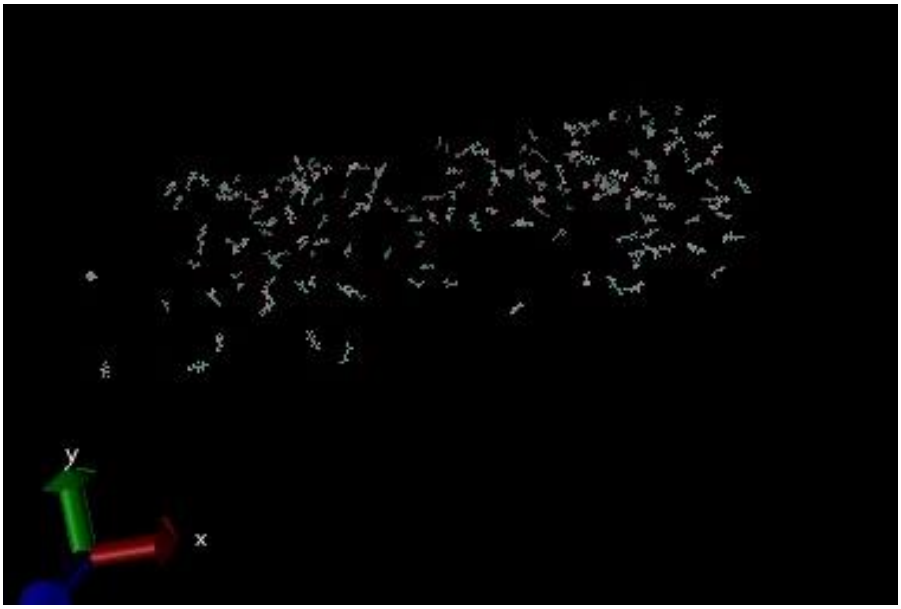

Figure 60: C_8F_{18} gas phase at 350K

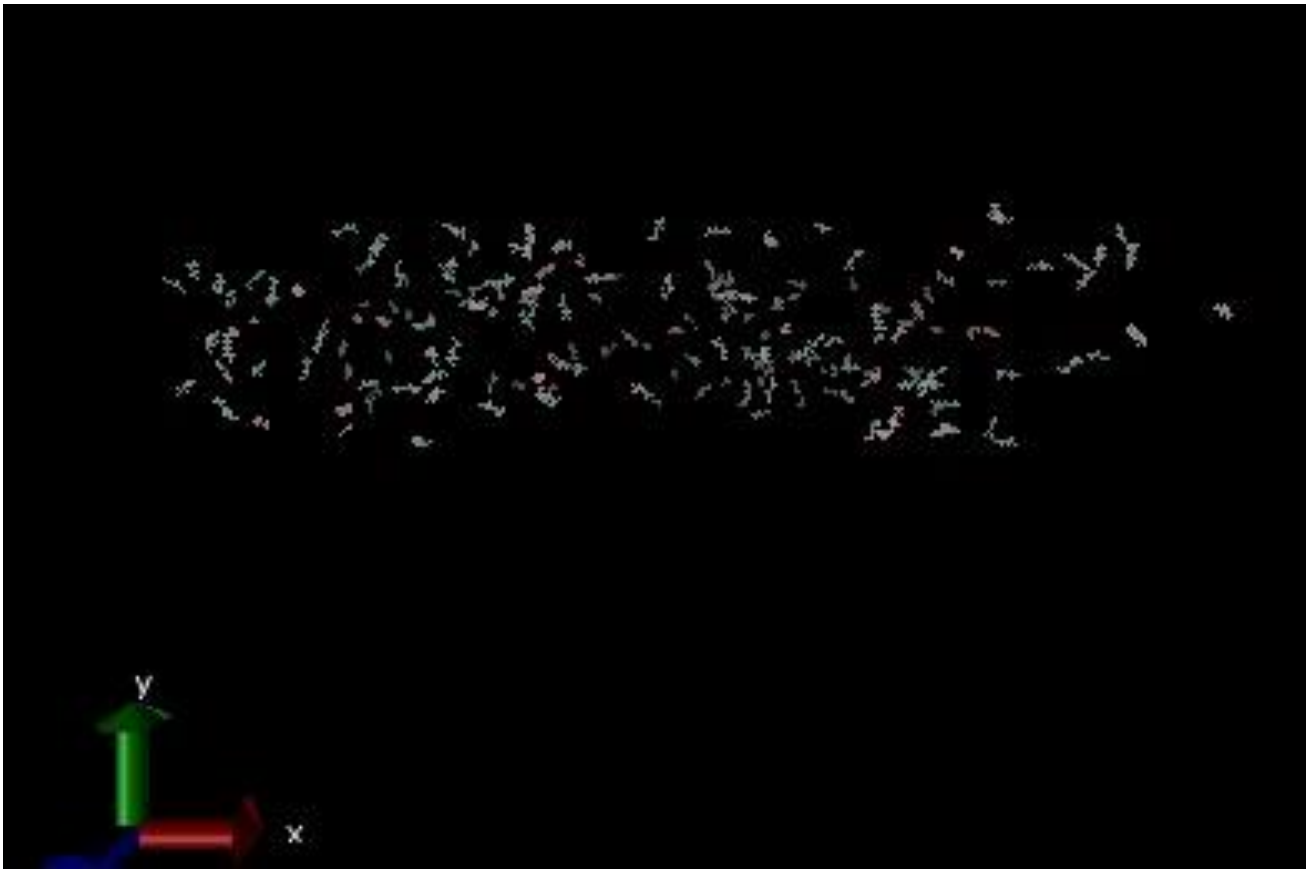

Figure 61: C_8F_{18} gas phase at 340K

The melt phase starts to appear at 330K as shown in Figure 62 and Figure 63, the simulations time was 100 ns

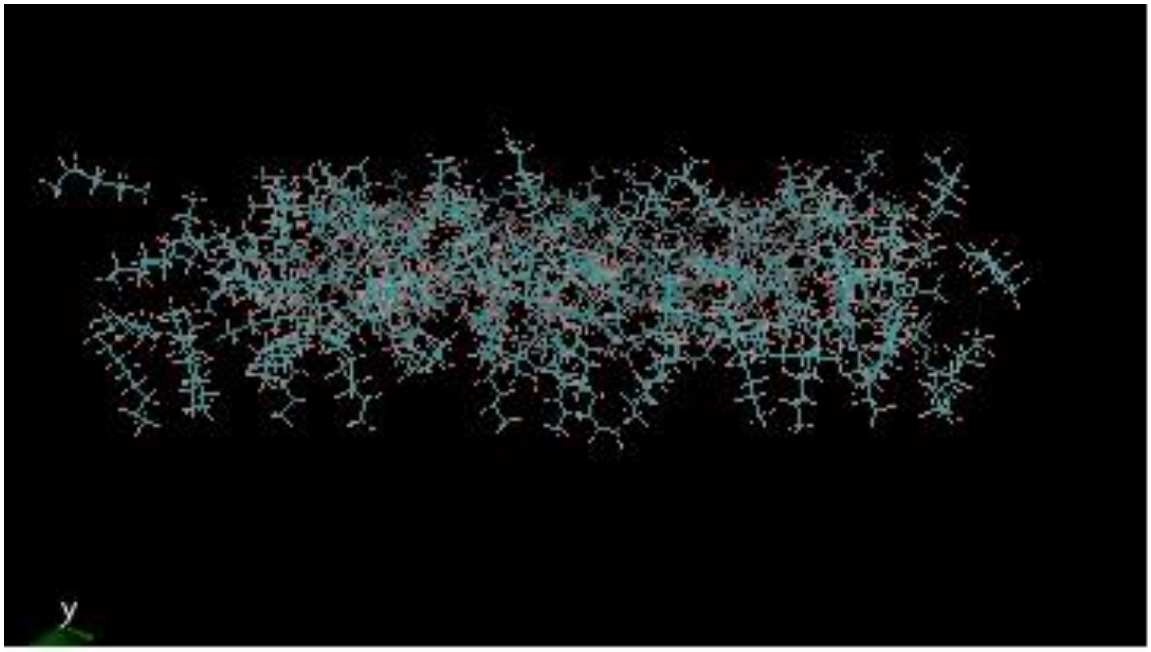

Figure 62: C_8F_{18} side view at 330K after 100 ns

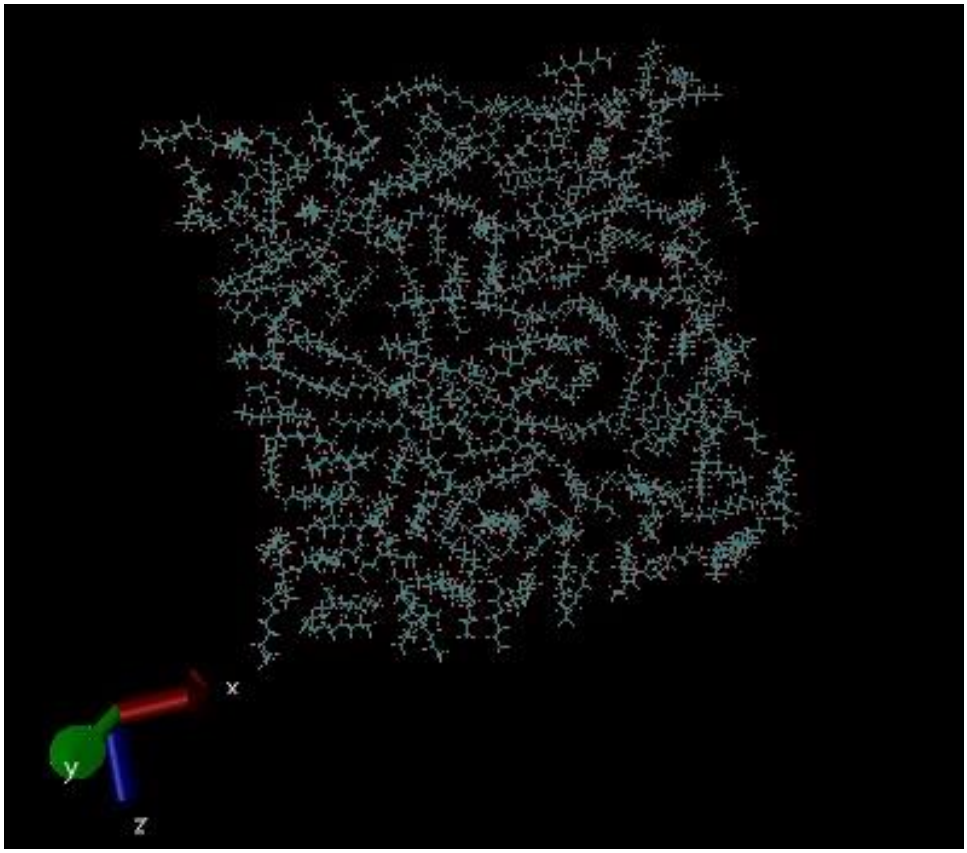

Figure 63: C_8F_{18} top view at 330K after 100 ns

6.2.3 $C_{11}F_{24}$ Melt Phase

MD simulations were performed for the cell that is tested under different temperatures to predict its phase, Table 26 shows in detail the phase at each temperature

Table 26: $C_{11}F_{24}$ phases at different temperatures

Temperature (K)	Phase
430	Gas
400	Gas
390	Gas
380	Gas
370	Liquid

Figure 64 and Figure 65 show the gas phase at 400K and 390 respectively. The melt phase for this cell appears at 370K as shown in Figure 66 and Figure 67. It should be noted that the liquid phase simulation was performed for 100 ns.

Figure 64: $C_{11}F_{24}$ gas phase at 400K

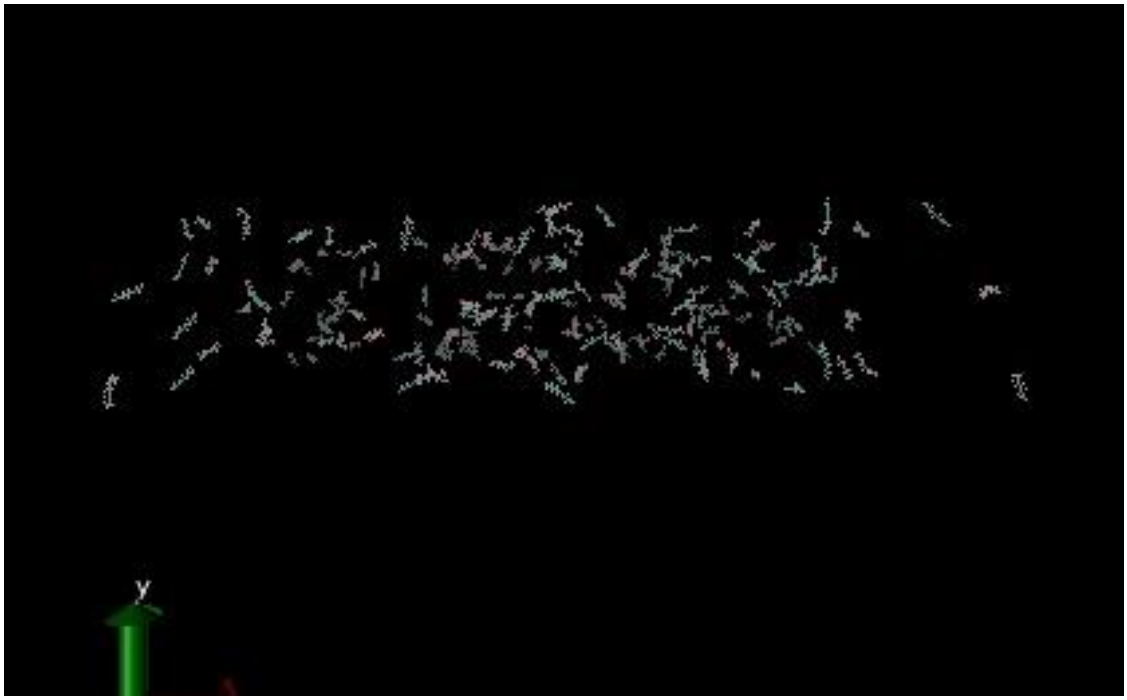

Figure 65: $C_{11}F_{24}$ gas phase at 390K

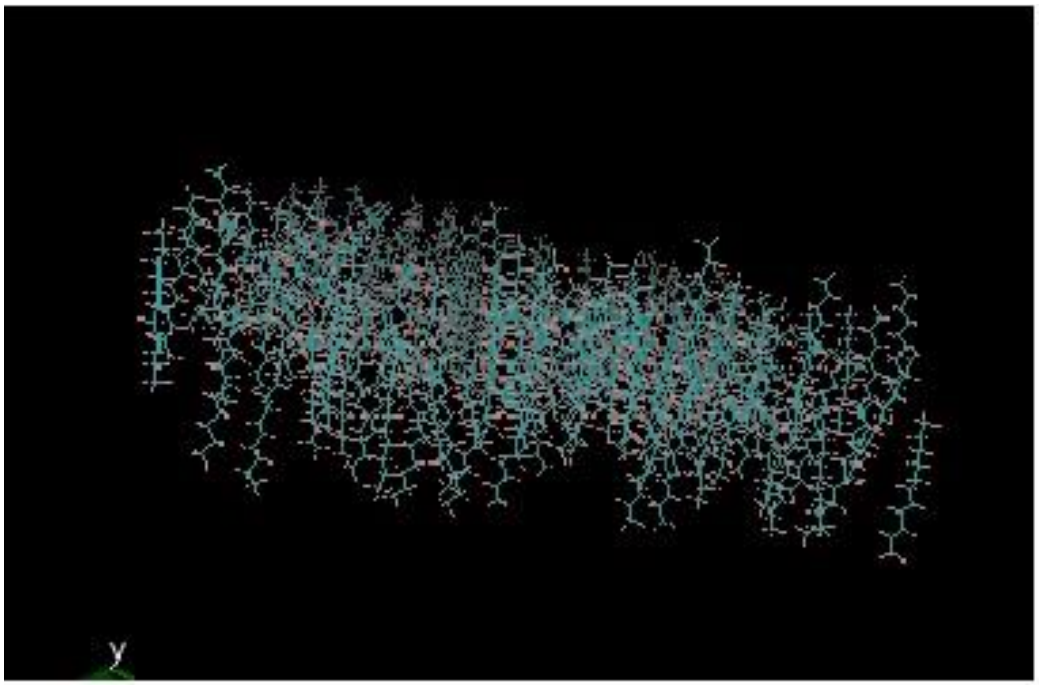

Figure 66: $C_{11}F_{24}$ side view at 370K after 100 ns

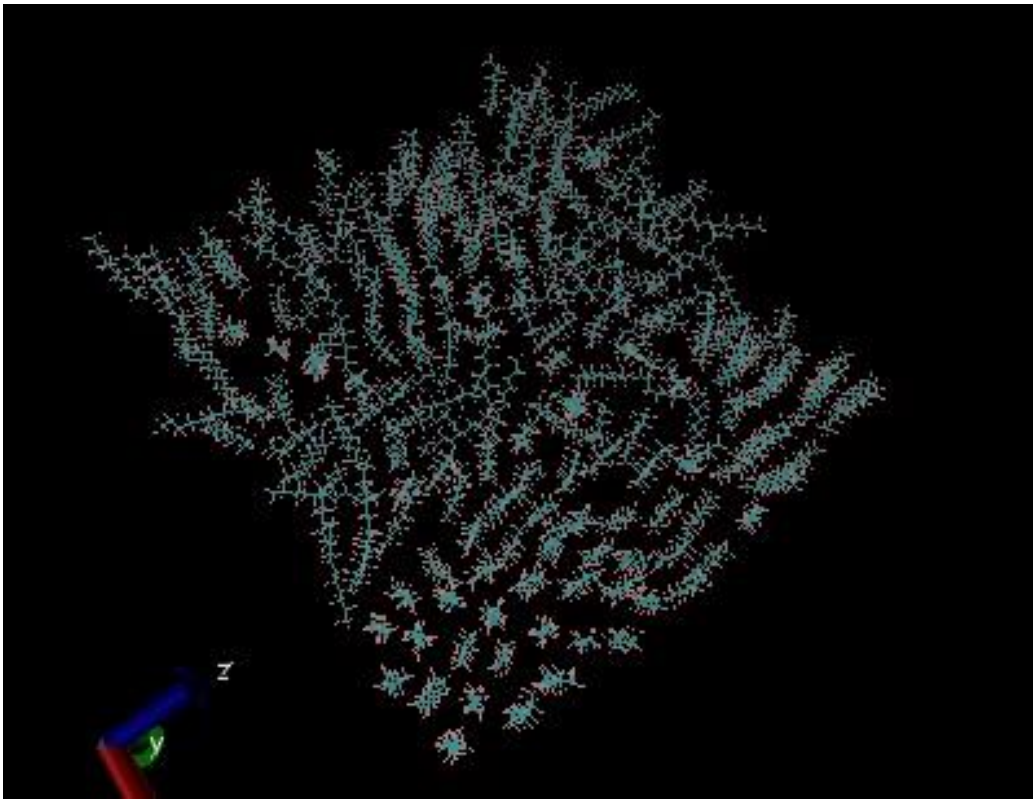

Figure 67: C11F24 side view at 370K after 100 ns

6.2.4 **Phase Assessment**

Phase in thermodynamic can be defined as state of matter in equilibrium (Venkataraman, 1997). Phases can be characterized using different method such as density. The density of solid phase and the liquid phase usually do not change dramatically, however in gas it does where the particles are far apart. As the temperature increases, the material expands or increases its volume. This indicate decrease in density, when the temperature goes down, the density usually becomes greater as illustrated in Figure 68 and Figure 70, for example in Figure 69 PTFE cell C_8F_{18} density for the melt at 330K was 1.70 gm/cm^3 ,while the gas phase at 340K the density was 0.07 gm/cm^3

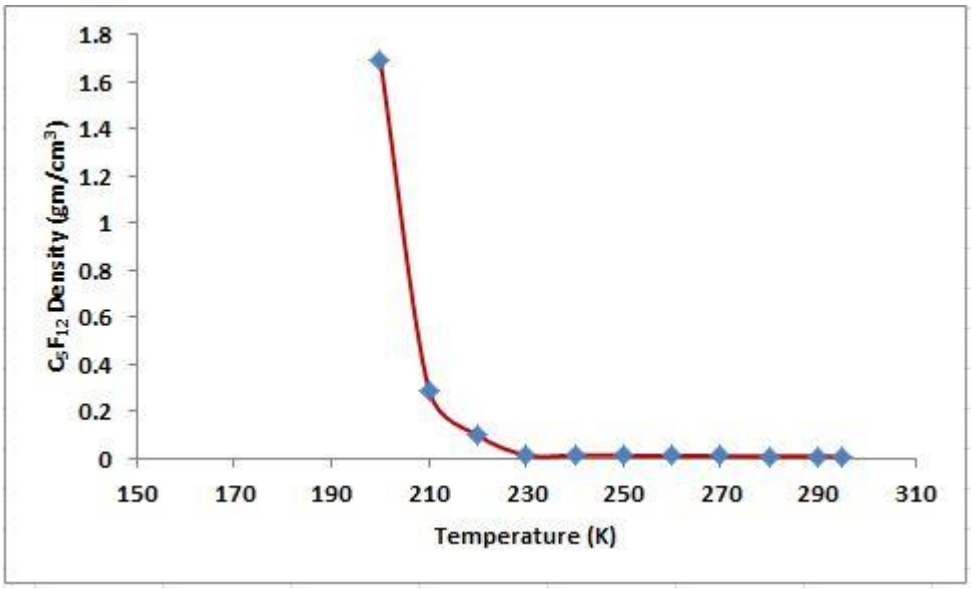

Figure 68: Density versus temperature for C_5F_{12}

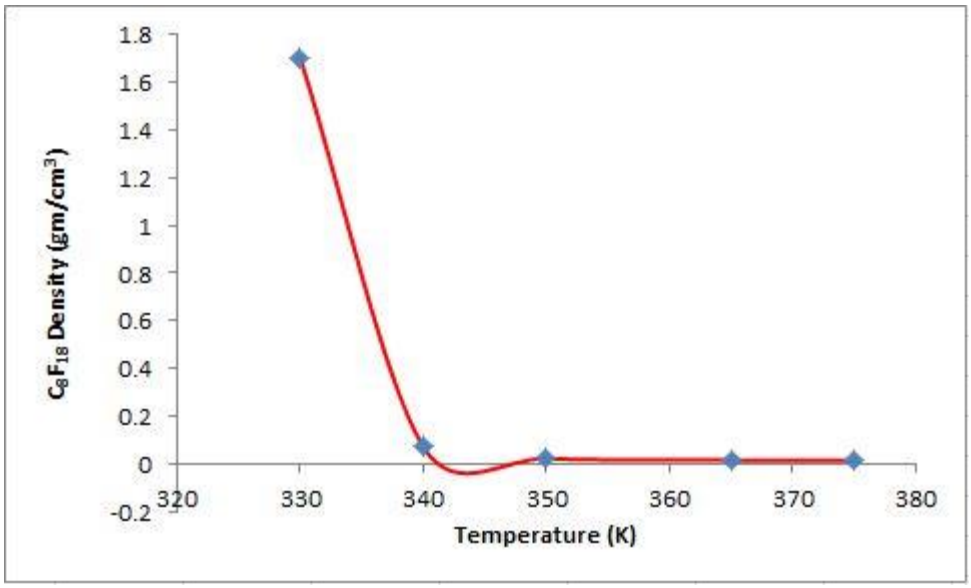

Figure 69: Density versus temperature for C_8F_{18}

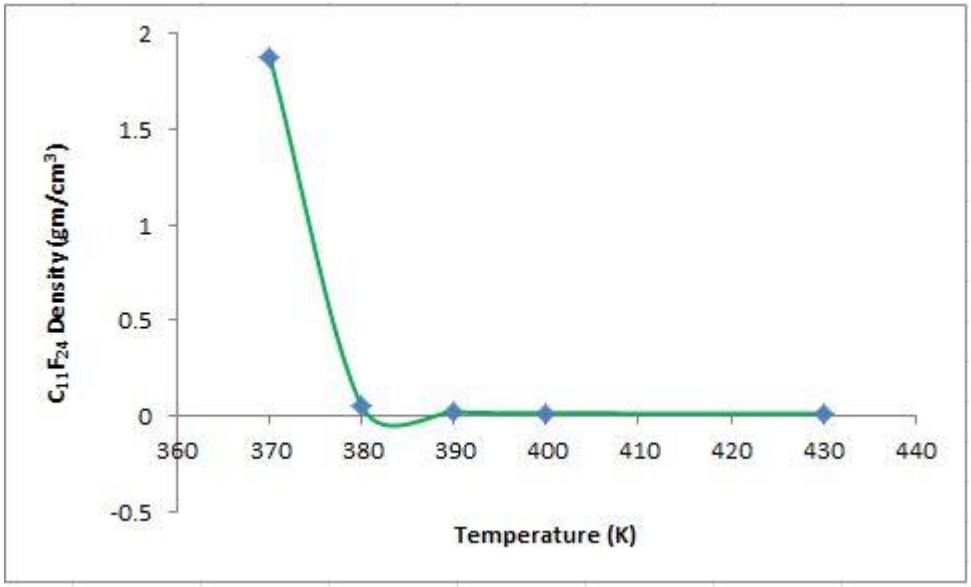

Figure 70: Density versus temperature for $C_{11}F_{24}$

In evaluating the polymer phase, reference experimental values for some cells in the melt phase exist to compare with, while for the gas phase there is no experimental nor MD simulations literature values to compare with, I use the ideal gas law to extract PTFE gas density from theory and compare it with this research finding.

$$PV = nRT \tag{6.1}$$

$$n = \frac{m}{M_w} \tag{6.2}$$

$$PV = \frac{mRT}{M_w} \tag{6.3}$$

$$\rho = \frac{PM_w}{1000RT} \tag{6.4}$$

where P is the pressure (atm), V is the volume (L), m is the mass (g) , R is the ideal gas constant (0.0821 L atm/K mol), T is the temperature (K), M_w is the molecular weight (g/mol), ρ is the density (g/cm^3). I listed an illustration for each cell at specific temperature in Table 27 to assure that PTFE at its gas phase follow the ideal gas theory for example, cell C_5F_{12} density value that is obtained from this work at 295K was about 0.012 g/cm^3 and the density value that is predicted at the same temperature using the ideal gas theory was very close and about 0.010 g/cm^3. The representations for PTFE cell using ideal gas theory are shown in Figure 71, Figure 72, and Figure 73 , where the vertical axes represents PTFE density in the logarithmic scale versus temperature, the blue line denotes this research MD simulations results while the red line displays the predicted results using ideal gas theory. The figures reassure that PTFE gas phase MD findings obey the ideal gas theory and this behavior is obvious from the corresponded two lines (i.e., MD blue line and ideal gas theory red line) in a range of temperatures until PTFE starts entering the liquid phase, at this point the two lines begin to separate, each line in different path, for example C_5F_{12} cell have the two matching lines until the temperature reach 200K where the sample enter the melt phase and at this point our sample no longer fit to the ideal gas theory.

Table 27: PTFE gas density comparison

Cell	Gas Density (ideal gas theory)(g/cm^3)	Gas Density (This research)(g/cm^3)
C_5F_{12} (295k)	0.012	0.010
C_8F_{18} (375K)	0.014	0.013
$C_{11}F_{24}$ (430K)	0.015	0.012

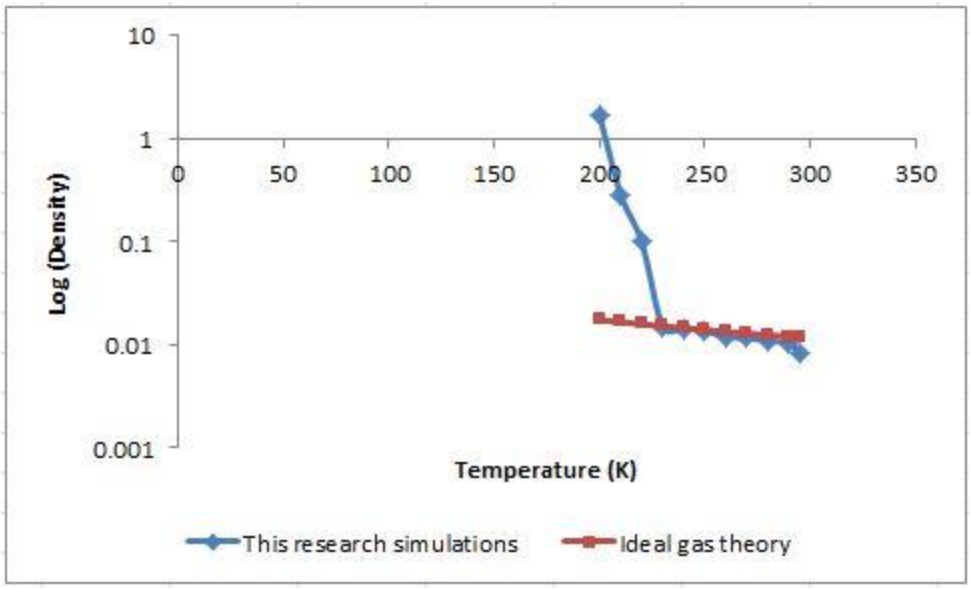

Figure 71: C_5F_{12} density versus temperature using logarithmic scale for density, the blue line shows this research values while the red line represents the ideal gas theory.

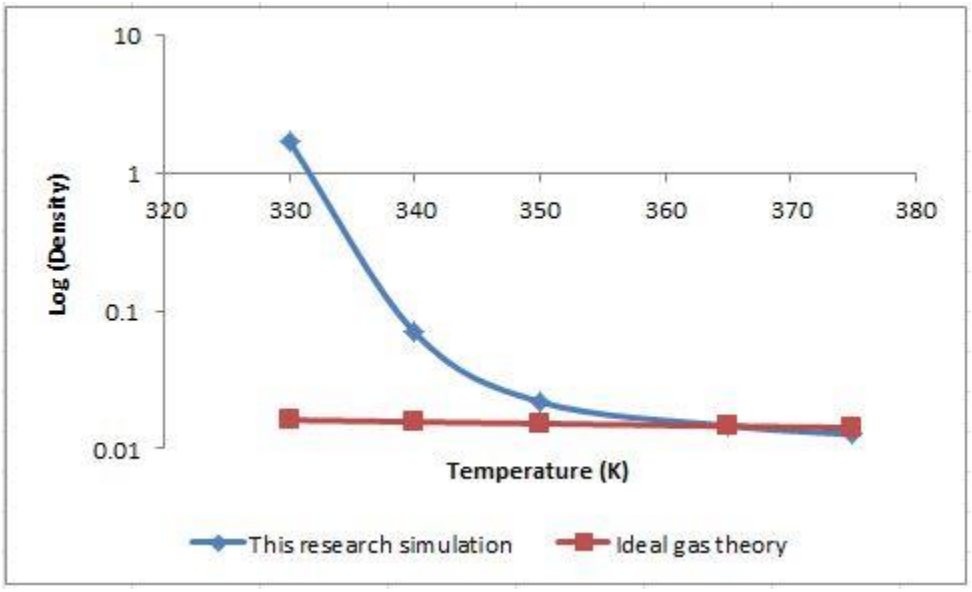

Figure 72: C_8F_{18} density versus temperature using logarithmic scale for density, the blue line shows this research values while the red line represents the ideal gas theory.

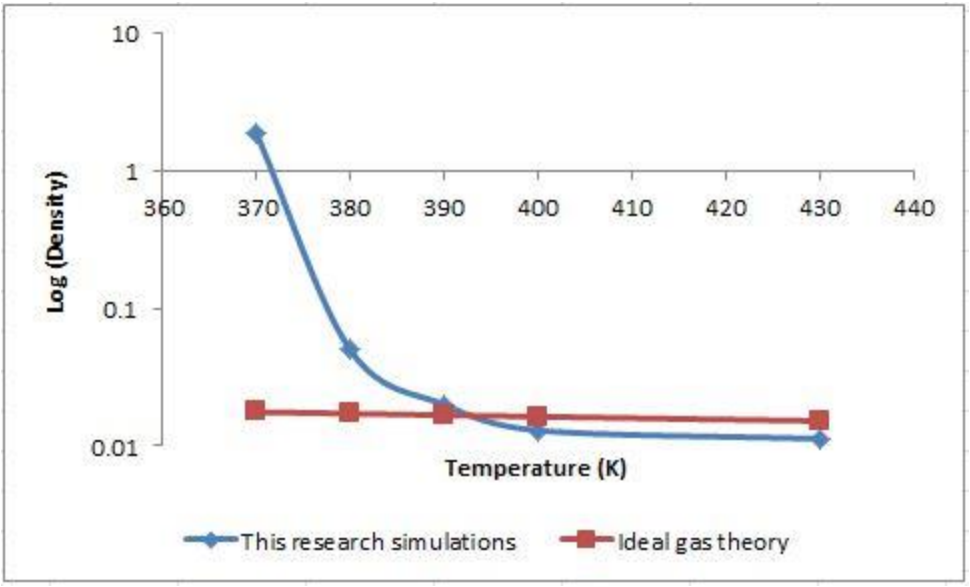

Figure 73: $C_{11}F_{24}$ density versus temperature using logarithmic scale for density, the blue line shows this research MD values while the red line represents the ideal gas theory values

6.3 Melt Phase Analysis

After obtaining the melt phase for the PTFE cells we extract some of the important properties such as boiling point, enthalpy of vaporization, density and specific heat.

6.3.1 **Boiling point**

The boiling point is defined as the point where the matter converted from the liquid phase to the gaseous phase at constant pressure. Therefore, I extract the boiling point using MD simulations by performing NPT ensemble at different temperatures, for example for PTFE cell $C_{11}F_{24}$ I submitted a simulation at 400K, the outcome was the gaseous phase as presented in Figure 64, I also the observed the phase when submitting another simulation at 380K and it was gaseous, however, at the simulation job that I submitted at 370K the melt phase was observed as Figure 66 illustrates. In conclusion, the boiling point was the point where the phase change from

the melt to gas and in our example the transition was at 380K. Table 28 represents the boiling point experimental values for PTFE mixture against the MD simulations predicted values for pure PTFE, the mixture experimental findings are closest values available to compare with under the fact that there is no pure PTFE samples in real laboratory work. For the cell C11there are no experimental PTFE mixture values to compare with, these are new results. As we see from the table the experimental values are higher than the predicted MD simulations findings from this research and this due to the difference in the materials that used in the different two approaches, I used pure PTFE in this research which is not available to be used in the experiments, in fact the researchers use PTFE mixture (i.e., also known as PTFE composite), however, this is the best available data to compare with.

Table 28: PTFE experimental and predicted boiling points

Cell	PTFE mixture experimental Boiling Point (K)	Pure PTFE predicted Boiling Point (K)
C_5F_{12}	295	210
C_8F_{18}	375	340
$C_{11}F_{24}$	N/A	380

I draw the relation between the number of carbon atoms versus the boiling point for both the predicted PTFE pure values from this research and for the PTFE mixture experimental findings. The property value increases with increasing of the molecular weight, the agreement between the predicted and the experimental is acceptable as shown in Figure 74

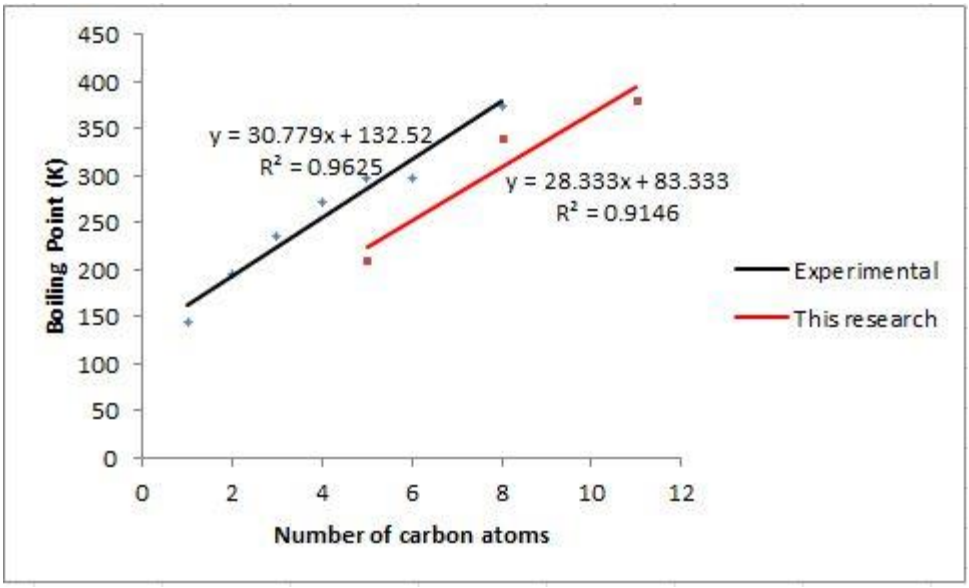

Figure 74: Molecular weight versus the boiling point

6.3.2 **Enthalpy of vaporization**

The heat of vaporization is defined as the sufficient amount of heat that is absorbed by one mole of liquid to convert it to the gaseous phase at constant temperature. Experimentally, heat of vaporization is detected by measuring the liquid enthalpy of vaporization around the boiling point using calorimetry or by predicting it using Clausius-Clapeyron equation. In MD simulations, it is measured using the total cohesive energy in the liquid phase plus the work done by volume variation or by the difference between the intramolecular and potential energies for the gaseous and liquid phase respectively (Watkins and Jorgensen, 2001, Wang and Hou, 2011).

$$\Delta H_{vap} = \Delta H_{gas} - \Delta H_{liq} = E(gas)_{intramolecular} - E(liq)_{total} + RT \quad (6.5)$$

where, ΔH_{vap} is the heat of vaporization, ΔH_{gas} is the enthalpy at the gaseous phase, ΔH_{liq} is the enthalpy at the liquid phase, $E(gas)_{intramolecular}$ is the intermolecular energy at the gaseous

phase, $E(liq)_{total}$ is the total energy at the liquid phase, R is the ideal gas constant, and T is the temperature. The term RT is equal to the PV work term and it is negligible for liquids.

The predicted enthalpy of vaporization for the PTFE cells is represented in Table 29. As we see from the table that the MD simulations values are higher than the experimental and that is due to the difference in time scales that are used in the two approaches in hand and to the difference in material as I mentioned before in the other hand, I used a pure PTFE while the experimental approach used the PTFE mixture. In addition, I compared this research results with PTFE MD simulations literature (Okada et al., 1999, Watkins and Jorgensen, 2001) and with experimental findings as shown in Figure 75 . There is a good agreement between the predicted values and the experimental ones. The enthalpy of vaporization as a property increases with increasing the molecular weight, this behavior is clear from this research results and from the experimental one as well, however, the C11F24 cell results in erratic trend where the heat of vaporization is about 20.13 cal/g that is lower than C8F18 with value of 25.10 cal/g. it seems that this inconsistent behavior had been noticed before in the experimental approach, more specifically for the cell C7F16 it has heat of vaporization about 19 cal/g, C6F14 heat of vaporization about 21 cal/g and C8F18 about 22 cal/g (Hougham, 1999). We noticed that cells with odd number of carbon atoms may have a trend that is inconsistent with the assumption that the property should increase with increasing the molecular weight and this is what exactly happens with C11 F24 cell

Table 29: PTFE experimental and calculated enthalpy of vaporization

Cell	Calculated Enthalpy of Vaporization (cal/g)	Experimental Enthalpy of Vaporization (cal/g)
C_5F_{12}	23.96±0.33	21.00
C_8F_{18}	25.10±0.42	22.00
$C_{11}F_{24}$	20.13±0.40	N/A

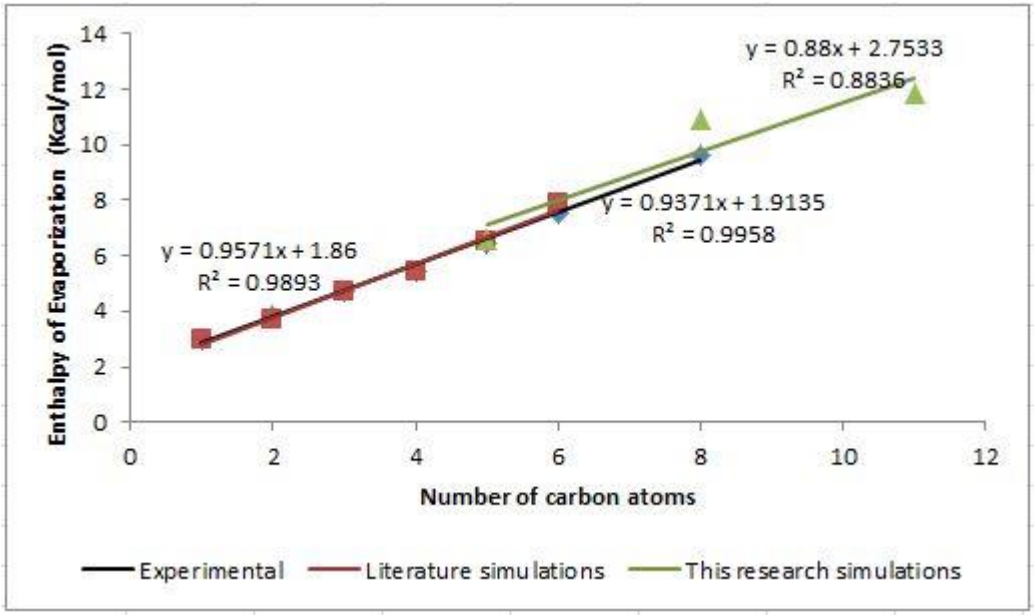

Figure 75: Enthalpy of vaporization vs MW

6.3.3 **Specific Heat**

Specific heat is a physical property defined as the amount of heat that is needed to raise unit mass by one degree of temperature. In MDS using NPT ensemble, specific heat is measured using energy fluctuations (Rajabpour et al., 2013, Li et al., 2008, Allen and Tildesley, 1987)

$$c_p = (\partial E/\partial T)_p \tag{6.6}$$

$$c_p = \frac{\langle \partial E^2 \rangle_{NPT}}{k_B T^2} \tag{6.7}$$

where c_p is the specific heat that is calculated at NPT ensemble, k_B is Boltzmann constant and T is the temperature. The fluctuations ∂E equal to$\langle E^2 \rangle - \langle E \rangle^2$, the most effective were the Columbic potential and Lennard Jones fluctuations as shown in Figure 76 and Figure 77 respectively for C11 cell, where the energy oscillates near its mean.

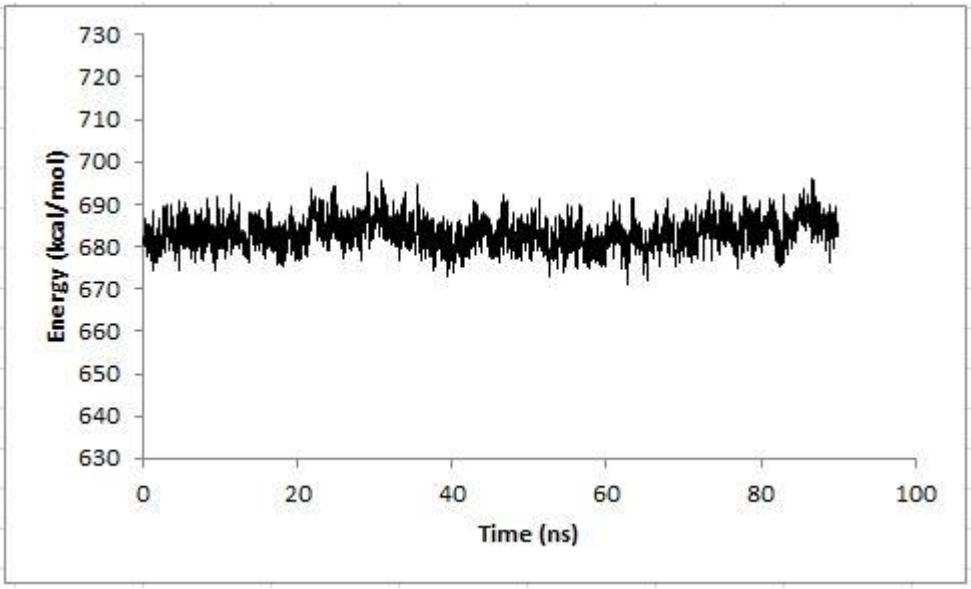

Figure 76: The electrostatic energy fluctuations

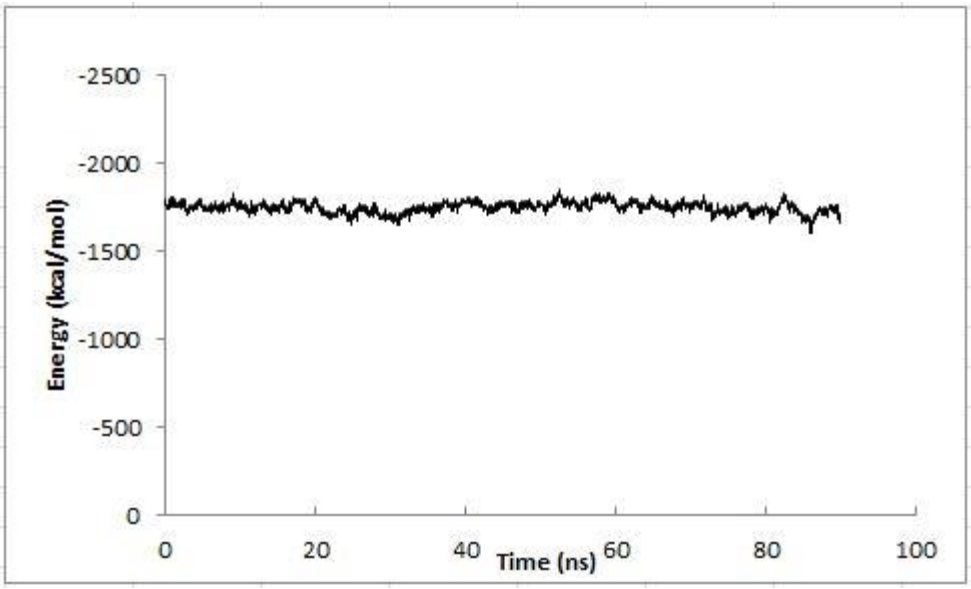

Figure 77: Van der Waals energy fluctuations

The specific heat values for the cells are presented in Table 30 , the table presents the calculated values and the experimental values (Yaws, 2008), for both approached the property increases with increasing the molecular weight. The agreement between the two approaches is acceptable although I use a pure PTFE and the experimental approach uses PTFE mixture, it should be noted that the MD simulations literature did not research the specific heat property for PTFE before.

Table 30: PTFE specific heat values

Cell	Predicted Specific Heat (KJ/mol K)	Experimental Specific Heat (KJ/mol K)	MDS Literature Specific Heat (KJ/mol K)
C_5F_{12} (200K)	0.1100±0.0007	0.2000	N/A
C_8F_{18} (330K)	0.1700±0.0009	0.2400	N/A
$C_{11}F_{24}$ (370K)	0.1710±0.0010	N/A	N/A

6.3.4 **Density**

Density, also known as the volumetric mass density is defined as the polymer mass per its volume. I calculated PTFE cells densities after 100 ns of complete equilibration with NPT ensemble simulations, where the property (i.e., density) equilibrate and fluctuates around its mean value as shown in Figure 78, Figure 79 and Figure 80, in MD simulations I calculate Density (ρ) where PTFE mass M divided by average volume $\langle V \rangle$ of the cell box.

$$\rho = M/\langle V \rangle \tag{6.8}$$

Table 31 represents the density values compared with the experimental ones (Hougham, 1999, Yaws, 2008), in addition I compared this research values with the MD simulations literature as shown in Figure 81, it should be noted that the MD simulations literature investigate density for PTFE small oligomers up to six carbon atoms and the experimental literature examines the oligomers with even number of carbon atoms, while this research investigate oligomers that are larger than six carbon atoms and molecules with odd number of carbon atoms such as $C_{11}F_{24}$.

The density as mechanical property show increase in its value with increasing the molecular weight (MW) for the experimental and MD approaches.

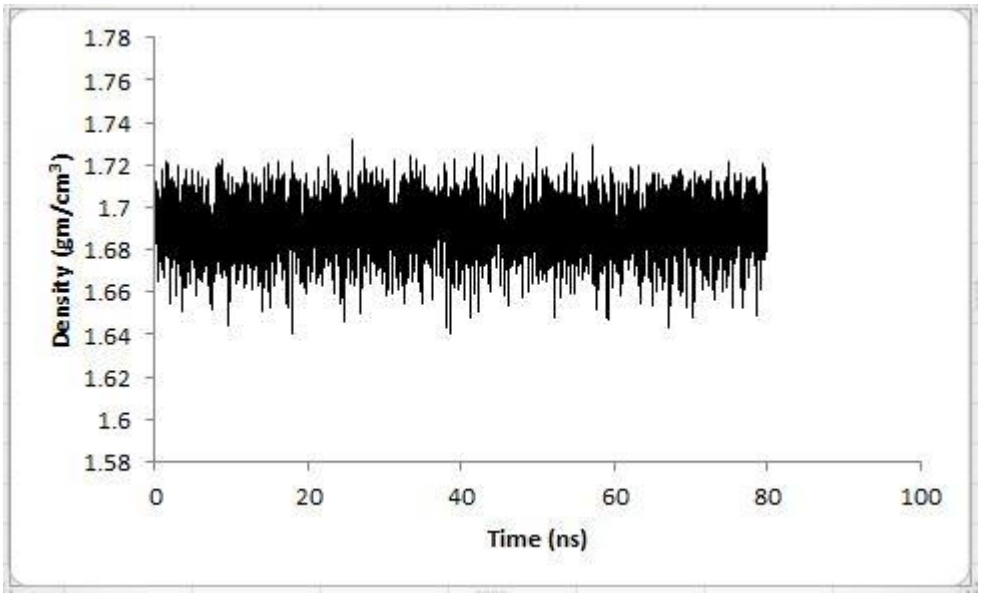

Figure 78: C_5F_{12} density versus simulation time

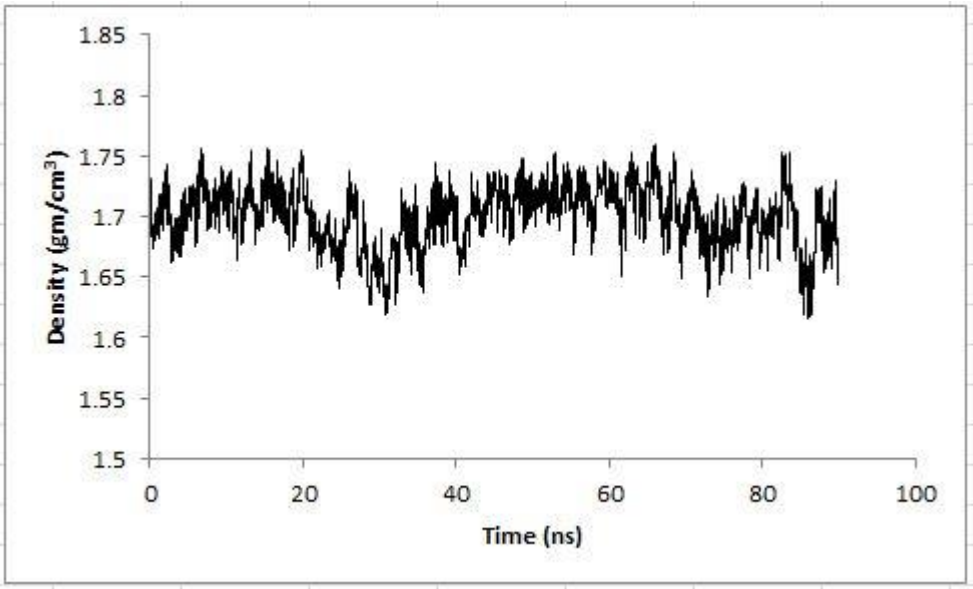

Figure 79: C_8F_{18} density versus simulation time

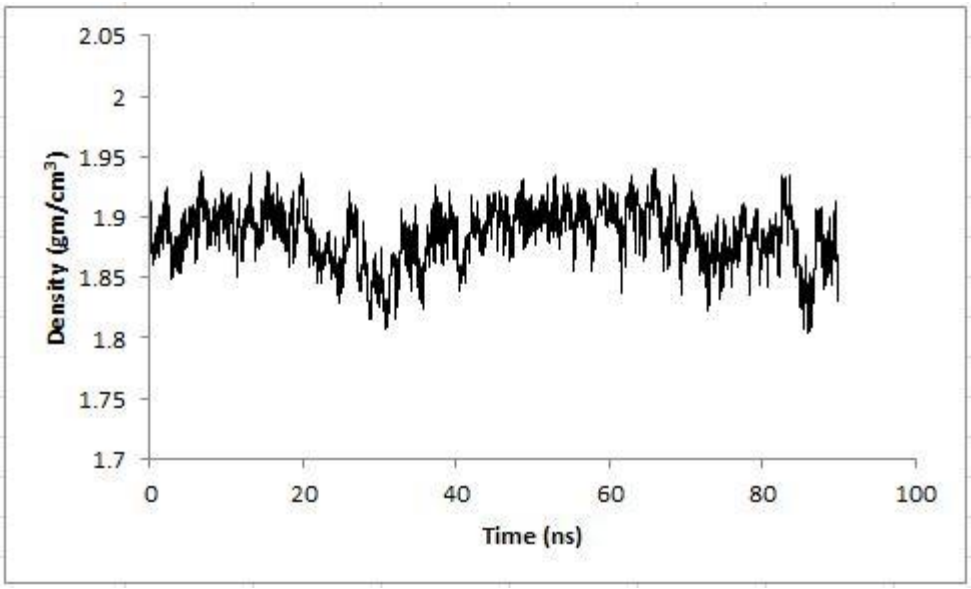

Figure 80: $C_{11}F_{24}$ density versus simulation time

Table 31: PTFE density values for different molecular weights

Cell	Predicted Density (gm/cm^3)	Experimental Density(gm/cm^3)
C_5F_{12}	1.69±0.017	1.60
C_8F_{18}	1.71±0.030	1.77
$C_{11}F_{24}$	1.88±0.031	N/A

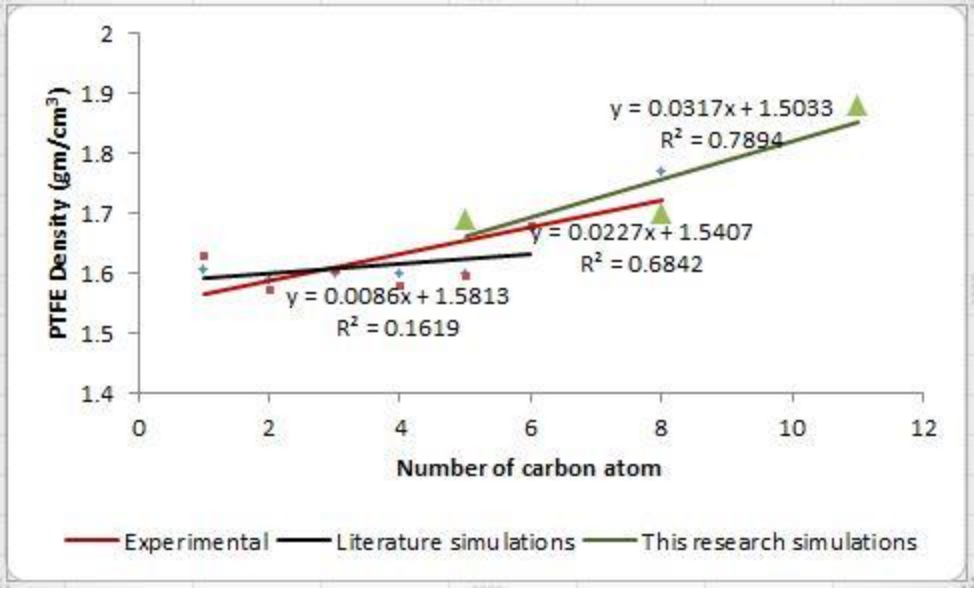

Figure 81: PTFE density versus molecular weight

6.4 Glassy Transition Temperature Analysis

The glassy transition temperature can be measured at the phase transition; that is when a change in the volume occurs due to the system passing the glassy transition temperature. At the point of transition, changes in the volume due to the annealing process versus the temperature The intersection between the high cooling rate line and the low cooling rate line determines the glassy transition temperature.

6.4.1 **Density**

Density is one of the properties that affected by temperature changing, and therefore phase transition due to glassy transition temperature where density deviates without volume discontinuity. I extract the glassy transition temperature for cell C_5F_{12}, which equals to 193K

using density as shown in Figure 82. In MD simulations I calculate Density (ρ) where PTFE mass M divided by average volume $\langle V \rangle$ of the cell box as indicated in equation 6.8

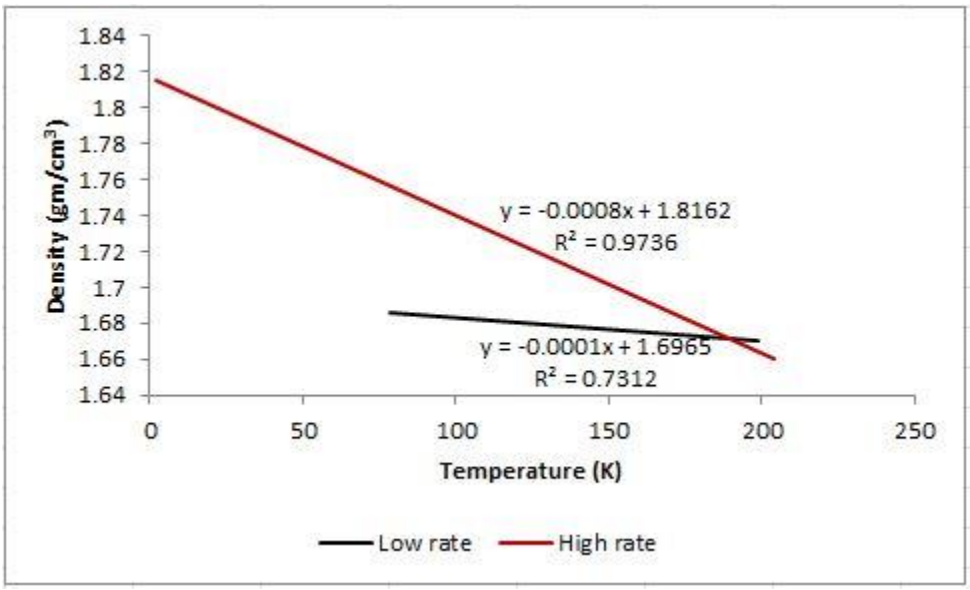

Figure 82: Density as a function of temperature for C_5F_{12}

6.4.2 **Specific Volume**

Specific volume is the reciprocal of density, this property is important in material science where it is used for many concepts such as the molar volume and partial molar volume. As density, specific volume is affected by cooling temperatures after passing the melting point, this cooling follows by entering the glass phase where specific volume differs without volume discontinuity. I extract the glassy transition temperature for cell $C_8F_{18,}$ which equals to 291K as shown in Figure 83, using MD simulations I calculate the specific volume as the inverse of Density (ρ)

$$\nu = 1/\rho \tag{6.9}$$

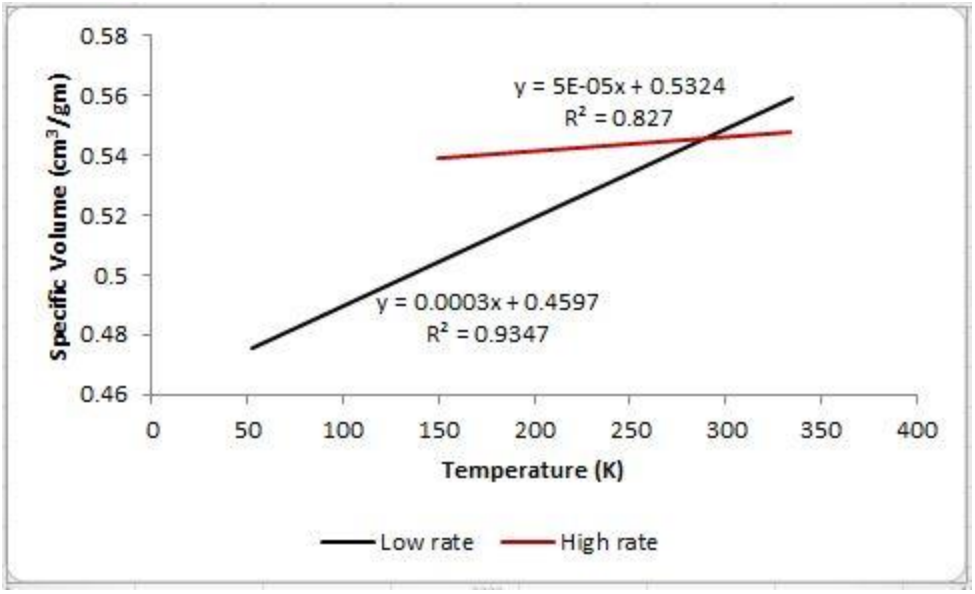

Figure 83: Specific volume as a function of temperature for C_8F_{18}

6.4.3 **Specific Heat**

Specific heat is used to extract the glassy transition temperature for $C_{11}F_{24,}$ Figure 84 represent the property that is measured on the high and slow rates, the glassy transition temperature for cell $C_{11}F_{24}$ equals to 324K. The way to calculate the specific heat in MD has been explained in 6.3.3 section

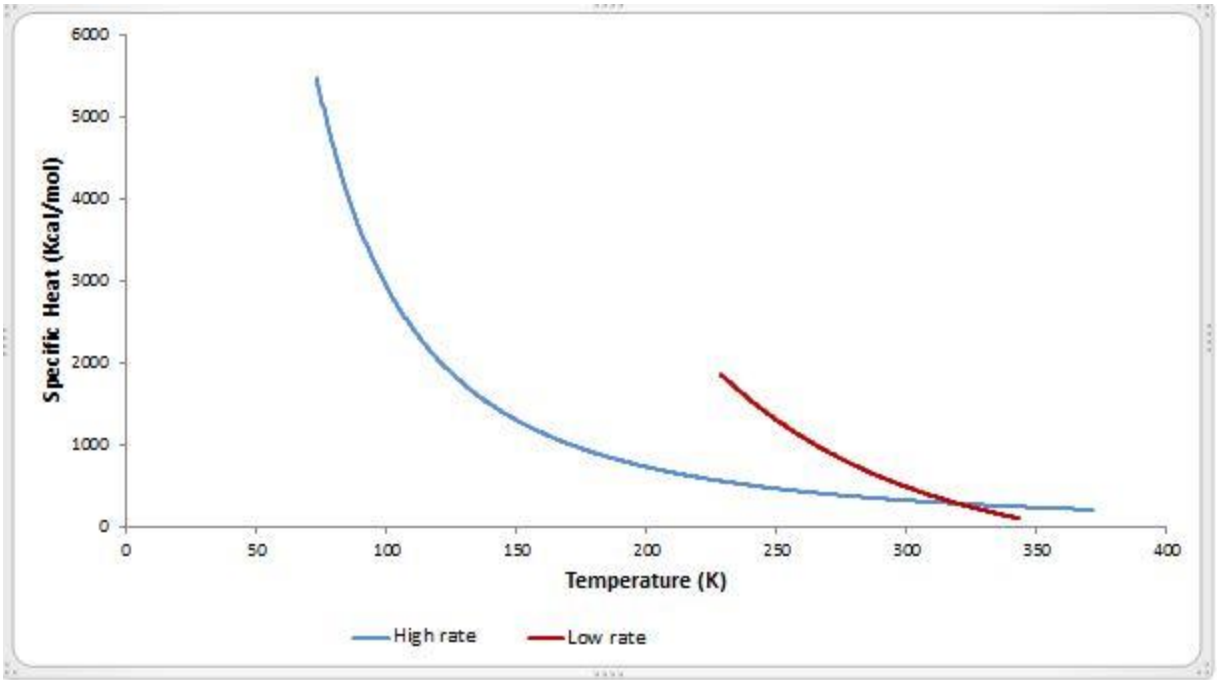

Figure 84: Specific heat as a function of temperature for $C_{11}F_{24}$

6.4.4 **Glassy Transition Temperature and the Molecular Weight Influence**

The mechanical properties such as the glassy transition temperature, modulus and toughness are affected by molecular weight, the relation between the mechanical behavior of polymers and their molecular weight is nearly proportional. (Fox Jr and Flory, 1950) describe the effect of the molecular weight on the glassy transition temperature in polystyrene as shown Figure 85 . In the current work PTFE glassy transition temperature increases with increasing the molecular weight. Flory–Fox equation is an expression which describes the influence of molecular weight on the glassy transition temperature property.

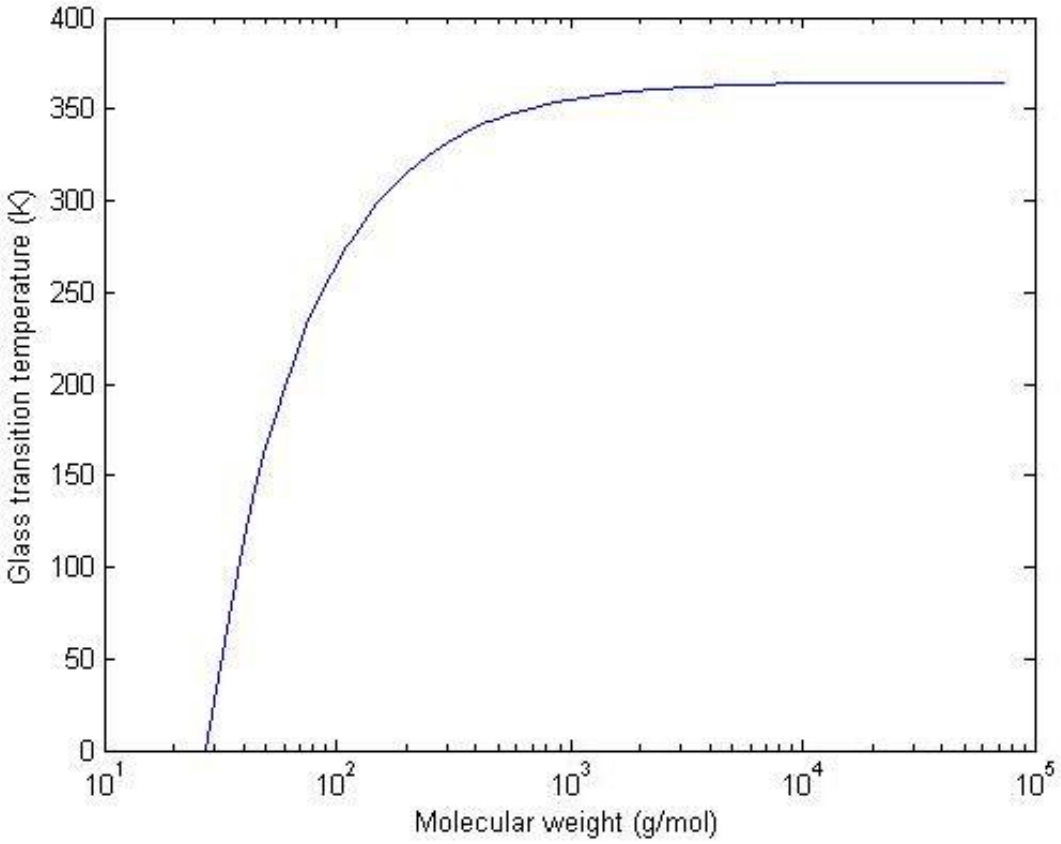

Figure 85: Molecular weight effect on Polystyrene GTT adopted from (Fox Jr and Flory, 1950)

$$T_g = T_{g,\infty} - \frac{K}{M_n} \tag{6.10}$$

where T_g is the glassy transition temperature, $T_{g,\infty}$ is the highest glassy transition value that can be reached by a polymer, K is a constant related to the polymer free volume, and M_n is the number average molecular weight. It should be noted that the value of K for PTFE is not available in both the experimental and MD approaches. PTFE highest glassy transition value (i.e., $T_{g,\infty}$) is offered in the experimental literature and it is about 400K (Araki, 1965) and it was not predicted using MD simulations studies. This research, contribute to the PTFE literature by the prediction of K and $T_{g,\infty}$, I fitted PTFE predicted glassy transition temperature values to Flory-Fox equation as illustrated in Figure 86, $K = 81464$ and $T_{g,\infty}$ equals to 476K, the latter

value is higher than its experimental counterpart and that is due to the MD simulations small time scale compared to the experimental approach big scale. I used the extracted parameters (i.e., K and $T_{g,\infty}$) to plot the relation between PTFE glassy transition temperature and the molecular weight as shown in Figure 87

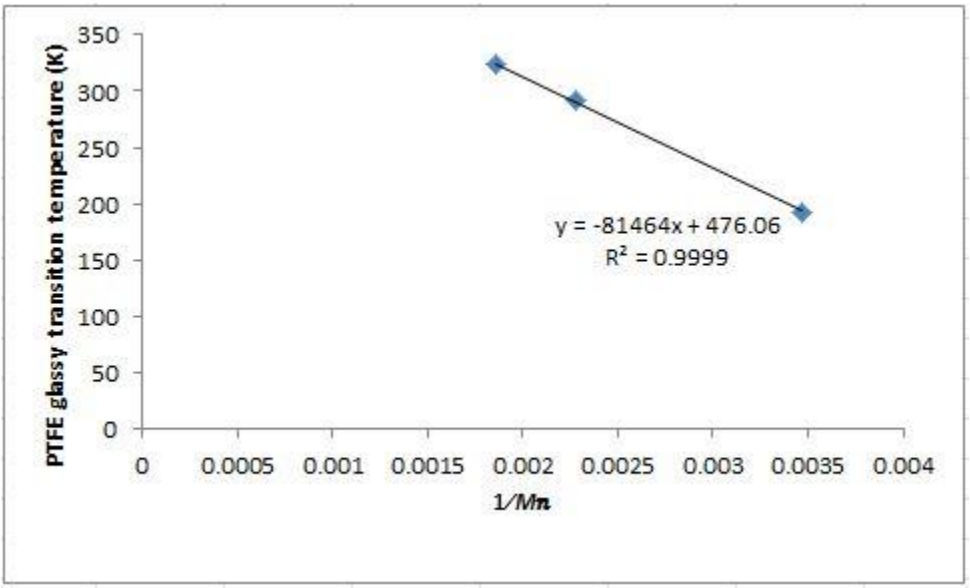

Figure 86: Effect of Flory-Fox equation on PTFE GTT

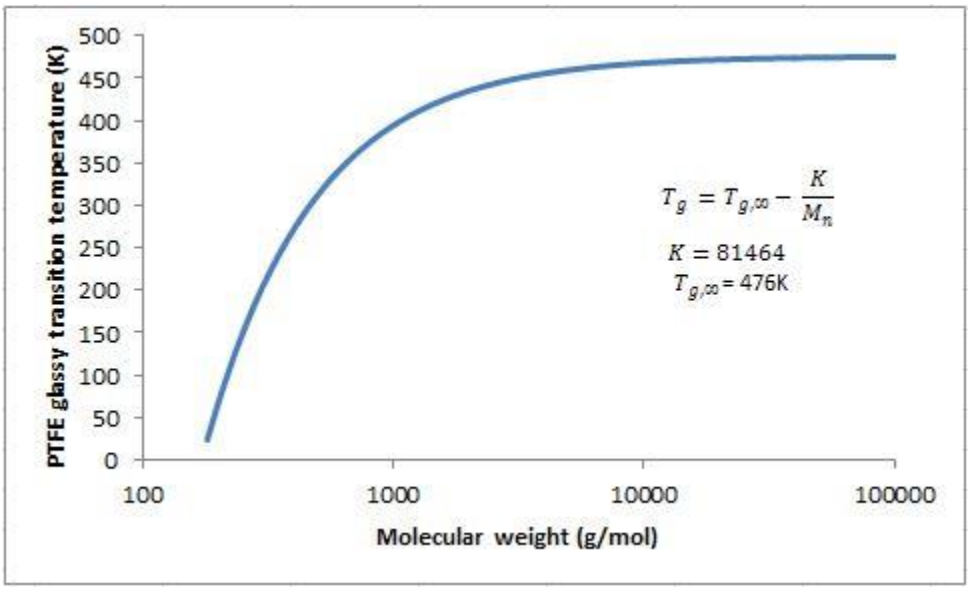

Figure 87: PTFE GTT versus MW using Flory-Fox parameters

6.4.5 **The Cooling Rate**

The glassy transition state for a polymer melt is characterized by the cooling rate under NPT conditions where the polymer melt, transfers from the liquid state to its solid glassy state. The glassy transition temperature would vary with the variation of the cooling rate. Therefore, the intersection between the high and the low rates would results in define the value of the glassy transition temperature (GTT), the low rates would give lower GTT and increase the time for relaxation, while the higher rates will result in higher GTT and less time for relaxation.

Changing the cooling rate would change GTT, experimentally; it is found that changing the cooling rate would predict variation in GTT value with range between 20 to 40 degree (Haward and Young, 1997). I apply this information in MD simulations with faster and slower rates for $C_{11}F_{24}$ cell and I have GTT equals to 350K, which is higher than the GTT, I predict in the previous section (i.e., 324K), comparison between the different rates illustrated in Figure 88

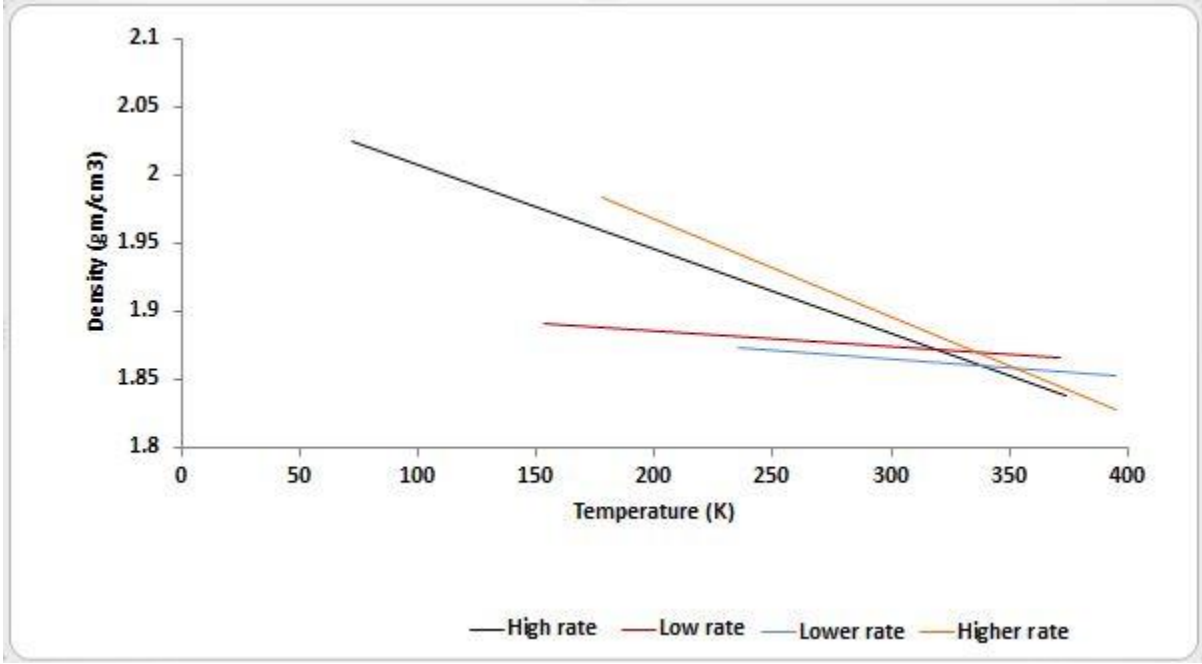

Figure 88: C11F24 GTT at different rates

6.4.6 **Governing Forces at the Molecular Level**

The influence of the glassy transition on the intramolecular and intermolecular energies has been examined MD simulations research. In this research, I computed PTFE glassy transition temperature and its impact on the potential energy. I utilized the potential energy information from the cell $C_{11}F_{24}$, and as shown in Figure 89 and Figure 90 that the bond and angle energy values for the simulated system have the same linearly trend while the non-bonding (i.e., the Van der Waals and electrostatic) and the dihedral energy values have a kink in the trend line as shown in Figure 91, Figure 92 and Figure 93. These outcomes declare the major role of the intermolecular and dihedral energies in PTFE thermal properties.

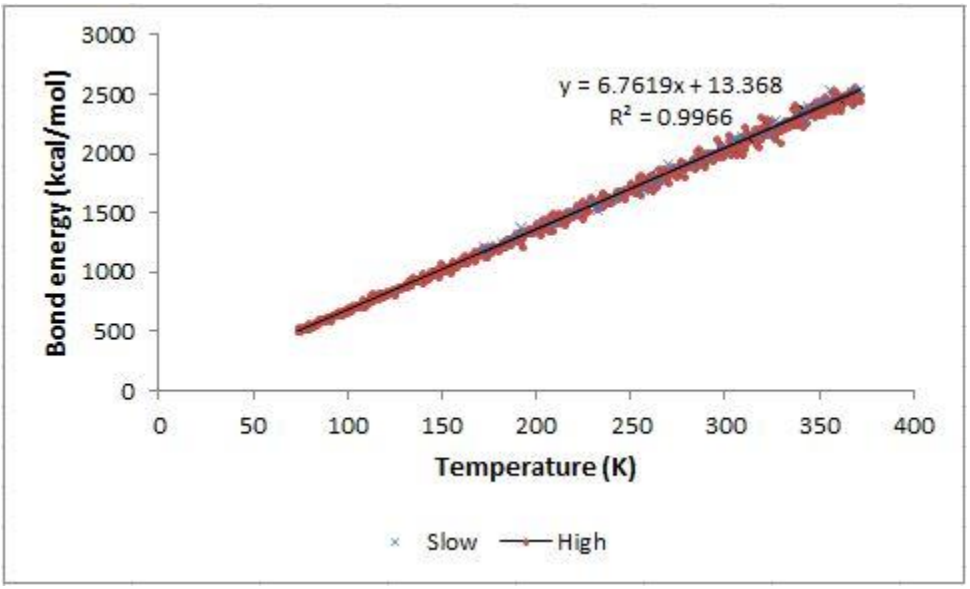

Figure 89: Bond energy versus temperature

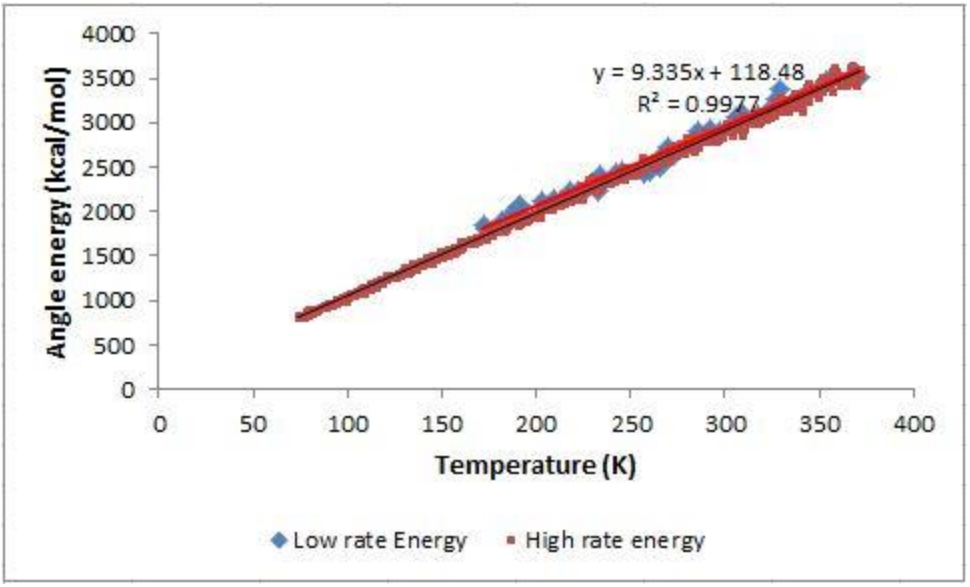

Figure 90: Angle energy versus temperature

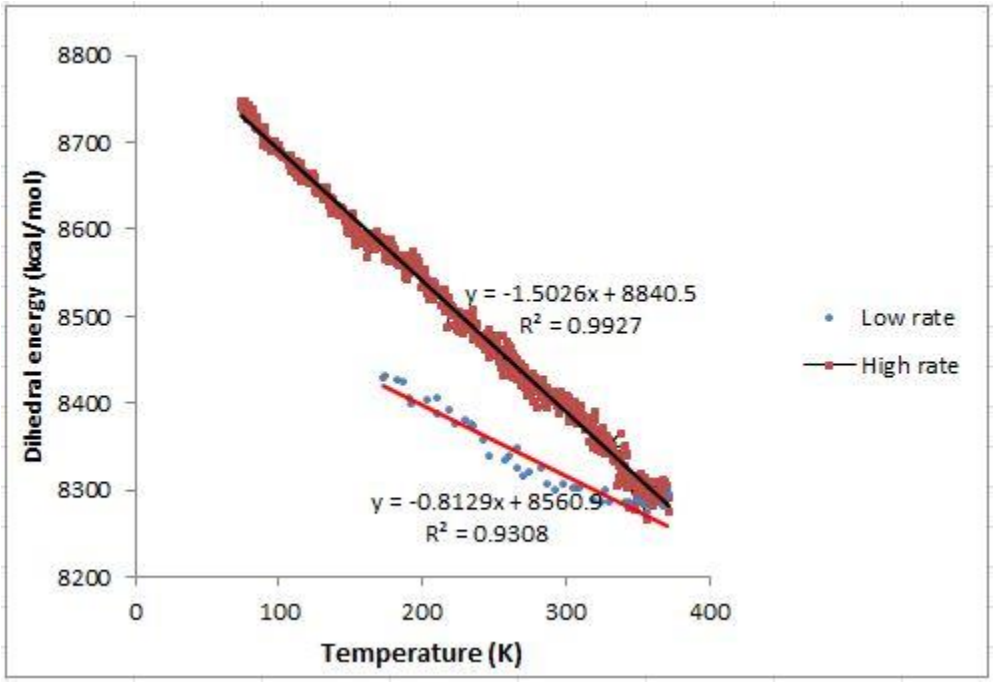

Figure 91: Dihedral energy versus temperature

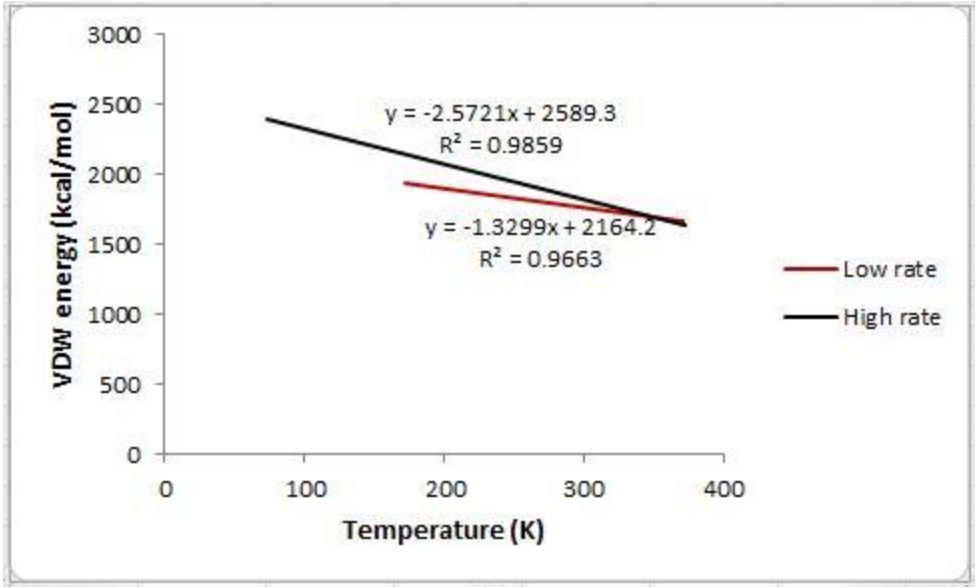

Figure 92: Van der Waals energy versus temperature

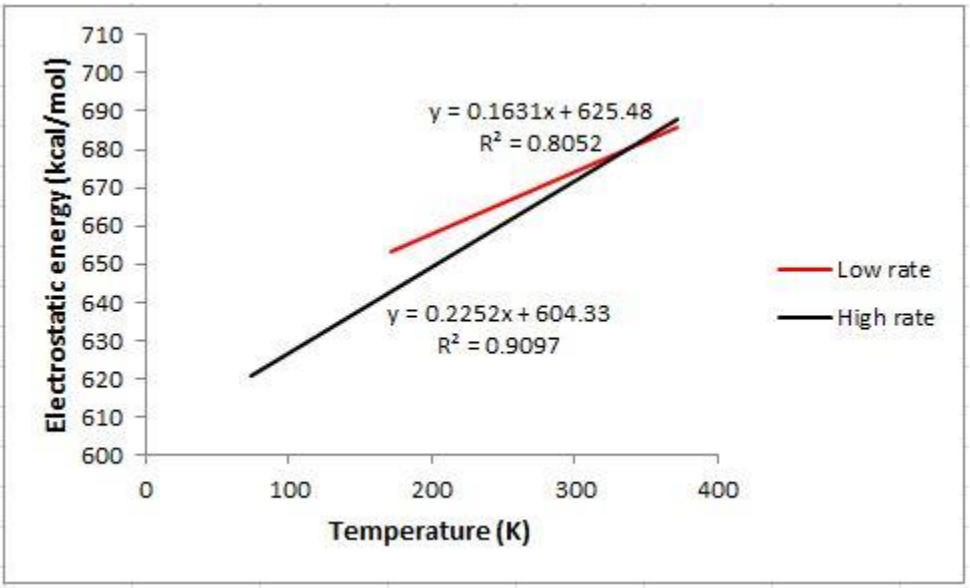

Figure 93: Electrostatic energy versus temperature

7 Concluding Remarks

Despite the recent advancements in MD simulations, there is yet to be a plausible effort utilizing this research approach to examine PTFE mechanical properties. The current research represents one of the earliest efforts in this regard. Specifically, this dissertation research utilizes MD simulations to predict PTFE glassy transition temperature and the thermal behavior near it. The remainder of this chapter proceeds as follows. Section 7.1 presents comparative analysis and establishes the contribution of the research, and section 7.2 presents the directions for future research.

.

7.1 Comparative Analysis and Contribution

This study contributes to the current body of knowledge on PTFE and MD simulations in several ways.

1. First, parameterization of new OPLS-AA force-field for PTFE polymer. Special handling was taken for fitting the dihedral angles using the nonlinear least squares algorithm. The intramolecular parameters were extracted using unique method (i.e., AFMM) instead of the tedious and traditional ways along with new charges. This research adds to and expands the current literature by offering a new set of PTFE force fields parameters to predict its behavior in diverse service environments and to improve bottom-up designs of polymers, among other avenues.
2. The present study is the first to exclusively analyze PTFE glassy transition temperature and the thermal behavior near it through MD simulations.

3. In addition, the current study adds to the overall MD research on characterizing the glassy transition temperatures. While the common practice within the MD research (Hossain et al., 2010) has been to compute the glassy transition temperature of polymers through considering the change in the specific volume property (volume method), this research utilizes both the volume method using density and specific volume and the thermal methods using specific heat.
4. Furthermore, the present study contributes to the PTFE experimental literature in that it's the first study to exclusively analyze the glassy transition temperature of PTFE at specific molecular weights, all while observing the changes in its density, specific volume and specific heat. This is contrary to PTFE experimental studies which offer values for PTFE glassy transition temperature but without specifying and controlling for the molecular weights at which these temperatures were measured. Not only does the current study consider the molecular weight but it also validates the influence of increasing molecular weight on improving the condensed phase properties such as the glassy transition temperature and specific heat.
5. In addition, the present study contributes to the PTFE experimental literature in that it analyzes the glassy transition temperature governing forces at the molecular level. This adds to the experimental literature which offers very little details regarding the exact molecular forces that control the glassy transition state. Specifically, this MD research shows that dihedral, Columbic and Lennard Jones potentials are the driving forces control the glassy state as explained with clear analysis in chapter 6.
6. This research is the first to extract the specific heat property for PTFE using MD simulations. This adds to both the PTFE MDS and experimental research which offer no such information for some PTFE oligomers. Specifically, this study provides new

findings about important melt phase properties for new PTFE oligomers. For example and as cleared in Table 32, studies within the experimental approach examined PTFE oligomers with even number of carbon atoms but not those oligomers with odd number of carbon atom such as $C_{11}F_{24}$. This research provides a complete set of essential properties for $C_{11}F_{24}$ such as density, specific heat, boiling point and heat of vaporization. In addition, MDS literature has primarily focused on small PTFE oligomers up to six carbon atoms and did not study bigger molecules.

7. Finally, this work contributes to PTFE literature by the prediction of PTFE Flory-Fox key values (i.e., K and $T_{g,\infty}$)

In conclusion, not only does the current work validate the measurements from experimental studies but it also offers additional predictions of PTFE properties. These predictions are important for understanding PTFE behaviors in varied conditions.

7.2 Future Research

The future research will include the following topics: yield and mechanical behavior of glassy PTFE, examine PTFE glassy transition temperature volume hysteresis, creep in PTFE glassy state and glassy state for PTFE composites.

Table 32: Comaparative analysis

Cell/Property (unit)	Experimental	MDS Literature	This Research
C_5F_{12} /Boiling point (K)	295(Barber and Cady, 1956)	N/A	210
C_8F_{18}/ Boiling point (K)	375(Lide, 2004)	N/A	340
$C_{11}F_{24}$/ Boiling point (K)	N/A	N/A	380
C_5F_{12} /Enthalpy of vaporization (g/cal)	21.00 (Hougham, 1999)	22.6 (Watkins and Jorgensen, 2001)	23.96±0.33
C_8F_{18}/ Enthalpy of vaporization (g/cal)	22.00 (Hougham, 1999)	N/A	25.10±0.42
$C_{11}F_{24}$/ Enthalpy of vaporization (g/cal)	N/A	N/A	20.13±0.40
C_5F_{12} /Specific Heat (KJ/mol K)	0.20 (Yaws, 2008)	N/A	0.1100±0.0007
C_8F_{18}/ Specific Heat (KJ /mol K)	0.24 (Yaws, 2008)	N/A	0.1700±0.0009
$C_{11}F_{24}$/ Specific Heat (KJ /mol K)	N/A	N/A	0.1710±0.0010
C_5F_{12} /Density (gm/cm^3)	1.60(Burger and Cady, 1951)	1.59 (Watkins and Jorgensen, 2001)	1.69±0.017
C_8F_{18}/Density (gm/cm^3)	1.77 (Hougham, 1999)	N/A	1.71±0.030
$C_{11}F_{24}$/Density (gm/cm^3)	N/A	N/A	1.88±0.031
C_5F_{12} /Glassy Transition Temperature	N/A	N/A	193
C_8F_{18}/ Glassy Transition Temperature	N/A	N/A	291
$C_{11}F_{24}$/ Glassy Transition Temperature	N/A	N/A	324
Flory-Fox PTFE free volume constant, K	N/A	N/A	81464
Flory-Fox PTFE highest GTT, $T_{g,\infty}$(K)	400 (Araki, 1965)	N/A	476

8 Appendix

8.1 Supplement Files

8.1.1 **PDB example**

```
*XXXXX
*
ATOM      1  CQ1 YZN A   1      -0.028  -2.006   0.000  1.00  0.00
C
ATOM      2  FQ2 YZN A   1       1.025  -2.891   0.000  1.00  0.00
F
ATOM      3  FQ3 YZN A   1      -0.795  -2.233   1.120  1.00  0.00
F
ATOM      4  FQ1 YZN A   1      -0.795  -2.233  -1.120  1.00  0.00
F
ATOM      5  CQ2 YZN A   1       0.522  -0.565   0.000  1.00  0.00
C
ATOM      6  FQ4 YZN A   1       1.322  -0.424  -1.132  1.00  0.00
F
ATOM      7  FQ5 YZN A   1       1.322  -0.424   1.132  1.00  0.00
F
ATOM      8  CQ3 YZN A   1      -0.523   0.565   0.000  1.00  0.00
C
ATOM      9  FQ6 YZN A   1      -1.322   0.424   1.132  1.00  0.00
F
ATOM     10  FQ7 YZN A   1      -1.322   0.424  -1.132  1.00  0.00
F
ATOM     11  CQV YZN A   1       0.028   2.006   0.000  1.00  0.00
C
ATOM     12  FR1 YZN A   1       0.795   2.233  -1.120  1.00  0.00
F
ATOM     13  FR2 YZN A   1      -1.025   2.891   0.000  1.00  0.00
F
ATOM     14  FR3 YZN A   1       0.795   2.233   1.120  1.00  0.00
F
END
```

8.1.2 **PSF example**

```
PSF CMAP CHEQ
       2 !NTITLE
* INPUT TEST

      14 !NATOM
       1 XXXX 1    YZN  CQ1     1    1.08000       12.0110           0
0.00000     -0.301140E-02
       2 XXXX 1    YZN  FQ2     2  -0.360000       18.9980           0
0.00000     -0.301140E-02
       3 XXXX 1    YZN  FQ3     2  -0.360000       18.9980           0
0.00000     -0.301140E-02
       4 XXXX 1    YZN  FQ1     2  -0.360000       18.9980           0
0.00000     -0.301140E-02
       5 XXXX 1    YZN  CQ2     1   0.632000       12.0110           0
0.00000     -0.301140E-02
       6 XXXX 1    YZN  FQ4     2  -0.316000       18.9980           0
0.00000     -0.301140E-02
       7 XXXX 1    YZN  FQ5     2  -0.316000       18.9980           0
0.00000     -0.301140E-02
       8 XXXX 1    YZN  CQ3     1   0.632000       12.0110           0
0.00000     -0.301140E-02
       9 XXXX 1    YZN  FQ6     2  -0.316000       18.9980           0
0.00000     -0.301140E-02
      10 XXXX 1    YZN  FQ7     2  -0.316000       18.9980           0
0.00000     -0.301140E-02
      11 XXXX 1    YZN  CQV     1    1.08000       12.0110           0
0.00000     -0.301140E-02
      12 XXXX 1    YZN  FR1     2  -0.360000       18.9980           0
0.00000     -0.301140E-02
      13 XXXX 1    YZN  FR2     2  -0.360000       18.9980           0
0.00000     -0.301140E-02
      14 XXXX 1    YZN  FR3     2  -0.360000       18.9980           0
0.00000     -0.301140E-02

      13 !NBOND: bonds
       1       4       1       2       1       3       1       5
      11      12      11      13      11      14       5       6
       5       7      11       8       5       8       8      10
       8       9

      24 !NTHETA: angles
       2       1       4       2       1       5       3       1
2
       3       1       4       3       1       5       4       1
5
       1       5       6       1       5       7       1       5
8
       6       5       7       6       5       8       7       5
8
```

```
         5        8        9        5        8       11        9        8
11
        10        8        5       10        8        9       10        8
11
        12       11        8       12       11       13       12       11
14
        13       11        8       13       11       14       14       11
8

        27 !NPHI: dihedrals
         1        5        8       10        1        5        8        9
         1        5        8       11        6        5        8       11
         7        5        8       11        3        1        5        6
         3        1        5        7        3        1        5        8
         2        1        5        6        2        1        5        7
         2        1        5        8        4        1        5        6
         4        1        5        7        4        1        5        8
        10        8       11       12        5        8       11       12
         9        8       11       12       10        8       11       13
         5        8       11       13        9        8       11       13
        10        8       11       14        5        8       11       14
         9        8       11       14        6        5        8       10
         6        5        8        9        7        5        8       10
         7        5        8        9

         0 !NIMPHI: impropers


         0 !NDON: donors


         0 !NACC: acceptors


         0 !NNB

         0        0        0        0        0        0        0        0
         0        0        0        0        0        0

         1        0 !NGRP NST2
         0        1        0

         1 !MOLNT
         1        1        1        1        1        1        1        1
         1        1        1        1        1        1

         0        0 !NUMLP NUMLPH

         0 !NCRTERM: cross-terms
```

8.1.3 **Topology example**

```
MASS 1 CTf   12.01100 C ! YZN
MASS 2 Fpf   18.99800 F ! YZN

Residue YZN
GROUP
  ATOM CQ1  CTf     1.080!
  ATOM FQ2  Fpf    -0.360!
  ATOM FQ3  Fpf    -0.360!
  ATOM FQ1  Fpf    -0.360!
  ATOM CQ2  CTf     0.632!
  ATOM FQ4  Fpf    -0.316!
  ATOM FQ5  Fpf    -0.316!
  ATOM CQ3  CTf     0.632!
  ATOM FQ6  Fpf    -0.316!
  ATOM FQ7  Fpf    -0.316!
  ATOM CQV  CTf     1.080!
  ATOM FR1  Fpf    -0.360!
  ATOM FR2  Fpf    -0.360!
  ATOM FR3  Fpf    -0.360!

  BOND CQ1  FQ1
  BOND CQ1  FQ2
  BOND CQ1  FQ3
  BOND CQ1  CQ2
  BOND CQV  FR1
  BOND CQV  FR2
  BOND CQV  FR3
  BOND CQ2  FQ4
  BOND CQ2  FQ5
  BOND CQV  CQ3
  BOND CQ2  CQ3
  BOND CQ3  FQ7
  BOND CQ3  FQ6


   ANGLE CQ1  CQ2  CQ3
   ANGLE CQ1  CQ2  FQ5
   ANGLE CQ1  CQ2  FQ4
   ANGLE FQ3  CQ1  CQ2
   ANGLE FQ3  CQ1  FQ1
   ANGLE FQ3  CQ1  FQ2
   ANGLE FQ2  CQ1  CQ2
   ANGLE FQ2  CQ1  FQ1
   ANGLE FQ1  CQ1  CQ2
   ANGLE FR1  CQV  CQ3
   ANGLE FR1  CQV  FR3
   ANGLE FR1  CQV  FR2
   ANGLE FR2  CQV  CQ3
   ANGLE FR2  CQV  FR3
   ANGLE FR3  CQV  CQ3
```

```
   ANGLE CQ2  CQ3  CQV
   ANGLE CQ2  CQ3  FQ6
   ANGLE FQ4  CQ2  CQ3
   ANGLE FQ4  CQ2  FQ5
   ANGLE FQ5  CQ2  CQ3
   ANGLE FQ6  CQ3  CQV
   ANGLE FQ7  CQ3  CQV
   ANGLE FQ7  CQ3  FQ6
   ANGLE FQ7  CQ3  CQ2


  DIHEDRAL CQ1  CQ2  CQ3  FQ7
  DIHEDRAL CQ1  CQ2  CQ3  FQ6
  DIHEDRAL CQ1  CQ2  CQ3  CQV
  DIHEDRAL CQV  CQ3  CQ2  FQ4
  DIHEDRAL CQV  CQ3  CQ2  FQ5
  DIHEDRAL FQ3  CQ1  CQ2  FQ4
  DIHEDRAL FQ3  CQ1  CQ2  FQ5
  DIHEDRAL FQ3  CQ1  CQ2  CQ3
  DIHEDRAL FQ2  CQ1  CQ2  FQ4
  DIHEDRAL FQ2  CQ1  CQ2  FQ5
  DIHEDRAL FQ2  CQ1  CQ2  CQ3
  DIHEDRAL FQ1  CQ1  CQ2  FQ4
  DIHEDRAL FQ1  CQ1  CQ2  FQ5
  DIHEDRAL FQ1  CQ1  CQ2  CQ3
  DIHEDRAL FR1  CQV  CQ3  FQ7
  DIHEDRAL FR1  CQV  CQ3  CQ2
  DIHEDRAL FR1  CQV  CQ3  FQ6
  DIHEDRAL FR2  CQV  CQ3  FQ7
  DIHEDRAL FR2  CQV  CQ3  CQ2
  DIHEDRAL FR2  CQV  CQ3  FQ6
  DIHEDRAL FR3  CQV  CQ3  FQ7
  DIHEDRAL FR3  CQV  CQ3  CQ2
  DIHEDRAL FR3  CQV  CQ3  FQ6
  DIHEDRAL FQ4  CQ2  CQ3  FQ7
  DIHEDRAL FQ4  CQ2  CQ3  FQ6
  DIHEDRAL FQ5  CQ2  CQ3  FQ7
  DIHEDRAL FQ5  CQ2  CQ3  FQ6

END
set echo=true end
```

8.1.4 **AFMM configuration file example**

[parameters]

a1 = 30.0 120.0 105.59

[general]

maxsteps = 100000

maxsigmasteps = 10000

mdexec = /home1/charmm

mdinp = ptfe.inp

qmout = ptfechrm.nw.out

qmfactor = 1.00

afmmfile = afma1.dat

weighting = projection

8.1.5 **NWCHEM input file example**

```
echo

start ptfe1

geometry units angstrom
  C     -1.92700000    0.09800000   -0.00400000
  F     -2.61200000   -0.63100000   -0.00200000
  F     -2.02900000    0.65900000   -0.82600000
  F     -2.03200000    0.66600000    0.81200000
  C     -0.55900000   -0.51700000    0.00100000
  F     -0.43600000   -1.14300000    0.91100000
  F     -0.41100000   -1.17000000   -0.88600000
  C      0.51600000    0.52900000    0.01000000
  F      0.42700000    1.18600000    0.90100000
  F      0.42300000    1.16600000   -0.89600000
  C      1.88500000   -0.08600000    0.00500000
  F      2.00200000   -0.72200000   -0.89800000
  F      2.67400000    0.69600000   -0.02300000
  F      2.04900000   -0.72400000    0.90000000
end

basis
* library 6-31G
end

dft; xc b3lyp; end

task dft optimize

task dft frequencies
```

8.2 Resume

Rawan A. Al- Nsour

Education

- Ph.D. Department of Mechanical & Nuclear Engineering, Virginia Commonwealth University, Richmond, Virginia, U.S.A. 2014
  Thesis: Molecular Dynamics and Simulations of Pure Polytetrafluoroethylene near the Glassy Transition Temperature at Different Molecular weights.
  - ❖ Advisor: Dr. Hani El Kaderi, Associate Professor of Chemistry, Virginia Commonwealth University, Richmond, Virginia
  - ❖ Co-Advisor: Dr. Brian Hinderliter, Associate Professor of Mechanical & Industrial Engineering, University of Minnesota, Duluth, Minnesota.
  - ❖ Co-Advisor: Dr. John Hackett, Associate Professor of Physiology & Biophysics, Goodwin Research Laboratory, VCU Massy Cancer Center, Virginia Commonwealth University, Richmond, Virginia.
  - ❖ Committee member: Dr. Karla Mossi, Associate Professor of Mechanical & Nuclear Engineering, Virginia Commonwealth University, Richmond, Virginia.
  - ❖ Committee member: Dr. James McLeskey, Associate Professor of Mechanical & Nuclear Engineering, Virginia Commonwealth University, Richmond, Virginia.
- M.Sc. Industrial Engineering, University of Jordan, Amman, Jordan, 2006.
- B.Sc. Mechanical Engineering, Jordan University of Science and Technology, Irbid, Jordan, 2002.

Research Interests

- Molecular Dynamics Simulations.
- Polymers Behavior near the Glassy Transition Temperature.
- Polymers and Composites Mechanical Behavior.
- Artificial Muscles, Protein Transporters.

Conferences, Symposia and Presentations

- Paper, Molecular Dynamics Simulations of Polytetrafluoroethylene at Glassy Transition Temperature. TechConnect World Conference and Expo 2014, Washington, DC, U.S.A, 2014.
- Paper, Parameterization of New Force Fields for Polytetrafluoroethylene. 13th Annual William & Mary Graduate Research Symposium, College of William & Mary, Williamsburg, Virginia, U.S.A, 2014.
- Abstract, 2013, Molecular Dynamics Simulations Study of Polytetrafluoroethylene. SciMeeting Conference for Molecular Simulations, Chicago, U.S.A.

- Abstract, 2013, Molecular Dynamics Simulations of Polytetrafluoroethylene near the Glassy Transition Temperature. ICCES'13: International Conference on Computational and Experimental Engineering and Sciences, Seattle, Washington, U.S.A.
- Poster & Presentation, 2013. Molecular Dynamics Simulations of Polytetrafluoroethylene. Graduate Student Association's 16th Annual Research Symposium and Exhibit, Virginia Commonwealth University, Richmond, Virginia, U.S.A.

Academic Honors and Certifications

- The Excellence in Scholarship Award at the prestigious 13th Annual William & Mary Graduate Research Symposium, College of William & Mary, U.S.A, 2014.
- Graduate School Dissertation Assistantship Award, Virginia Commonwealth University, U.S.A, 2013-2014.
- Graduate School Award for the best poster and presentation at the Graduate Student Association's 16th Annual Research Symposium and Exhibit, Virginia Commonwealth University, U.S.A, 2013.
- Graduate Teaching Assistantship Award, Department of Mechanical & Nuclear Engineering, Virginia Commonwealth University, U.S.A.; Fall 2009–Fall 2011.
- Certification in Modern Cars Technology (189 Hours), Ministry of Work, Amman, Jordan, 2000.

Professional Societies

- Member of Institute of Electrical and Electronics Engineers (IEEE).
- Member of American Society of Mechanical Engineers (ASME).
- Member of Dominion Six Sigma Blue Belt Organization, Virginia Commonwealth University, Richmond, Virginia, U.S.A.

VCU Activities

- Member of Graduate Mechanical Engineering Organization, Virginia Commonwealth University, Richmond, Virginia, U.S.A.
- Member of Engineering Graduate Student Association, Virginia Commonwealth University, Richmond, Virginia, U.S.A.
- Member of Chemical Safety Organization, Virginia Commonwealth University, Richmond, Virginia, U.S.A.

Professional Experience

- Manager, Sales and Commercial Correspondence Section at the Regional Company for Elevators and Escalators, Amman, Jordan, Jan, 2008 to Aug, 2008.
- Manager, Sales and Commercial Correspondence Section at the AL-MAJAL Company for Mechanical Works Projects Managements & Supply & Solar System, Amman, Jordan, Nov, 2006 to Dec, 2007.
- Project Engineer at the Ideal Trading Group Company, Amman, Jordan, Dec. 2005 to Oct. 2006.
- Account Executive in the International Market at the Commercial Group for Trading Company, Amman, Jordan, Feb. 2005–Nov. 2005.
- Manager, New Cars Pre-Delivery Inspection Section at T. Gargour & Fils Company (Mercedes-Benz General Distributor for DaimlerChrysler AG in Jordan), Amman, Jordan, Dec, 2001 to Sep, 2004.
- Engineer on the Maintenance Section at FORD Company, Amman, Jordan, Feb, 2001–Nov, 2001.

Teaching Experience

Teaching Assistant, Department of Mechanical & Nuclear Engineering, Virginia Commonwealth University, Richmond, Virginia, U.S.A., Fall 2009 to Spring 2013. In charge of holding office hours, preparing and grading homeworks, in addition to exams for the following classes:

- Engineering Statics (90 students).
- Heat Transfer (130 students).
- Radiation Safety and Shielding (40 students).
- Nuclear Power Plants (25 students).
- Economics of Nuclear Power Production (24 students).
- Introduction to Nuclear Engineering (29 students).
- Dynamics and Kinematics (180 students).
- Thermal Systems Design (50 students).
- Mechanics of Deformable Solids (90 students).
- Technical Writing (40 students).

Graduate Courses

- Advanced Engineering Mathematics.
- Design Optimization.
- Smart Materials.
- Special Topics in Solid Mechanics.
- Special Topics in Self Assemble Membranes.

- Special Topics in Applied Membrane Biophysics.
- Advanced Molecular Modeling.
- Survey of Molecular Modeling Methods.
- Technical Writing.
- Industrial Quality Control.
- Operation Research I.
- Operation Research II.
- Special Topics in Engineering Management.
- Applied Engineering Statistics.
- Production Planning and Control.
- System Simulation.
- Project Management and Network Models.
- Human Factors.
- Computer Integrated Manufacturing.
- Analysis and Design of Production Systems.
- Information Systems Analysis and Design.

Programming Languages and Software Skills

- LINUX.
- TCL Scripting Language.
- VMD, Visual Molecular Dynamics.
- NAMD, Molecular Simulations.
- NWCHEM, Quantum Mechanics.
- AFMM, Molecular Mechanics.
- C++ programing Language.
- Mathematica.
- MATLAB.
- Microsoft Office (Word, Excel, PowerPoint).

9 References

ACCELRYS, I. Cerius2. 2000. *Accelrys Inc: San Diego, CA*.

ACHARYA, B. 2010. 2.2. Mathematical Chemistry: Basic Issues. *GRAPH THEORY APPLIED TO CHEMISTRY*, 27.

ALDER, B. & WAINWRIGHT, T. 1957a. Phase transition for a hard sphere system. *The Journal of Chemical Physics,* 27**,** 1208-1209.

ALDER, B. & WAINWRIGHT, T. E. 1957b. Phase transition for a hard sphere system. *The Journal of Chemical Physics,* 27**,** 1208.

ALLEN, M. P. & TILDESLEY, D. J. 1987. Computer simulation of liquids.

AMARO, R., DHALIWAL, B. & LUTHEY-SCHULTEN, Z. 2007. Parameterizing a novel residue.

ANDERSON, O. L. 1995. *Equations of state of solids for geophysics and ceramic science,* Oxford University Press on Demand.

ARAKI, Y. 1965. Thermal expansion coefficient of polytetrafluoroethylene in the vicinity of its glass transition at about 400 K. *Journal of Applied Polymer Science,* 9**,** 421-427.

ARKLES, B. & SCHIRESON, M. 1976. The molecular weight of PTFE wear debris. *Wear,* 39**,** 177-180.

ARORA, J. S. 2004. *Introduction to optimum design*, Academic Press.

AVERILL, F. & PAINTER, G. 1992. Steepest-descent determination of occupation numbers and energy minimization in the local-density approximation. *Physical Review B,* 46**,** 2498.

BADER, A. & PARKER, L. 2001. Joseph Loschmidt, physicist and chemist. *Physics Today,* 54**,** 45.

BANERJEA, A. & TAYLOR, P. 1982. Theoretical calculation of conformational energies of polytetrafluoroethylene. *Journal of Applied Physics,* 53**,** 6532-6535.

BANERJEA, A. & TAYLOR, P. 1984. Devil's staircase in a one-dimensional model. *Physical Review B,* 30**,** 6489.

BARBER, E. J. & CADY, G. H. 1956. Vapor pressures of perfluoropentanes. *The Journal of Physical Chemistry,* 60**,** 504-505.

BARTON, D. & COOKSON, R. 1956. The principles of conformational analysis. *Q. Rev. Chem. Soc.,* 10**,** 44-82.

BASAŘOVÁ, P. & SVOBODA, V. 1991. Calculation of heats of vaporization of halogenated hydrocarbons from saturated vapour pressure data. *Fluid phase equilibria,* 68**,** 13-34.

BATES, T. 1967. Conformational energies of perfluoroalkanes. Part 1.—Semi-empirical calculations. *Trans. Faraday Soc.,* 63**,** 1825-1834.

BATES, T. & STOCKMAYER, W. 1966. Conformational Properties of Isolated Polytetrafluoroethylene Chains. *Journal of Chemical Physics,* 45**,** 2321-2322.

BATES, T. & STOCKMAYER, W. 1968a. Conformational energies of perfluoroalkanes. II. Dipole moments of H (CF2) nH. *Macromolecules,* 1**,** 12-17.

BATES, T. & STOCKMAYER, W. 1968b. Conformational energies of perfluoroalkanes. III. Properties of polytetrafluoroethylene. *Macromolecules,* 1**,** 17-24.

BAYLY, C. I., CIEPLAK, P., CORNELL, W. & KOLLMAN, P. A. 1993. A well-behaved electrostatic potential based method using charge restraints for deriving atomic charges: the RESP model. *The Journal of Physical Chemistry,* 97**,** 10269-10280.

BILLMEYER, F. W. 1957. *Textbook of Polymer Chemistry*, Interscience Publishers New York.

BORODIN, O., SMITH, G. D. & BEDROV, D. 2002. A quantum chemistry based force field for perfluoroalkanes and poly (tetrafluoroethylene). *The Journal of Physical Chemistry B,* 106**,** 9912-9922.
BOYD, R., BREITLING, S. & MANSFIELD, M. 1973. Application of conformational analysis techniques to the prediction of heats of formation and gas-phase thermodynamic functions. *AIChE Journal,* 19**,** 1016-1024.
BRASILE, L. & CLARKE, J. 1997. Method and solution for organ preservation comprising retinal-derived growth factor, cyclodextrin, mucopolysaccharide and fluorocarbon. Google Patents.
BRENEMAN, C. M. & WIBERG, K. B. 2004. Determining atom-centered monopoles from molecular electrostatic potentials. The need for high sampling density in formamide conformational analysis. *Journal of computational chemistry,* 11**,** 361-373.
BROOKS, B. R., BRUCCOLERI, R. E. & OLAFSON, B. D. 1983. CHARMM: A program for macromolecular energy, minimization, and dynamics calculations. *Journal of computational chemistry,* 4**,** 187-217.
BUNN, C., COBBOLD, A. & PALMER, R. 1958. The fine structure of polytetrafluoroethylene. *Journal of Polymer Science,* 28**,** 365-376.
BUNN, C. & HOWELLS, E. 1954. Structures of molecules and crystals of fluoro-carbons.
BURGER, L. L. & CADY, G. H. 1951. Physical Properties of Perfluoropentanes1a. *Journal of the American Chemical Society,* 73**,** 4243-4246.
BYLASKA, E. J., DE JONG, W., GOVIND, N., KOWALSKI, K., STRAATSMA, T., VALIEV, M., WANG, D., APRA, E., WINDUS, T. & HAMMOND, J. 2007. NWChem, A computational chemistry package for parallel computers, version 5.1. *Pacific Northwest National Laboratory, Richland, Washington,* 99352**,** 0999.
BYRD, E. F. & RICE, B. M. 2008. A comparison of methods to predict solid phase heats of formation of molecular energetic salts. *The Journal of Physical Chemistry A,* 113**,** 345-352.
CAPALDI, F. M., BOYCE, M. C. & RUTLEDGE, G. C. 2004. Molecular response of a glassy polymer to active deformation. *Polymer,* 45**,** 1391-1399.
CARDELLI, L. 1986. Amber. *Combinators and functional programming languages***,** 21-47.
CARRAHER, C. E. 1996. *Polymer chemistry: an introduction*, M. Dekker.
CENGEL, Y. A., BOLES, M. A. & KANOĞLU, M. 2011. *Thermodynamics: an engineering approach*, McGraw-Hill New York.
CHABRIER, F., LLOYD, C. & SCRIMGEOUR, S. 1999. Measurement at low strain rates of the elastic properties of dental polymeric materials. *Dental materials: official publication of the Academy of Dental Materials,* 15**,** 33.
CLARK, E. 1999. The molecular conformations of polytetrafluoroethylene: forms II and IV. *Polymer,* 40**,** 4659-4665.
CLARK, E. & MUUS, L. 1962. Partial disordering and crystal transitions in polytetrafluoroethylene*. *Zeitschrift für Kristallographie,* 117**,** 119-127.
CLARK, E. S. 2006. The crystal structure of polytetrafluoroethylene, forms I and IV. *Journal of Macromolecular Science, Part B: Physics,* 45**,** 201-213.
COMBES, J., DUCLOS, P. & SEILER, R. 1977. The Born-Oppenheimer approximation. *Acta Phys. Austriaca,* 17**,** 139-159.

CORRADINI, P. & GUERRA, G. 1977. On the Chain Conformation of Poly (tetrafluoroethylene) in the Crystalline Modification above 30 C. *Macromolecules,* 10**,** 1410-1413.
D'ILARIO, L. & GIGLIO, E. 1974. Calculation of the van der Waals potential energy for polyethylene and polytetrafluoroethylene as two-atom and three-atom chains: rotational freedom in the crystals. *Acta Crystallographica Section B: Structural Crystallography and Crystal Chemistry,* 30**,** 372-378.
DAI, Z. W., LING, J., HUANG, X. J., WAN, L. S. & XU, Z. K. 2011. Molecular Simulation on the Interactions of Water with Polypropylene Surfaces. *The Journal of Physical Chemistry C,* 115**,** 10702-10708.
DALTON, J. 1805. Memoirs and Proceedings of the Manchester Literary and Philosophical Society. *Manchester,* 6**,** 271.
DARDEN, T., YORK, D. & PEDERSEN, L. 1993. Particle mesh Ewald: An N· log (N) method for Ewald sums in large systems. *The Journal of Chemical Physics,* 98**,** 10089.
DE SANTIS, P., GIGLIO, E., LIQUORI, A. & RIPAMONTI, A. 1963. Stability of helical conformations of simple linear polymers. *Journal of Polymer Science Part A: General Papers,* 1**,** 1383-1404.
DURRELL, W. S., STUMP JR, E. C. & SCHUMAN, P. D. 1965. The glass transition temperature of polytetrafluoroethylene. *Journal of Polymer Science Part B: Polymer Letters,* 3**,** 831-833.
EBNESAJJAD, S. 2011. Introduction to Fluoropolymers. Applied Plastics Engineering Handbook, Elsevier Inc.
EBY, R., CLARK, E., FARMER, B., PIERMARINI, G. & BLOCK, S. 1990. Crystal structure of poly (tetrafluoroethylene) homo-and copolymers in the high pressure phase. *Polymer,* 31**,** 2227-2237.
EBY, R. & SINNOTT, K. 1961. Transitions and relaxations in polytetrafluoroethylene. *Journal of Applied Physics,* 32**,** 1765-1771.
ELEUTERIO, H. S. 1991. Fluoropolymers: an explorer's vantage point.
ETTEN, B. V. A System Administrator's Introduction to Bioinformatics. 2004.
FARMER, B. & EBY, R. 1981. Energy calculations of the crystal structure of the low temperature phase (II) of polytetrafluoroethylene. *Polymer,* 22**,** 1487-1495.
FARMER, B. & EBY, R. 1985. Energy calculations for the crystal structure of the high temperature phases (I and IV) of poly (tetrafluoroethylene). *Polymer,* 26**,** 1944-1952.
FEIRING, A. E., BANKS, R., SMART, B. & TATLOW, J. 1994. Fluoroplastics. *Organofluorine Chemistry: Principles and Commercial Applications,* 15**,** 339-372.
FISCHER, C. F. 1977. Hartree--Fock method for atoms. A numerical approach.
FLOM, D. & PORILE, N. 1955. Friction of teflon sliding on teflon. *Journal of Applied Physics,* 26**,** 1088-1092.
FOWLER, J. & FARMER, F. 1954. Conductivity induced in polytetrafluoroethylene by X-rays.
FOX JR, T. G. & FLORY, P. J. 1950. Second-order transition temperatures and related properties of polystyrene. I. Influence of molecular weight. *Journal of Applied Physics,* 21**,** 581-591.
FREDDOLINO, P. & SHIH, A. 2006. Case Study: Membranes.
FRISCH, M. J., FRISCH, A. & FORESMAN, J. B. 1995. *Gaussian 94 user's reference,* Gaussian.
GOODMAN, S. H. 1998. *Handbook of thermoset plastics,* William Andrew Publishing.

GROSS, E. K. U. & DREIZLER, R. M. 1995. *Density functional theory*, Springer.
GROSS, U., PAPKE, G. & RÜDIGER, S. 1993. Fluorocarbons as blood substitutes: critical solution temperatures of some perfluorocarbons and their mixtures. *Journal of fluorine chemistry,* 61**,** 11-16.
GRULKE, E. A. 1999. Solubility parameter values. *Polymer handbook,* 3**,** 519-559.
GUIDE, D. U. 1993. Biosym Technologies. *San Diego*.
GULLINGSRUD, J., SAAM, J. & PHILLIPS, J. 2006. psfgen User's Guide. *Urbana,* 51**,** 61801.
GUNTHER, H. 1994. *NMR spectroscopy*, Wiley.
HAN, J., GEE, R. H. & BOYD, R. H. 1994. Glass transition temperatures of polymers from molecular dynamics simulations. *Macromolecules,* 27**,** 7781-7784.
HANFORD, W. & JOYCE, R. 1946. Polytetrafluoroethylene. *Journal of the American Chemical Society,* 68**,** 2082-2085.
HANSEN, C. M. 1969. The universality of the solubility parameter. *Industrial & Engineering Chemistry Product Research and Development,* 8**,** 2-11.
HARIHARAN, A. & HARRIS, J. G. 1994. Structure and thermodynamics of the liquid–vapor interface of fluorocarbons and semifluorinated alkane diblocks: A molecular dynamics study. *The Journal of Chemical Physics,* 101**,** 4156-4165.
HAVENS JR, W. W. 1968. Nuclear research as a source of technology. *Physics Today,* 21**,** 46.
HAWARD, R. N. & YOUNG, R. J. 1997. *The physics of glassy polymers*, Springer.
HEARLE, J. W. S. 1982. *Polymers and their properties*, Ellis Horwood.
HEHRE, W. J. & HUANG, W. W. 1995. *Chemistry with computation: an introduction to SPARTAN*, Wavefunction, Inc.
HEINONEN, O. & TAYLOR, P. 1989. Dynamic helicity-reversal defects in polytetrafluoroethylene chains. *Polymer,* 30**,** 585-589.
HILDEBRAND, J. & SCOTT, R. The Solubility of Nonelectrolytes, 1964. *Reinhold, New York*.
HIRAKAWA, S. & TAKEMURA, T. 1969. Transitions and Phases of Polytetrafluoroethylene. *Japanese Journal of Applied Physics,* 8.
HOLT, D. & FARMER, B. 1999a. Modeling of helix reversal defects in polytetrafluoroethylene: I. Force field development and molecular mechanics calculations. *Polymer,* 40**,** 4667-4672.
HOLT, D. & FARMER, B. 1999b. Modeling of helix reversal defects in polytetrafluoroethylene: II. Molecular dynamics simulations. *Polymer,* 40**,** 4673-4684.
HOLT, D., FARMER, B., MACTURK, K. & EBY, R. 1996. Fluoropolymer force fields derived from semiempirical molecular orbital calculations. *Polymer,* 37**,** 1847-1855.
HOPEWELL, J., DVORAK, R. & KOSIOR, E. 2009. Plastics recycling: challenges and opportunities. *Philosophical Transactions of the Royal Society B: Biological Sciences,* 364**,** 2115-2126.
HOPFINGER, A. J. & HOPFINGER, A. 1973. *Conformational properties of macromolecules*, Academic Press New York.
HOSSAIN, D., TSCHOPP, M., WARD, D., BOUVARD, J., WANG, P. & HORSTEMEYER, M. 2010. Molecular dynamics simulations of deformation mechanisms of amorphous polyethylene. *Polymer,* 51**,** 6071-6083.
HOUGHAM, G. 1999. *Fluoropolymers: Properties*, Springer.
HUMPHREY, W., DALKE, A. & SCHULTEN, K. 1996. VMD: visual molecular dynamics. *Journal of molecular graphics,* 14**,** 33-38.

ISGRO, T., PHILLIPS, J., SOTOMAYOR, M. & VILLA, E. 2003. NAMD TUTORIAL. Theoritical and Computational Biophysics Group, University of Illinois and Beckman Institute, Illinois.

IWASAKI, M. 1963. On the helical structure of polytetrafluoroethylene. *Journal of Polymer Science Part A: General Papers,* 1**,** 1099-1104.

JANG, S. S., BLANCO, M., GODDARD III, W. A., CALDWELL, G. & ROSS, R. B. 2003. The source of helicity in perfluorinated N-alkanes. *Macromolecules,* 36**,** 5331-5341.

JANG, S. S., LIN, S. T., ÇAGIN, T., MOLINERO, V. & GODDARD III, W. A. 2005. Nanophase segregation and water dynamics in the dendrion diblock copolymer formed from the Frechet polyaryl ethereal dendrimer and linear PTFE. *The Journal of Physical Chemistry B,* 109**,** 10154-10167.

JENKINS, H. D. B. 2008. *Chemical thermodynamics at a glance*, John Wiley & Sons.

JENSEN, F. 2007. *Introduction to computational chemistry*, Wiley.

JORGENSEN, W. L., MAXWELL, D. S. & TIRADO-RIVES, J. 1996. Development and testing of the OPLS all-atom force field on conformational energetics and properties of organic liquids. *Journal of the American Chemical Society,* 118**,** 11225-11236.

JORGENSEN, W. L. & TIRADO-RIVES, J. 1988. The OPLS [optimized potentials for liquid simulations] potential functions for proteins, energy minimizations for crystals of cyclic peptides and crambin. *Journal of the American Chemical Society,* 110**,** 1657-1666.

KAUFMAN, H. S. & FALCETTA, J. J. 1977. *Introduction to polymer science and technology: an SPE textbook*, Wiley.

KENDALL, R. A., APRÀ, E., BERNHOLDT, D. E., BYLASKA, E. J., DUPUIS, M., FANN, G. I., HARRISON, R. J., JU, J., NICHOLS, J. A. & NIEPLOCHA, J. 2000. High performance computational chemistry: An overview of NWChem a distributed parallel application. *Computer Physics Communications,* 128**,** 260-283.

KHAN, A. & ZHANG, H. 2001. Finite deformation of a polymer: experiments and modeling. *International Journal of Plasticity,* 17**,** 1167-1188.

KING, R. & TABOR, D. 2002. The effect of temperature on the mechanical properties and the friction of plastics. *Proceedings of the Physical Society. Section B,* 66**,** 728.

KIRBY, R. K. 1956. Thermal Expansion of Polytetrafluoroethylene (Teflon) From-190 to+ 300 C. *Journal of research of the National Bureau of Standards,* 57**,** 91-94.

KOO, G. P., RIDDELL, M. N. & O'TOOLE, J. L. 1967. Fatigue properties of polytetrafluoroethylene and related fluoropolymers. *Polymer Engineering & Science,* 7**,** 182-188.

LAU, S. F., WESSON, J. P. & WUNDERLICH, B. 1984. Glass transition of polytetrafluoroethylene. *Macromolecules,* 17**,** 1102-1104.

LEACH, A. & KIER, L. B. 1997. Molecular modeling: principles and applications. *Journal of Medicinal Chemistry,* 40**,** 2969.

LEACH, A. R. 1996. Molecular modeling. *Principles & Application, Person Education Limited,* 701.

LENNTECH. 1998. Lenntech. Available: http://www.lenntech.com/teflon.htm.

LEONARD JR, W., JERNIGAN, R. & FLORY, P. 1965. Dipole Moments in Relation to Configuration of n-Alkane Chains Bearing α, ω Dipolar Substituents. *The Journal of Chemical Physics,* 43**,** 2256.

LI, L., ZHANG, Y., MA, H. & YANG, M. 2008. An investigation of molecular layering at the liquid-solid interface in nanofluids by molecular dynamics simulation. *Physics Letters A,* 372**,** 4541-4544.
LI, M., LIU, X., QIN, J. & GU, Y. 2009. Molecular dynamics simulation on glass transition temperature of isomeric polyimide. *Ex-press Polym Lett,* 3**,** 665.
LIDE, D. R. 2004. *CRC Handbook of Chemistry and Physics 2004-2005: A Ready-Reference Book of Chemical and Physical Data*, CRC press.
LIPKOWITZ, K. B. & BOYD, D. B. 1995. *Reviews in Computational Chemistry 6*, Wiley Online Library.
LONG, D. A. & LONG, D. 1977. *Raman spectroscopy*, McGraw-Hill New York.
LONG JR, D. M. 1998. Fluorocarbon blood substitutes. EP Patent 0,231,070.
MARGOLIS, J. 1985. Engineering thermoplastics: properties and applications. *Plast. Eng.,* 41**,** 63.
MARK, H. F. 1970. *Encyclopedia of Polymer Science and Technology: Reinforced plastics to starch*, Interscience publishers.
MARQUARDT, D. W. 1963. An algorithm for least-squares estimation of nonlinear parameters. *Journal of the Society for Industrial & Applied Mathematics,* 11**,** 431-441.
MARTYNA, G. J., TOBIAS, D. J. & KLEIN, M. L. 1994. Constant pressure molecular dynamics algorithms. *The Journal of Chemical Physics,* 101**,** 4177.
MATSUSHIGE, K., ENOSHITA, R., IDE, T., YAMAUCHI, N., TAKI, S. & TAKEMURA, T. 1977. Fine structure of the III-I transition and molecular motion in polytetrafluoroethylene. *Japanese Journal of Applied Physics,* 16**,** 681-687.
MAUSKOPF, S. H. 1969. The Atomic Structural Theories of Ampère and Gaudin: Molecular Speculation and Avogadro's Hypothesis. *Isis,* 60**,** 61-74.
MAYO, S. L., OLAFSON, B. D. & GODDARD, W. A. 1990. DREIDING: a generic force field for molecular simulations. *Journal of Physical Chemistry,* 94**,** 8897-8909.
MCCULLOUGH, R. & MCMAHON, P. 1964. Contributions to conformational energy from interactions between nonbonded atoms and groups. Part 1.—General formulation. *Trans. Faraday Soc.,* 60**,** 2089-2096.
MCMAHON, P. & MCCULLOUGH, R. 1965. Contributions to conformational energy from interactions between nonbonded atoms and groups. Part 3.—Stable conformations of linear polyethylene and polytetrafluoroethylene. *Transactions of the Faraday Society,* 61**,** 201-206.
MODULE, F. 2011. Material Studio 6.0. *Accelrys Inc., San Diego, CA*.
NAKAFUKU, C. & TAKEMURA, T. 1975. Crystal Structure of High Pressure Phase of Polytetrafluoroethylene. *Japanese Journal of Applied Physics,* 14.
NAKANISHI, K. 1962. Infrared absorption spectroscopy: practical.
NAMD, S. T. 2004. *Gradient Tolerance* [Online]. Available: http://www.ks.uiuc.edu/Research/namd/mailing_list/namd-l/.
NAPOLITANO, R., PUCCIARIELLO, R. & VILLANI, V. 1990. Conformational and packing energy calculations on the low-temperature phase (phase II) of poly (tetrafluoroethylene). *Die Makromolekulare Chemie,* 191**,** 2755-2765.
NEESE, F. 2009. ORCA Quantum Chemistry Program.
NELSON, M. T., HUMPHREY, W., GURSOY, A., DALKE, A., KALÉ, L. V., SKEEL, R. D. & SCHULTEN, K. 1996. NAMD: a parallel, object-oriented molecular dynamics program. *International Journal of High Performance Computing Applications,* 10**,** 251-268.

NICHOLSON, J. W. 2011. *The chemistry of polymers*, Royal Society of Chemistry.
OKADA, O., OKA, K., KUWAJIMA, S. & TANABE, K. 1999. Molecular Dynamics Studies of Amorphous Poly (tetrafluoroethylene). *Molecular simulation,* 21**,** 325-342.
PAULECHKA, E., KROENLEIN, K., KAZAKOV, A. & FRENKEL, M. 2012. A Systematic Approach for Development of an OPLS-Like Force Field and Its Application to Hydrofluorocarbons. *The Journal of Physical Chemistry B.*
PETERSEN, H. G. 1995. Accuracy and efficiency of the particle mesh Ewald method. *The Journal of Chemical Physics,* 103**,** 3668.
PETERSON, M. D. 1945. POLYMERIZATION PROCESS. Google Patents.
PLUNKETT, R. J. 1986. The history of polytetrafluoroethylene: discovery and development. *High Performance Polymers: Their Origin and Development***,** 261-266.
PRIME, R. B. 2010. An introduction to thermosets.
QUINN, F. A., ROBERTS, D. E. & WORK, R. 1951. Volume-Temperature Relationships for the Room Temperature Transition in Teflon. *Journal of Applied Physics,* 22**,** 1085-1086.
RAE, P. & BROWN, E. 2005. The properties of poly (tetrafluoroethylene)(PTFE) in tension. *Polymer,* 46**,** 8128-8140.
RAE, P. & DATTELBAUM, D. 2004. The properties of poly (tetrafluoroethylene)(PTFE) in compression. *Polymer,* 45**,** 7615-7625.
RAHMAN, A. 1964. Correlations in the motion of atoms in liquid argon. *Physical Review,* 136**,** 405-411.
RAJABPOUR, A., AKIZI, F. Y., HEYHAT, M. M. & GORDIZ, K. 2013. Molecular dynamics simulation of the specific heat capacity of water-Cu nanofluids. *International Nano Letters,* 3**,** 58.
RIESS, J. G. 1992. Overview of progress in the fluorocarbon approach to in vivo oxygen delivery. *Artificial Cells, Blood Substitutes and Biotechnology,* 20**,** 183-202.
RIGBY, D. & ROE, R. J. 1987. Molecular dynamics simulation of polymer liquid and glass. I. Glass transition. *The Journal of Chemical Physics,* 87**,** 7285.
ROOS, B. & LAWLEY, K. 1987. Ab Initio Methods in Quantum Chemistry II. *Advances in Chemical Physics,* 69**,** 399-446.
RYLAND, A. L. 1958. X-ray diffraction. *Journal of Chemical Education,* 35**,** 80.
SADLEJ, J. & COOPER, I. L. 1985. *Semi-empirical methods of quantum chemistry,* Ellis Horwood Chichester, West Sussex.
SAUER, J. & KLINE, D. 1955. Dynamic mechanical properties of polystyrene, polyethylene, and polytetrafluoroethylene at low temperatures. *Journal of Polymer Science,* 18**,** 491-495.
SCHLEGEL, H. B. 1987. Optimization of equilibrium geometries and transition structures. *Advances in Chemical Physics; Ab Initio Methods in Quantum Chemistry-I***,** 249.
SCOTT, W. R. P., HÜNENBERGER, P. H., TIRONI, I. G., MARK, A. E., BILLETER, S. R., FENNEN, J., TORDA, A. E., HUBER, T., KRÜGER, P. & VAN GUNSTEREN, W. F. 1999. The GROMOS biomolecular simulation program package. *The Journal of Physical Chemistry A,* 103**,** 3596-3607.
SHOOTER, K. & THOMAS, P. 1949. Frictional properties of some plastics. *Research; a journal of science and its applications,* 2**,** 533.
SIMON, D. & MCQUARRIE, J. 1997. Physical Chemistry: A Molecular Approach. University Science Books: Sausalito, CA.

SMITH, G. D., JAFFE, R. L. & YOON, D. Y. 1994. Conformational characteristics of poly (tetrafluoroethylene) chains based upon ab initio electronic structure calculations on model molecules. *Macromolecules,* 27**,** 3166-3173.
SPEERSCHNEIDER, C. & LI, C. 1962. Some observations on the structure of polytetrafluoroethylene. *Journal of Applied Physics,* 33**,** 1871-1875.
SPERATI, C. & STARKWEATHER, H. 1961. Fluorine-containing polymers. II. Polytetrafluoroethylene. *Fortschritte Der Hochpolymeren-Forschung***,** 465-495.
SPRIK, M., RÖTHLISBERGER, U. & KLEIN, M. L. 1997. Structure of solid poly (tetrafluoroethylene): A computer simulation study of chain orientational, translational, and conformational disorder. *The Journal of Physical Chemistry B,* 101**,** 2745-2749.
SPRIK, M., RÖTHLISBERGER, U. & KLEIN, M. L. 1999. Conformational and orientational order and disorder in solid polytetrafluoroethylene. *Molecular Physics,* 97**,** 355-373.
STEWART, J. J. P. 1990. MOPAC: a semiempirical molecular orbital program. *Journal of Computer-Aided Molecular Design,* 4**,** 1-103.
ŠTICH, I., CAR, R., PARRINELLO, M. & BARONI, S. 1989. Conjugate gradient minimization of the energy functional: A new method for electronic structure calculation. *Physical Review B,* 39**,** 4997.
STILLE, J. K. 1962. *Introduction to polymer chemistry*, Wiley New York.
STILLINGER, F. H. & RAHMAN, A. 1974. Improved simulation of liquid water by molecular dynamics. *The Journal of Chemical Physics,* 60**,** 1545.
TANGRAM, T. L. 2012. *Shrinkage in plastics processing* [Online]. Available: http://www.tangram.co.uk/TI-Polymer-Shrinkage_in_plastics.html.
TIELEMAN, D. P., MARRINK, S.-J. & BERENDSEN, H. J. 1997. A computer perspective of membranes: molecular dynamics studies of lipid bilayer systems. *Biochimica Et Biophysica Acta-Reviews on Biomembranes,* 1331**,** 235-270.
TIPLER, P. A. & MOSCA, G. 2007. *Physics for scientists and engineers,* WH Freeman & Company.
TUCKERMAN, M. 2009. *Statistical mechanics: theory and molecular simulation*, Oxford University Press, USA.
TURNBULL, D. & COHEN, M. H. 1961. Free-volume model of the amorphous phase: glass transition. *The Journal of Chemical Physics,* 34**,** 120.
UNAL, H., MIMAROGLU, A., KADıOGLU, U. & EKIZ, H. 2004. Sliding friction and wear behaviour of polytetrafluoroethylene and its composites under dry conditions. *Materials & design,* 25**,** 239-245.
VAIANA, A., COURNIA, Z., COSTESCU, I. & SMITH, J. 2005. AFMM: A molecular mechanics force field vibrational parametrization program. *Computer Physics Communications,* 167**,** 34-42.
VALIEV, M., BYLASKA, E. J., GOVIND, N., KOWALSKI, K., STRAATSMA, T. P., VAN DAM, H. J. J., WANG, D., NIEPLOCHA, J., APRA, E. & WINDUS, T. L. 2010. NWChem: a comprehensive and scalable open-source solution for large scale molecular simulations. *Computer Physics Communications,* 181**,** 1477-1489.
VAN LAARHOVEN, P. J. & AARTS, E. H. 1987. *Simulated annealing*, Springer.
VENKATARAMAN, G. 1997. *Many Phases Of Matter,* Universities Press.
VILLANI, V., PUCCIARIELLO, R. & FUSCO, R. 1991. Conformational analysis of fluorinated copolymers of tetrafluoroethylene. *Colloid & Polymer Science,* 269**,** 477-482.

VISHNYAKOV, A. & NEIMARK, A. V. 2000. Molecular simulation study of Nafion membrane solvation in water and methanol. *The Journal of Physical Chemistry B,* 104**,** 4471-4478.
WALKER, J. 1913. Van't Hoff Memorial Lecture. *Journal of the Chemical Society, Transactions,* 103**,** 1127-1143.
WANG, J. & HOU, T. 2011. Application of Molecular Dynamics Simulations in Molecular Property Prediction. 1. Density and Heat of Vaporization. *Journal of chemical theory and computation,* 7**,** 2151-2165.
WARFIELD, R. W., CUEVAS, J. E. & BARNET, F. 1970. Single specimen determination of Young's and bulk moduli of polymers. *Rheologica Acta,* 9**,** 439-446.
WATKINS, E. K. & JORGENSEN, W. L. 2001. Perfluoroalkanes: Conformational analysis and liquid-state properties from ab initio and Monte Carlo calculations. *The Journal of Physical Chemistry A,* 105**,** 4118-4125.
WEEKS, J., CLARK, E. & EBY, R. 1981. Crystal structure of the low temperature phase (II) of polytetrafluoroethylene. *Polymer,* 22**,** 1480-1486.
WEIR, C. E. 1953. Transitions and phases of polytetrafluoroethylene (Teflon). *Journal of research of the National Bureau of Standards,* 50**,** 95-97.
WESTBROOK, J., FENG, Z., CHEN, L., YANG, H. & BERMAN, H. M. 2003. The protein data bank and structural genomics. *Nucleic Acids Research,* 31**,** 489-491.
YAWS, C. L. 2008. *Thermophysical properties of chemicals and hydrocarbons,* William Andrew.
YU, K. Q., LI, Z. S. & SUN, J. 2001. Polymer structures and glass transition: A molecular dynamics simulation study. *Macromolecular theory and simulations,* 10**,** 624-633.